Aus der Medizinischen Klinik und Poliklinik I der Ludwig-Maximilians-Universität München
Direktor: Prof. Dr. med. Steffen Massberg

und der Neurologischen Klinik und Poliklinik der Ludwig-Maximilians-Universität München
Direktorin: Prof. Dr. med. Marianne Dieterich

Novel pathomechanisms implicated in defects of neuromuscular transmission

Dissertation
zum Erwerb des Doktorgrades der Naturwissenschaften
an der Medizinischen Fakultät
der Ludwig-Maximilians-Universität München

vorgelegt von

Marina Dusl

aus

Freising

2014

Gedruckt mit Genehmigung der Medizinischen Fakultät
der Ludwig-Maximilians-Universität München

Eingereicht am:	06. Mai 2014
Betreuer:	Prof. Dr. rer. nat. Robert David
Zweitgutachter:	Prof. Dr. rer. nat. Roland Kappler
Mitbetreuung durch die habilitierte Mitarbeiterin:	Priv.-Doz. Dr. med. Angela Abicht
Dekan:	Prof. Dr. med. Dr. h.c. Maximilian Reiser, FACR, FRCR
Tag der mündlichen Prüfung:	23. Februar 2015

Teile dieser Arbeit wurden veröffentlicht in oder sind in Vorbereitung zur Publikation:

Senderek J[#], Muller JS[#], **Dusl M**, Strom TM, Guergueltcheva V, Diepolder I, Laval SH, Maxwell S, Cossins J, Krause S, Muelas N, Vilchez JJ, Colomer J, Mallebrera CJ, Nascimento A, Nafissi S, Kariminejad A, Nilipour Y, Bozorgmehr B, Najmabadi H, Rodolico C, Sieb JP, Steinlein OK, Schlotter B, Schoser B, Kirschner J, Herrmann R, Voit T, Oldfors A, Lindbergh C, Urtizberea A, von der Hagen M, Hubner A, Palace J, Bushby K, Straub V, Beeson D, Abicht A, Lochmuller H. Hexosamine biosynthetic pathway mutations cause neuromuscular transmission defect. *Am J Hum Genet* 2011;88(2):162-72.

Chaouch A, Muller JS, Guergueltcheva V, **Dusl M**, Schara U, Rakocevic-Stojanovic V, Lindberg C, Scola RH, Werneck LC, Colomer J, Nascimento A, Vilchez JJ, Muelas N, Argov Z, Abicht A, Lochmuller H. A retrospective clinical study of the treatment of slow-channel congenital myasthenic syndrome. *J Neurol* 2012;259(3):474-81.

Guergueltcheva V[#], Muller JS[#], **Dusl M**, Senderek J, Oldfors A, Lindbergh C, Maxwell S, Colomer J, Mallebrera CJ, Nascimento A, Vilchez JJ, Muelas N, Kirschner J, Nafissi S, Kariminejad A, Nilipour Y, Bozorgmehr B, Najmabadi H, Rodolico C, Sieb JP, Schlotter B, Schoser B, Herrmann R, Voit T, Steinlein OK, Najafi A, Urtizberea A, Soler DM, Muntoni F, Hanna MG, Chaouch A, Straub V, Bushby K, Palace J, Beeson D, Abicht A, Lochmuller H. Congenital myasthenic syndrome with tubular aggregates caused by GFPT1 mutations. *J Neurol* 2011;259(5):838-50.

Abicht A, **Dusl M**, Gallenmuller C, Guergueltcheva V, Schara U, Della Marina A, Wibbeler E, Almaras S, Mihaylova V, von der Hagen M, Huebner A, Chaouch A, Muller JS, Lochmuller H. Congenital myasthenic syndromes: achievements and limitations of phenotype-guided gene-after-gene sequencing in diagnostic practice: a study of 680 patients. *Hum Mutat* 2012;33(10):1474-84.

Gallenmuller C, Muller-Felber W, **Dusl M**, Stucka R, Guergueltcheva V, Blaschek A, von der Hagen M, Huebner A, Muller JS, Lochmuller H, Abicht A. Salbutamol-responsive limb-girdle congenital myasthenic syndrome due to a novel missense mutation and heteroallelic deletion in MUSK. *Neuromuscul Disord* 2014;24(1):31-5.

Dusl M, Senderek J, Müller JS, Vogel JG, Pertl A, Stucka R, Lochmüller H, David R[#], Abicht A[#]. A 3'-UTR mutation creates a potential microRNA target site in the *GFPT1* gene of LG-CMS patients. Im Begutachtungsverfahren.

[#] These authors contributed equally to this work

Poster Präsentation:

M. Dusl, V. Guergueltcheva, J. Müller, S., C. Rodolico, J.P. Sieb, J.J. Vilchez, Kirschner, J., T. Voit, O.K. Steinlein, A. Abicht, H. Lochmüller (November 2009) Limb-girdle congenital myasthenic syndrome with tubular aggregates – phenotypic clues for the entity. TREAT-NMD International Conference, Brussels, Belgium

Vortrag:

M. Dusl, V. Guergueltcheva, J. Müller, S. Nafissi, A. Kariminejad, C. Rodolico, J.P. Sieb, J.J. Vilchez, J. Colomer, J. Kirschner, B. Schlotter, B. Schoser, R. Herrmann, T. Voit, O.K. Steinlein, M. von der Hagen, A. Huebner, J. Senderek, A. Abicht, H. Lochmüller (April 2011) Limb-girdle congenital myasthenic syndrome with frequent tubular aggregates. 20th Congress of the *German* Society *for Muscle* Diseases, Neu-Ulm, Germany

Meinen Eltern

Table of contents

A Acknowledgments

I would like to thank Prof. Dr. Marianne Dieterich for offering me the opportunity to work on an exciting project and for the good work environment at the Friedrich-Baur-Institute.

Prof. Dr. Robert David, I thank for the helpful discussions and guidance of my research projects.

I am thankful to PD Dr. Angela Abicht, Prof. Dr. Hanns Lochmüller and Dr. Juliane Müller for their continual guidance, support and advice throughout the thesis.

I want to emphasize special thanks to all past and present members of the institute for their valuable personal support and help whenever needed, especially Prof. Dr. Maggie Walter, Prof. Dr. Jan Senderek, Dr. Rolf Stucka, PD Dr. Dr. Sabine Krause, Christiana Kubny, Manuela Zitzelsberger, Dr. Sarah Feldkirchner, Irene Kammermeier, Dr. Cordula Pertl, Anja Pertl, Swanhild Meyer, Dr. Sarah Baumeister, Dr. Steffanie Bulst, Dr. Velina Guergueltcheva and Dr. Christian Thirion. Thank you very much for the perfect atmosphere and the many hours at the vegi!

I would like to thank my parents Anneliese and Jakob Dusl for their love and their support throughout my studies.

My love, thank you for being you and for being mine. You and Luise are the greatest gift for me! I love you!

B Summary

Limb-girdle congenital myasthenic syndrome (LG-CMS) is a rare inherited neuromuscular disorder in humans. One major objective of the present study was the molecular genetic characterization of LG-CMS patients with tubular aggregates (TAs) in muscle biopsies. Mutations in glucosamine-fructose-6-phosphate aminotransferase 1 (GFPT1) were identified as underlying molecular defect by a genome-wide linkage analysis and DNA sequencing of positional candidate genes. The bifunctional enzyme GFPT1 catalyses the first and rate limiting step of the hexosamine biosynthetic pathway (HBP) leading to the formation of UDP-N-acetylglucosamine (UDP-GlcNAc) which is essential for posttranslational modification of serine and threonine residues of nuclear and cytoplasmic proteins. Although glutaminase and isomerase activities have been attributed to GFPT1, little is known about the regulation and subcellular localization of GFPT1. A defect in glycosylation is a novel underlying pathomechanism in a synaptic transmission disorder and the role of GFPT1 in CMS pathogenesis has not been defined yet.

Immunoblot analysis revealed reduced GFPT1 protein levels in LG-CMS patients' myoblast lysates. Furthermore, decreased levels of *O*-linked N-acetylglucosamine (*O*-GlcNAc) on proteins were observed in patients' myoblasts and in mouse myoblasts (C2C12 cells) treated with *Gfpt1* siRNA.

The analysis of the effects of LG-CMS associated *GFPT1* mutations on enzymatic activity demonstrated that selected GFPT1 missense mutations have only small effects on the enzyme activity of the GFPT1 protein. Furthermore, the subcellular localization of mutant GFPT1 species, transiently expressed in SW13 cells, is almost consistent with that of wild-type GFPT1. Therefore, a deficiency of GFPT1 protein due to decreased synthesis or stability of the GFPT1 mutants seems to result in reduced levels of *O*-linked N-acetylglucosamine on proteins in LG-CMS patients' myoblasts and might be the major factor at least in the pathogenesis of some GFPT1 associated LG-CMS.

A second major objective was to elucidate the pathogenic mechanisms of a particular mutation in the 3'- untranslated region (UTR) of *GFPT1* (c.*22C>A) observed in four independent families from Spain and Germany. Because this variant does not alter the *GFPT1* open reading frame, its pathogenic relevance has not yet been established. The GFPT1 protein levels were reduced in patients' myoblast samples carrying c.*22C>A heterozygously compared to controls, similarly as it had been observed in patients carrying other disease causing mutations of *GFPT1*. In a controlled assay, the association of *GFPT1* c.*22C>A with reduced GFPT1 protein levels was confirmed. Furthermore, my data demonstrate that the c.*22C>A mutation in the *GFPT1* gene allows for illegitimate binding of miR-206* and miR-600 resulting in reduced GFPT1 protein

expression. I found that reduced GFPT1 protein levels resulted from repression of translation rather than degradation of the mRNA. While it has been demonstrated before that miR-206 is expressed in muscle and involved in myogenesis, I first confirmed that the miR-206* (star-strand) is expressed in skeletal muscle. The overlapping expression profiles of hsa-miR-206*, hsa-miR-600 and *GFPT1* support the assumption that the binding of these miRNAs to the 3'-UTR of mutant *GFPT1* mRNA might be pathogenetically relevant. Therefore, my results support a model in which the point mutation c.*22C>A in the *GFPT1* 3'-UTR creates a target site for miR-206* and miR-600, which influences *GFPT1* expression. Notably, the miR-206* is considerably upregulated in GFPT1 patients' muscle compared to control muscle.

In contrast to most other CMS causing genes which encode post-, pre- or synaptic proteins at the neuromuscular junction (NMJ), *GFPT1* is ubiquitously expressed. Consequently, one challenge of the present thesis was to understand how reduction in GFPT1 protein levels results in selective vulnerability at the NMJ. The skeletal muscle-specific expression of miR-206* could explain the muscle-specific phenotype of CMS patients with the *GFPT1* 3'-UTR mutation.

For the diagnosis, counseling and therapy of a patient, a precise molecular classification of CMS is of paramount importance. The identification of GFPT1 mutations in LG-CMS patients allows, in contrast to most other inherited disorders, an effective therapy since CMS patients with GFPT1 mutations response well to acetylchoninesterase inhibitor treatment.

My results suggest that formation of miRNA binding sites by mutations might be a relevant pathogenic factor in CMS and most likely in other Mendelian disorders as well. In keeping with this consideration, variants in the 3'-UTRs should be carefully evaluated during routine genetic diagnostic procedures.

C Zusammenfassung

Die kongenitalen myasthenen Syndrome (CMS) bilden eine klinisch und genetisch heterogene Gruppe von neuromuskulären Erkrankungen, denen eine Signalübertragungsstörung der motorischen Endplatte zugrunde liegt. Im Fokus dieser Arbeit stand die seit längerem bekannte, distinkte Unterform der autosomal-rezessiv vererbten CMS mit Gliedergürtelbetonung (LG-CMS) und tubulären Aggregaten in der Muskelbiopsie. Durch genomweite Kopplungsanalyse und die anschließende Sequenzanalyse positionaler Kandidatengene gelang es, Mutationen im *GFPT1*-Gen, das für das bifunktionelle Enzym glutamine—fructose-6-phosphate transaminase 1 (GFPT1) kodiert, als Ursache der LG-CMS zu identifizieren. GFPT1 ist das Schlüsselenzym des Hexosamin-Stoffwechselweges (HBP) und essentiell für die posttranslationale Modifikation von Serin- und Threonin-Resten von nukleären und cytoplasmatischen Proteinen mit *O*-glykosidisch gebundenem N-Acetylglucosamin (*O*-GlcNAc). Der Zusammenhang zwischen CMS und einem Glykosylierungsdefekt ist ein neuer Pathomechanismus für neuromuskuläre Signalübertragunsstörungen, so dass diese Arbeit das Ziel verfolgte, die molekularen und zellulären Auswirkungen der GFPT1-Mutationen zu charakterisieren, um die Rolle von GFPT1 in der CMS-Pathogenese zu verstehen.

Es konnte gezeigt werden, dass die GFPT1-Proteinmengen in Myoblasten von Patienten mit GFPT1-Mutationen deutlich vermindert sind. Außerdem finden sich in Myoblasten von Patienten und in Mausmyoblasten (C2C12-Zellen), in denen die *Gfpt1*-Expression mit siRNA unterdrückt wird, verminderte Level von *O*-GlcNAc modifizierten Proteinen. Dahingegen konnte durch transient exprimiertes GFPT1 in HEK293 Zellen und nachfolgendem GDH Aktivitätstest nachgewiesen werden, dass GFPT1-Missensmutationen nur geringe Auswirkungen auf die Enzymaktivität haben. Zudem stimmt die subzelluläre Lokalisation von mutiertem GFPT1 mit der des Wildtyp Proteins weitgehend überein, so dass es vermutlich aufgrund verminderter Synthese oder Stabilität der GFPT1-Mutanten zum Verlust der Proteinfunktion kommt, die sich in reduzierten Levels von *O*-GlcNAc modifizierten Proteinen zeigt.

Ein weiterer Schwerpunkt der vorliegenden Arbeit war die Analyse der c.*22C>A Mutation in der 3`-untranslatierten Region (UTR) von *GFPT1*, die in vier unabhängigen LG-CMS Familien aus Spanien und Deutschland identifiziert wurde. Auch bei diesen Patienten waren in Muskelbiopsien und kultivierten Myoblsaten deutlich verminderte GFPT1-Proteinmengen nachweisbar. Es konnte gezeigt werden, dass durch die Mutation in der 3`-UTR von *GFPT1* eine Bindestelle der miRNAs miR-600 und miR-206* entsteht. In Experimenten mit Reporterkonstrukten konnte bestätigt werden, dass durch die Bindung der miRNAs an die Zielsequenz die Expression von GFPT1 tatsächlich vermindert wird. Dabei ergeben sich die verringerten GFPT1-Proteinmengen in

Myoblasten und Muskel von Patienten mit der Mutation c.*22C>A eher aus der Repression der Translation als dem Abbau der mRNA. Während bereits bekannt war, dass der sog. „Leitstrang" der miR-206 im Muskel exprimiert wird und als muskelspezifische miRNA eine Rolle bei der Myogenese spielt, zeigt diese Arbeit, dass auch die miR-206* (star), der sog. „Folgestrang" in humanem Muskel, Myoblasten, Myotuben und C2C12-Zellen vorliegt. Im Unterschied zu den meisten anderen CMS-Genen, die Komponenten der neuromuskulären Endplatte kodieren, wird *GFPT1* ubiquitär exprimiert. Da durch die *GFPT1* 3'-UTR-Mutation eine Zielsequenz für die muskelspezifische miRNA miR-206* entsteht, ergibt sich hierfür zumindest für Patienten mit dieser Mutation ein plausibler Erklärungsansatz. Mit der Identifizierung von Mutationen im *GFPT1*-Gen konnten in der vorliegenden Arbeit Glykosylierungsdefekte als gänzlich neuer Pathomechanismus für kongenitale myasthene Syndrome beschrieben werden. Für die betroffenen Patienten bedeutet der Nachweis einer GFPT1-Mutation nicht nur die Möglichkeit einer gezielten genetischen Beratung, sondern erlaubt – im Gegensatz zu den meisten anderen erblichen Erkrankungen – auch eine wirksame Therapie, da bei Patienten mit GFPT1-Mutationen Acetylcholinesterasehemmer gut wirksam sind. Untersuchungen zu einer Mutation außerhalb des kodierenden Leserahmens des *GFPT1*-Gens weisen darauf hin, dass die Entstehung einer miRNA Bindestelle durch Mutationen im 3'-UTR eine Ursache monogenetischer Erkrankungen darstellen kann und die Analyse der 3'-UTR in der genetischen Diagnostik berücksichtigt werden muss.

D Introduction

1 Neuromuscular junction (NMJ)

The NMJ is a specialized synapse to communicate the electrical impulse from the motor neuron to the skeletal muscle in order to signal contraction. The synapse consists of the following three major structural elements [1, 2]: the presynaptic region containing the nerve terminal, the synaptic cleft and the postsynaptic surface of the muscle cell. It is designed to transmit the impulses from the nerve terminal to the muscle via the chemical transmitter acetylcholine (ACh). This neurotransmitter is synthesized in the motor nerve terminal by the enzyme choline acetyltransferase (ChAT) and packed into synaptic vesicles. Following the arrival of an action potential and the subsequent influx of presynaptic calcium by voltage-gated calcium channels (VGCC), the vesicles are released. They fuse with the plasma membrane of the nerve terminus and release the neurotransmitter acetylcholine (ACh) into the synaptic cleft. The neurotransmitter binds to the acetylcholine receptor (AChR) at the postsynaptic surface at a ratio of two ACh molecules per receptor. Ligand binding leads to the opening of the AChR ion channel, positively charged sodium ions enter through the central pore of the receptor and results in the depolarization of the postsynaptic membrane. The depolarization of the membrane potential leads to the activation of voltage-gated sodium channels (sodium channel isoform Nav1.4, the muscle sodium channel which is predominantly expressed in skeletal muscle [3, 4]) on the postsynaptic side. An action potential is generated and propagated, eventually leading to contraction of the muscle. ACh is hydrolyzed by the enzyme acetylcholinesterase (AChE) in the synaptic cleft of the NMJ. Its breakdown product, choline, can be re-synthesized into ACh in the motor neuron. The membrane potential of the presynaptic membrane is restored when voltage-gated potassium channels open.

During development, the formation of the postsynaptic apparatus is induced by agrin, which is released from the nerve terminal [5]. Binding of agrin to the low-density lipoprotein receptor-related protein 4 (Lrp4) activates the muscle specific tyrosine kinase (MuSK) [6-8] which in turn is able to bind downstream of kinase 7 (Dok7) [9]. Activated MuSK also leads to the tyrosine phosphorylation of the AChR β-subunit [10]. It was shown that phosphorylation of this motif fosters binding of the membrane protein rapsyn to each AChR [11]. Rapsyn also interacts with the f-actin cytoskeleton, thus attaching the receptor to the cytoskeleton and being essential for AChR clustering [12].

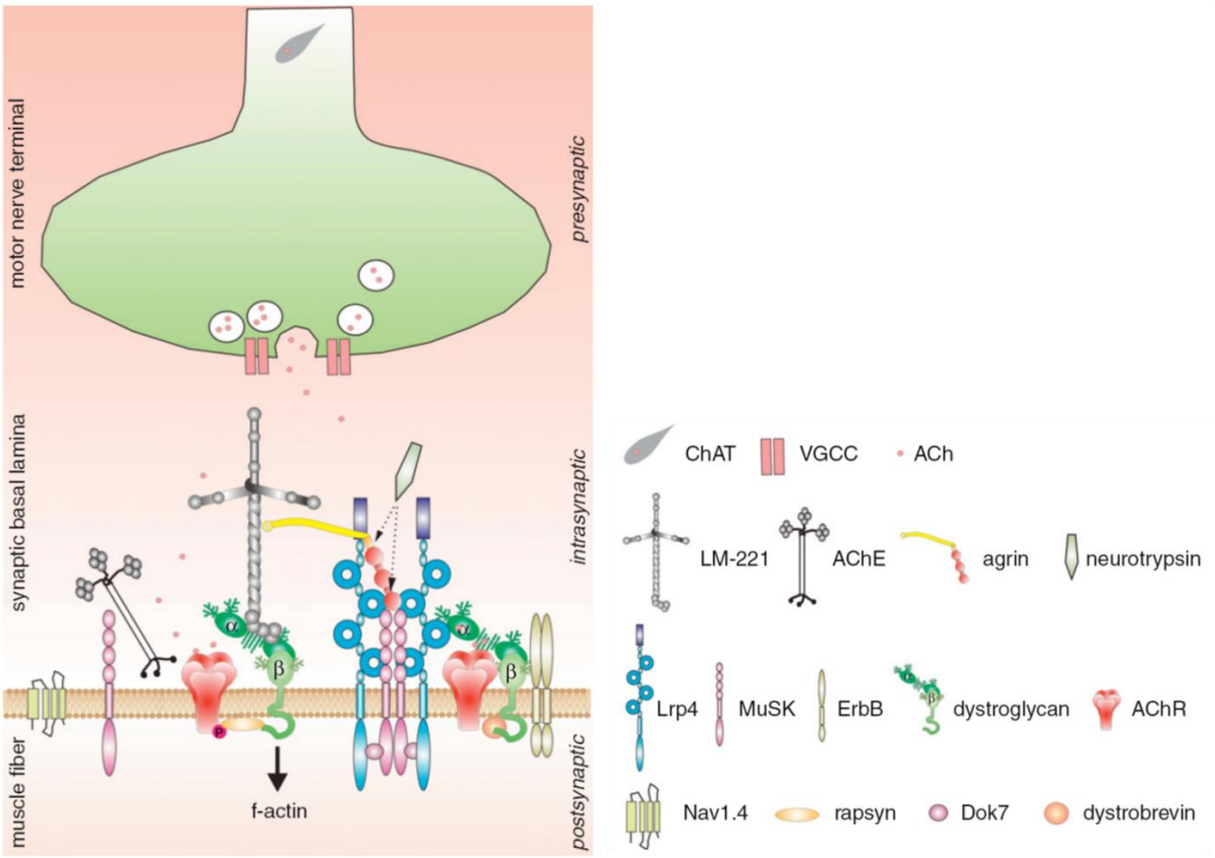

Figure 1: Schematic representation of the neuromuscular junction (NMJ).

The scheme presents the molecular signaling at the neuromuscular junction and the involved molecules in signal transmission and development of the apparatus [13]. See text for abbreviations and explanations.

2 Congenital myasthenic syndromes (CMS)

Impaired neuromuscular transmission causes some different neurological conditions, varying from poisoning with botulinum and snake venom toxins through the autoimmune mediated disorders such as the Lambert-Eaton myasthenic syndrome and myasthenia gravis to the hereditary congenital myasthenic syndromes (CMS) [14, 15]. Diseases of the NMJ affect presynaptic, synaptic or postsynaptic components and cause skeletal muscle fatigue. Congenital myasthenic syndromes are inherited human disorders characterized by defects in neuromuscular transmission [16, 17]. These rare hereditary neuromuscular disorders are caused by mutations in a number of different genes. There are no current information on the prevalence of CMS in Germany, but a recent study in the United Kingdom (UK) revealed that the UK detected prevalence of genetically confirmed CMS was about 9.2 cases per million children under 18 years of age [18]. To date, 14 genes are known to cause CMS and as the majority of them are coding for NMJ proteins, the

disorder is classified according to the location of the mutant protein at the NMJ into presynaptic, synaptic and postsynaptic CMS [19, 20].

2.1 Main clinical symptoms

In general, the onset of the disease is shortly after birth or during early childhood. Some sporadic or late-onset CMS have been described as well [19, 20]. The main clinical features of CMS include abnormal fatigue and fluctuating muscle weakness. The disorder may be very severe, resulting in progressive muscle weakness, respiratory insufficiency, loss of ambulation and death [21]. The symptoms of CMS are sometimes similar to those of two other NMJ disorders, myasthenia gravis and Lambert-Eaton myasthenic syndrome. However, these disorders occur when the immune system attacks parts of the NMJ [22]. In contrast to autoimmune disorders, tests for AChR and MuSK antibodies are negative in CMS patients.

2.2 Classification of CMS

2.2.1 Presynaptic CMS

2.2.1.1 CHAT mutations

Presynaptic CMS is rare and only mutations in the protein choline acetyltransferse (ChAT), encoded by the *CHAT* gene, have been identified so far. The ChAT protein catalyses the production of ACh at the nerve terminals. Experiments in knockout mice have shown that ChAT affects synaptogenesis and coordinates synaptic maturation [23]. The *CHAT* mutations in CMS patients alter the stability, expression or kinetics of the ChAT protein. The onset of these CMS is at birth or in the neonatal period. Patients harboring mutations in *ChAT* show sudden episodic crises with apnea and they respond well to anti-AChE therapy [24-26].

2.2.2 Synaptic CMS

2.2.2.1 COLQ mutations

Acetylcholinesterase (AChE) hydrolyses acetylcholine in the synaptic cleft of the NMJ. This asymmetric enzyme consists of one, two or three homotetramers of catalytic subunits ($AChE_T$) attached to a triple-stranded collagenic tail (ColQ) that anchors it in the synaptic basal lamina [27]. ColQ comprises an N-terminal proline-rich region attachment region (PRAD), a collagenic central domain and a C-terminal region enriched in charged residues and cysteines. Each ColQ

strand binds to the proline-rich region of an $AChE_T$ tetramer [28]. In order to anchor the enzyme in the postsynaptic membrane, two binding domains in the collagen domain and residues in the C-terminal domain interact with perlecan and the extracellular domain of muscle-specific kinase (MuSK). Pathogenic mutations causing synaptic CMS have been identified in each ColQ domain. The resulting endplate AChE deficiency can be caused by mutations preventing the attachment of $AChE_T$ to ColQ, producing a short single-stranded and insertion-incompetent ColQ or by impairing the triple-helical assembly of the collagenic domain and/or hindering insertion into the basal lamina [16]. These different consequences depend on the localization of the *COLQ* mutations. The first symptoms usually arise neonatally or during infancy and they are severe with significant lethal risk or less severe, respectively. ColQ patients do not benefit from anti-AChE therapy but they can be treated by ephedrine [29] or albuterol [30].

2.2.2.2 LAMB2 mutations

In the literature, one case has been reported presenting with symptoms and signs of CMS associated with congenital nephrosis and ocular malformations. The molecular genetic analysis of this patient confirmed compound heterozygous mutations in the *LAMB2* gene, encoding the beta2 subunit of laminins. The patient did not benefit from cholinesterase inhibitors but the therapy with ephedrine was beneficial [31]. Laminins are glycoproteins of the basal lamina located at the NMJ and they seem to play an important role in synaptogenesis [32].

2.2.3 Postsynaptic CMS

2.2.3.1 AChR subunit mutations

The most common type of CMS is postsynaptic CMS. Most cases are caused by mutations in AChR subunit genes. The adult muscle AChR is a pentamer comprising two α subunits, one β, one δ and one ε subunit. There is also a fetal form in which a γ subunit is expressed instead of the ε subunit. The five homologous subunits consist of a large N-terminal extracellular domain followed by three transmembrane domains (M1–3), an intracellular cytoplasmic domain, a final transmembrane domain (M4) and an extracellular C-terminus [33]. Each receptor has two ACh binding pockets, one at the α/ε interface and one at the α/δ interface.

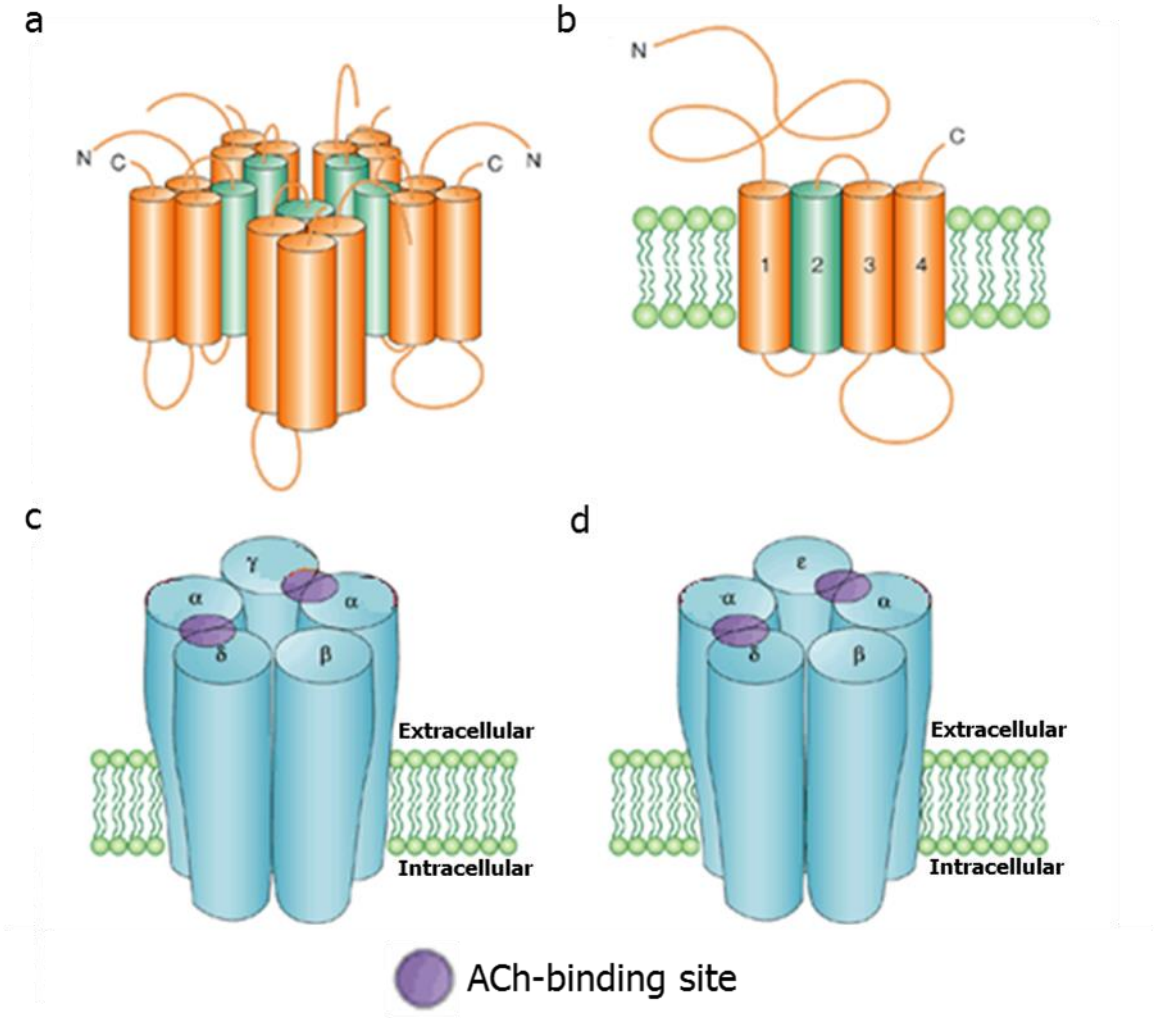

Figure 2: Schematic representation of the acetylcholine receptor (AChR).

(a) AChR is a pentameric membrane protein. (b) Each subunit consist of a large N-terminal extracellular domain followed by three transmembrane domains (1–3), an intracellular cytoplasmic domain, a final transmembrane domain (4) and an extracellular C-terminus. (c) The fetal form expresses the γ subunit instead of the ε subunit. (d) The adult muscle AChR comprising two α subunits, one β, one δ and one ε subunit. The figure was adapted and modified from [34].

AChR mutations can be classified into two major classes: kinetic mutations with or without subtle AChR deficiency and mutations leading to major deficiency of AChR at the endplate by altering its expression. Kinetic mutations are subdivided into two types depending on their kinetic effect: 'slow-channel' and 'fast-channel' mutations. Prolonged opening of the AChR channel and the following slow decay of the synaptic current are caused by slow-channel mutations. Physiologically, the fast-channel syndrome is the opposite of the slow-channel syndrome. Slow-channel syndromes are caused by autosomal-dominant gain-of-function mutations, while all other CMS types are caused by autosomal-recessive loss-of-function mutations [16, 35-37].

2.2.3.2 RAPSN mutations

Mutations in the gene encoding rapsyn (receptor-associated protein of the synapse) are also classified as postsynaptic CMS. The rapsyn protein comprises several functional domains: a myristoylated N-terminal, 7 tetratricopeptide repeats (TPR) important for self-aggregation and binding to the muscle kinase MuSK, the coiled coil domain and the C-terminal domain that binds to β dystroglycan. Together with agrin, LRP4 (low-density lipoprotein receptor-related protein 4), MuSK and Dok-7 (downstream of tyrosine kinase 7) rapsyn clusters the muscle nicotinic ACh receptor at the postsynaptic membrane and connects it to the subsynaptic cytoskeleton through dystroglycan [7, 9, 38, 39]. The majority of the identified *RAPSN* mutations are located in the tetratricopeptide repeat domain of the rapsyn protein. Expression studies of cells co-expressing mutant rapsyn and AChR subunits revealed impaired recruitment of the receptor to rapsyn clusters [40]. Mutations in the *RAPSN* gene are a relatively common cause of CMS and most *RAPSN* CMS patients harbour the p.Asn88Lys mutation in exon 2 either homozygously or heterozygously [41, 42]. Both early and late onset phenotypes have been described and the clinical picture varies from severe to mild. Ptosis is seen in most patients with *RAPSN* mutations. Other frequent symptoms include respiratory crises and high arched palate. The patients respond well to AChE inhibitor therapy.

2.2.3.3 MUSK and AGRN mutations

Defects in MuSK and agrin are also known to cause CMS. There are two publications on mutations in agrin [43, 44] and three on mutations in MuSK [45-47]. The clinical phenotype and the disease severity of patients with *MUSK* mutations is very variable. Only the presence of ocular symptoms and fatigable limb weakness are common. The two CMS patients with *AGRN* mutations described so far presented with a fairly mild phenotype without bulbar and respiratory difficulties. *MUSK* as well as *AGRN* patients benefit from ephedrine treatment while the therapy with cholinesterase inhibitors is ineffective.

2.2.3.4 DOK7 mutations

First described in 2006, mutations in the *DOK7* gene have been established as a common cause of CMS. The mutations in *DOK7* are supposed to result in abnormal activation of MuSK signalling which leads to unstable NMJ with simplified pre- and post-synaptic structures [48-50]. Furthermore, experiments in zebrafish suggested that Dok-7 deficiency also impairs slow muscle fibre organisation independent of Musk [51]. First symptoms of the disease may become manifest either in childhood or adulthood. Patients with *DOK7* mutations show predominant limb-girdle weakness, facial weakness and mild ptosis while the extra-ocular muscles are usually

spared. These patients do not benefit from AChE inhibitor therapy but they can be treated with ephedrine [52] or albuterol [30].

2.2.3.5 SCN4A and PLEC mutations

Only one CMS patient with mutations in the gene *SCN4A* encoding the voltage-gated sodium channel of skeletal muscle (Nav1.4) has been observed so far [53]. Recently, four CMS patients have been reported with mutations in the *PLEC* gene coding for the intermediate filament-linking protein plectin [54-56].

2.3 Therapeutic strategies for CMS

Dependent on a precise molecular genetic diagnosis, there are some strategies for therapy of CMS available. These are based on whether the underlying genetic defect decreases or increases the synaptic response to ACh. Acetylcholinesterase (AChE) inhibitors are used to increase the synaptic response to ACh. When the synaptic response to ACh is attenuated, 3,4-diaminopyridine (3,4-DAP) is also a beneficial treatment as it increases ACh release [36]. By contrast, if the AChR opening is prolonged, followed by an increased synaptic response, drugs like ephedrine, quinidine or fluoxetine are the treatment of choice. Under this condition, the use of AChE-inhibitors is ineffective or symptoms might even get worse.

Molecular defect	Treatment	Reference
Presynaptic defects		
Choline acetyltransferase deficiency (*CHAT* mutation)	AChE inhibitors	[24-26]
Synaptic defects		
Endplate AChE deficiency (*COLQ* mutation)	Ephedrine or albuterol	[29] or [30]
Laminin beta2 subunit (*LAMB2* mutation)	Ephedrine	[31]
Postsynaptic defects		
AChR deficiency without kinetic abnormality	AChE inhibitors; 3,4-diaminopyridine plus AChE inhibitors	[57, 58]
Fast-channel syndrome	AChE inhibitors and 3,4-diaminopyridine	[59, 60]
Slow-channel syndrome	Fluoxetine, Quinidine	[61, 62]
Rapsyn (impaired AChR clustering)	AChE inhibitors	[63]
MuSK	Ephedrine and 3,4-diaminopyridine	[45-47]
Agrin	Ephedrine	[43, 44]
Sodium channel, voltage-gated (*SCN4A* mutation)	AChE inhibitors and acetazolamide	[53]
Plectin	3,4-diaminopyridine	[64]
Dok-7	Ephedrine or albuterol	[52] or [30]

Table 1: Treatment of CMS with different molecular genetic diagnoses

3 Novel clinical and molecular entity

3.1 Limb-girdle (LG-) CMS with frequent tubular aggregates and *GFPT1* mutations

3.1.1 LG-CMS symptoms

LG-CMS patients show shoulder and pelvic girdle weakness and fatigue. No or only minimal involvement of ocular and facial muscles is observed. The onset of the disease usually occurs in the first decade of life. Repetitive nerve stimulation (RNS) reveals a significant decrement in proximal muscles. The majority of patients show tubular aggregates (TAs) in skeletal muscle and esterase inhibitor treatment is beneficial for the patients [65, 66]. Unlike patients with *GFPT1* mutation, CMS patients with *DOK7* mutation who suffer from limb-girdle weakness as well do not benefit from ACh esterase inhibitor treatment and they show involvement of eye movements [48].

3.1.2 Tubular aggregates

Tubular aggregates (TAs) were first described by Engel as granular "crystal-like" inclusions in skeletal muscles, associated with mitochondrial aggregates [67]. To date, the presence of TAs has been described in the skeletal muscle of patients with a wide range of neuromuscular disorders. The mechanisms which underlie the formation of TAs are still unknown. In addition, their functional significance in skeletal muscle has not been fully understood and it is unknown whether they represent pathological structures or compensatory reactions to diverse pathogenic events such as periodic paralysis, dyskalaemia, intoxication, inflammatory myopathies, cramps and myalgias, myotonia congenita, familial myopathies, and several other myopathies of uncertain etiology [68, 69]. TAs are composed of long tubules containing one or more inner tubules and some saccular dilations [69]. By light microscopy, the aggregates can be seen as dark inclusions in the nicotinamide-adenine dinucleotide (NADH) stain of muscle biopsies and as they stain positive with the NADH-tetrazolium reductase reaction, they were initially thought to originate from mitochondria. However, work of several groups has shown that TAs rather arise from the sarcoplasmatic reticulum [70].

3.1.3 GFPT1

The enzyme glutamine-fructose-6-phosphate transaminase (GFPT) catalyses the first and rate limiting step of the hexosamine biosynthetic pathway (HBP) leading to UDP-GlcNAc production. It is highly conserved among species and it is encoded by the two highly homologous genes *GFPT1* and *GFPT2* [71, 72] which are localized on different chromosomes (in humans: *GFPT1* maps to chromosome 2p13-p1 while *GFPT2* maps to chromosome 5q34-q35). There are also differences in the expression pattern. Both genes are ubiquitously expressed but while *GFPT1* is highly expressed in the testis, pancreas and placenta, *GFPT2* is more abundant in the heart and central nervous system [72]. In skeletal and heart muscle, an additional *GFPT1* splice variant was discovered [73]. The so called *GFPT1-L* or muscle-specific variant has a 54 base pair insertion (additional muscle-specific exon; 18 amino acid insertion) and is more abundant in muscle than the shorter ubiquitous splice variant *GFPT1* [73].

The GFPT enzyme consists of three catalytic domains: the N-terminal 27 kDa glutamine amidotransferase domain, which transfers amide nitrogen from glutamine to the substrate fructose-6-phosphate, and the two C-terminal sugar isomerase domains which are phosphosugar-binding domains [74-76]. The bacterial counterpart (GlmS) has been purified to homogeneity and extensively structurally analysed [76-79]. The *Escherichia coli* (*E.coli*) GlmS enzyme is supposed to function as a dimer. The glutamine amidotransferase and sugar isomerase domains are connected by a linker and a hydrophobic channel responsible for ammonia transfer between the domains. The overall structure of human GFPT1 is similar to the structure of GlmS and the amino acid sequence of the isomerase domain of GFPT1 has 43 % identity with GlmS [80]. Recent studies on the human GFPT1 enzyme revealed that it exists in at least two different oligomerization states (symmetric dimer and tetramer) during the reaction process [80, 81].

3.2 Hexosamine biosynthetic pathway (HBP)

Cellular glucose is rapidly phosphorylated to glucose-6-phosphate (glucose-6-P) by hexokinases, trapping the glucose within the cell. There are multiple pathways for the cellular fate of glucose including glycolysis, glycogen synthesis, pentose phosphate pathway and the HBP. The majority enters the glycolytic pathway and serves as energy source. Only 2-3 % of total cellular glucose is metabolized via the HBP (Figure 3) [82-84].

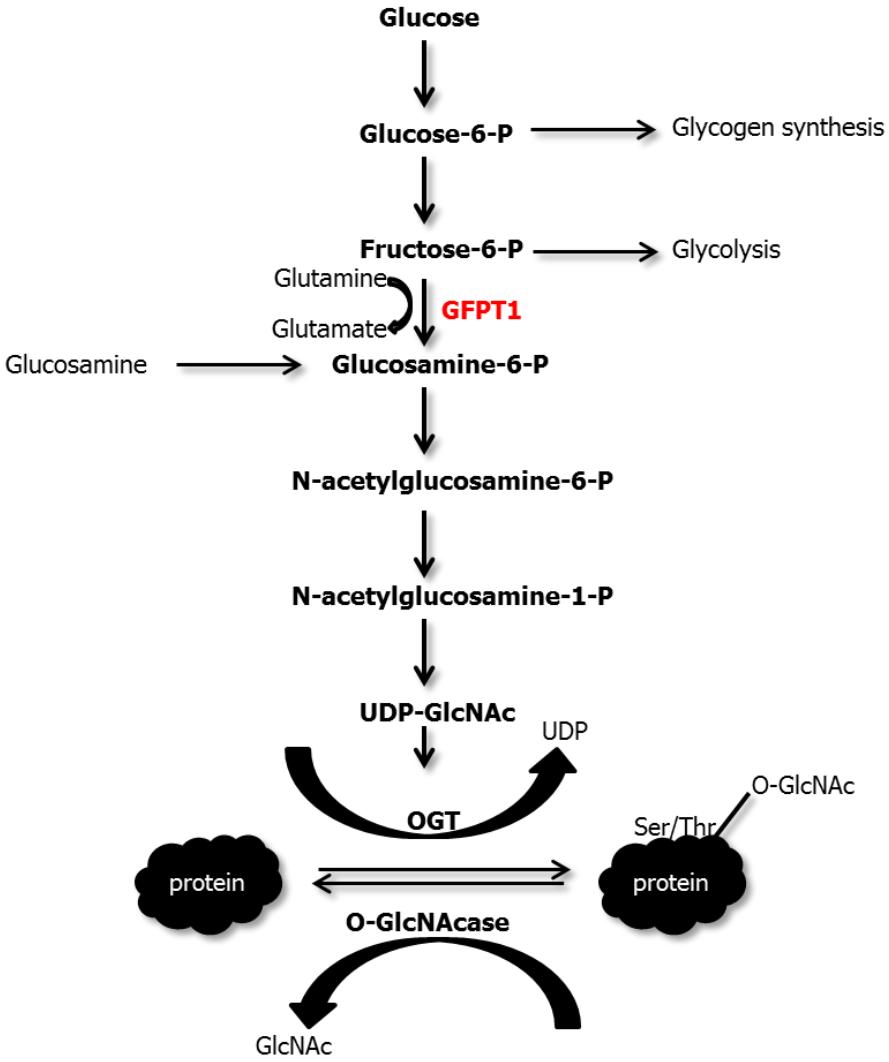

Figure 3: The hexosamine biosynthetic pathway (HBP) and protein *O*-GlcNAc modification.
After phosphorylation of glucose to glucose-6-phosphate (glucose-6-P) it is converted to fructose-6-phosphate (fructose-6-P) which is metabolized to glucosamine-6-phosphate by glucosamine-fructose-6-phosphate aminotransferase 1 (GFPT1). The major end product of the HBP is uridine diphosphate *N*-acetylglucosamine (UDP-GlcNAc). UDP-GlcNAc serves as substrate for uridine-diphospho-*N*-acetylglucosamine:polypeptide β-*N*-acetylglucosaminyltransferase (OGT), leading to the formation of *O*-linked β-*N*-acetylglucosamine (*O*-GlcNAc) modified proteins. The figure was adapted and modified from [85].

Glucosamine-fructose-6-phosphate aminotransferase 1 (GFPT1) catalyses the first and rate limiting step of the hexosamine biosynthetic pathway (HBP) by converting fructose-6-phosphate to glucosamine-6-phosphate with glutamine as amine donor [86]. The metabolization of glucosamine-6-P, via different hexosamine intermediates, leads to the formation of uridine diphosphate *N*-acetylglucosamine (UDP-GlcNAc). GFPT1 activity is subject to feedback inhibition by the end product of the pathway UDP-GlcNAc and has been shown to be regulated by glucose in cultured rat adipocytes [87]. Kinetic differences between GFPT1 and GFPT1-L enzyme activities

are known. The major kinetic difference is a greater susceptibility of GFPT1-L to feed-back inhibition by UDP-GlcNAc [73, 88]. UDP-GlcNAc is a substrate of uridine-diphospho-*N*-acetylglucosamine:polypeptide β-*N*-acetylglucosaminyltransferase (OGT) for the synthesis of glycoproteins, glycolipids, proteoglycans and it is the donor for the formation of *O*-GlcNAc modified proteins [89]. The removal of *O*-GlcNAc from proteins is catalysed by the enzyme β-*N*-acetylglucosaminidase (*O*-GlcNAcase).

The modification of nuclear and cytoplasmatic proteins by *O*-GlcNAc is very dynamic and plays a role in the alteration of activity [90], function [91], protein stability [92, 93] and subcellular localization of target proteins [94-96]. Since some serine and threonine residues modified by *O*-GlcNAc are also subject to phosphorylation, GlcNAc is in some cases in direct competition with phosphorylation [97].

In contrast, classical and complex *N*- and *O*-linked glycosylation occurs on membrane-bound or secreted proteins that are synthesized in the endoplasmic reticulum (ER) and the Golgi apparatus.

3.2.1 Glycosylation

More than 20 posttranslational modifications (PTMs) of proteins are known that occur in eukaryotes [98]. The dynamically regulated phosphorylation of proteins might be the most studied form. But there are many others including the modification of proteins by addition of carbohydrate moieties (glycosylation). Nearly half of all proteins are estimated to be glycosylated, making glycosylation the most common form of posttranslational modification *in vivo* [99]. *N*-linked glycosylation is characterized by remarkably long chains of carbohydrates whereby the carbohydrates are added to secreted proteins at the consensus sequence Asn-X-Ser/Thr, (where X can be any amino acid except proline) [99, 100]. *O*-linked glycosylation does not require a consensus sequence and is often restricted to a few carbohydrate units [101]. However, it may be elaborated to great lengths and structural diversity. Classical and complex *N*- and *O*-linked glycosylation occurs on membrane-bound or secreted proteins during their synthesis and transport through the endoplasmic reticulum (ER) and the Golgi apparatus.

3.2.1.1 O-GlcNAc Glycosylation

The attachment of the monosaccharide β-*N*-acetylglucosamine (*O*-GlcNAc) to serine and threonine residues of nuclear and cytoplasmatic proteins is a rapid and dynamic modification [102, 103]. First described by Hart and Torres in 1984 in lymphocyte cells [103], *O*-GlcNAc is distinguished from other classical forms of glycosylation by occurring predominantly on

intracellular proteins rather than those secreted to membrane compartments [102]. Furthermore, unlike other carbohydrate modifications, but similar to phosphorylation, the attachment of *O*-GlcNAc appears to be dynamically regulated. Since some serine and threonine residues modified by *O*-GlcNAc are also subject to phosphorylation, GlcNAc is in some cases in direct competition with phosphorylation [97]. Recent studies revealed that *O*-GlcNAc levels are strongly upregulated in response to a number of cell stress stimuli [104]. It has been shown that the global extent of *O*-GlcNAc modification is tightly dependent of the flux through the hexosamine biosynthetic pathway (HBP) [105].

E Objectives

Since 1998, our laboratory has collected DNA and clinical data of more than 900 independent CMS patients of various ethnic origins. Molecular genetic analysis and characterization of these patients led to the identification of numerous disease-causing mutations in known CMS genes providing novel insights into synaptic function. The main aspect of this thesis was the identification and characterization of genetic alterations which lead to defects in neuromuscular transmission at the neuromuscular junction and thereby to CMS. The analysis of the pathology of mutations is the basis for the classification of the syndrome and has direct impact on the clinical management of CMS patients.

The aim of the first part of this thesis was the identification of the underlying gene defect in LG-CMS with frequent tubular aggregates. Using genome-wide homozygosity mapping and DNA sequencing of positional candidate genes, mutations in *GFPT1* were identified in a unique collection of LG-CMS families.

The second aim of my thesis was the molecular genetic analysis of the *GFPT1* gene in additional LG-CMS patients to characterize unsolved CMS patients molecular genetically and to establish genotype-phenotype correlations.

In contrast to other CMS genes, GFPT1 is a ubiquitous enzyme expressed in most tissues. Consequently, one challenge of the present thesis was to understand how mutated GFPT1 results in a selective vulnerability of the NMJ and leads to LG-CMS. To address this question, the subcellular localization, enzyme activity and expression levels of GFPT1 carrying LG-CMS causing missense mutations were studied.

Furthermore, I aimed to analyse in more detail a peculiar change in the 3'- untranslated region (UTR) of *GFPT1*: c.*22C>A which leads to reduced GFPT1 levels in patient muscle samples. To get a hint whether reduced protein amounts resulted from repression of translation or altered mRNA stability, real-time qRT-PCR, *in silico* investigation and experimental validation of miRNA binding sites were employed.

F Materials and Methods

1 Materials

1.1 Laboratory equipment

Camera: Zeiss AxioCam HR photo camera (Zeiss, Oberkochen, Germany)

Centrifuges: Centrifuge 5417, 5417R (Eppendorf, Hamburg, Germany); Varifuge 3.0R (Heraeus, Buckinghamshire, UK)

Cell culture incubator (37°C): Functional line (Heraeus, Buckinghamshire, UK)

ELISA: Spectra Max 250 microplate reader (Molecular Devices, Sunnyvale, CA)

-80°C Freezer: HERA freeze (Heraeus, Buckinghamshire, UK)

Gel documentation system: Herolab, Wiesloch, Germany

37°C Incubator/ bacteria: Heraeus Instruments (Heraeus, Buckinghamshire, UK)

Laminar airflow cabinet: BDK, Sonnenbühl-Genkingen, Germany

Luminometer: Berthold Technologies TriStar LB 941

Microscope: Zeiss Axiovert 200 M fluorescence microscope (Zeiss, Oberkochen, Germany)

pH-meter: HI9321 Microprocessor pH Meter (Hanna Instruments, Kehl am Rhein, Germany)

Pipetes: Pipetman, Gilson (2 µl, 20 µl, 200 µl, 1000 µl)

Power supply: Bio-Rad Power Pac Basic (Bio-Rad Laboratories, Hercules, USA)
Proteingel chamber: Bio-Rad Mini Protean II (Bio-Rad Laboratories, Hercules, USA)

Software: Photoshop CS2 (Adobe); Illustrator CS2 (Adobe); ImageJ (national institute of health, USA)

Spectrophotometer: Nanodrop ND-1000 (PeqLab, Erlangen, Germany)

Thermocycler: Mastercycler personal (Eppendorf, Hamburg, Germany); CFX96 Real-Time System (Bio-Rad Laboratories, Hercules, USA)

Western blot imager: ChemoCam Imager (INTAS, Göttingen, Germany)

1.2 Chemicals

All used chemicals were purchased from Sigma-Aldrich, PAA Laboratories or Roth.
Exceptions are listed below:
Agarose (Invitrogen); dNTPSet (Fermentas); Fluorescence Mounting Medium (Dako); Horse Serum (Invitrogen); Running Buffer (MP Biomedicals, LLC); Transfer Buffer (MP Biomedicals, LLC)

1.3 Kits and enzymes

The following enzymes and kits were used:
Restriction endonucleases with 10x restriction buffer system (NewEngland BioLabs, Roche, Fermentas); AccuPrime™ *Pfx* DNA Polymerase (Invitrogen); *PfuULTRA*™ High-Fidelity DNA Polymerase (Agilent Technologies, Inc.); T4 DNA Ligase (NewEngland BioLabs); Calf Intestine Alkaline Phosohatase (Fermentas); RNeasy Kit (Qiagen); RNeasy MinElute Cleanup Kit (Qiagen); miRNeasy Kit (Qiagen); miScript PCR Starter Kit (Qiagen); Hs_miR-600_1 miScript Primer Assay (Qiagen); Oan-miR-206* miScript Primer Assay (Qiagen); BCA Protein Assay Reagent Kit (Pierce); Bio-Rad Protein Assay (Bio-Rad Laboratories GmbH); NucleoSpin Extract II (MachereyNagel); NucleoBond PC 500 (MachereyNagel); Dual-Luciferase® Reporter Assay (Promega); Restriction endonucleases (NewEngland BioLabs, Fermentas); M-MuLV RT (Fermentas); Polyplus jetPEI transfection reagent (Biomol); FuGene6 transfection reagent (Roche Diagnostics); Lipofectamine 2000 transfection reagent (Invitrogen); Wizard® Genomic DNA Purification Kit (Promega); RNase-Free DNase Set (Qiagen)

1.4 Plasmids

Plasmids	Description	Supplier
pCMVmyc	1. *E. coli* origin of replication for plasmid propagation in *E. coli* 2. ampicillin resistance marker for selection of *E. coli* transformants 3. mammalian expression vector (CMV promoter) 4. allows to express a protein of interest fused to the c-Myc tag 5. multiple cloning site (MCS)	Clontech
pCMVmycL-GFPT1wt	pCMVmyc vector containing a *EcoRI*/*NotI* digested L-GFPT1 wt fragment	this study
pCMVmycT15A	pCMVmyc vector containing a *EcoRI*/*NotI* digested L-GFPT1 T15A fragment	this study
pCMVmycD348Y	pCMVmyc vector containing a *EcoRI*/*NotI* digested L-GFPT1 D348Y fragment	this study
pCMVmycR434H	pCMVmyc vector containing a *EcoRI*/*NotI* digested L-GFPT1 R434H fragment	this study
pCMVmycD43V	pCMVmyc vector containing a *EcoRI*/*NotI* digested L-GFPT1 D43V fragment	this study
pCMVmycM492T	pCMVmyc vector containing a *EcoRI*/*NotI* digested L-GFPT1 M492T fragment	this study
pCMVmycI121T	pCMVmyc vector containing a *EcoRI*/*NotI* digested L-GFPT1 I121T fragment	this study
pCMVmycR385H	pCMVmyc vector containing a *EcoRI*/*NotI* digested L-GFPT1 R385H fragment	this study
pCMVmycR111C	pCMVmyc vector containing a *EcoRI*/*NotI* digested L-GFPT1 R111C fragment	this study
pEGFP-N1	1. *E. coli* origin of replication for plasmid propagation in *E. coli* 2. kanamycin resistance marker for selection of *E. coli* transformants 3. mammalian expression vector (CMV promoter) 4. allows to express a protein of interest fused to EGFP 5. multiple cloning site (MCS)	Clontech
pCMVL-GFPT1wt	pEGFP-N1 vector with removed EGFP open reading frame and containing a *KpnI*/*NotI* digested L-GFPT1 wt fragment	this study
pCMVT15A	pEGFP-N1 vector with removed EGFP open reading frame and containing a *KpnI*/*NotI* digested L-GFPT1 T15A fragment	this study
pCMVD348Y	pEGFP-N1 vector with removed EGFP open reading frame and containing a *KpnI*/*NotI* digested L-GFPT1 D348Y fragment	this study
pCMVR434H	pEGFP-N1 vector with removed EGFP open reading frame and containing a *KpnI*/*NotI* digested L-GFPT1 R434H fragment	this study
pCMVD43V	pEGFP-N1 vector with removed EGFP open reading frame and containing a *KpnI*/*NotI* digested L-GFPT1 D43V fragment	this study
pCMVM492T	pEGFP-N1 vector with removed EGFP open reading frame and containing a *KpnI*/*NotI* digested L-GFPT1 M492T fragment	this study

pCMVI121T	pEGFP-N1 vector with removed EGFP open reading frame and containing a *Kpn*I/*Not*I digested L-GFPT1 I121T fragment	this study
pCMVR385H	pEGFP-N1 vector with removed EGFP open reading frame and containing a *Kpn*I/*Not*I digested L-GFPT1 R385Hfragment	this study
pCMVR111C	pEGFP-N1 vector with removed EGFP open reading frame and containing a *Kpn*I/*Not*I digested L-GFPT1 R111C fragment	this study
pCMVL-GFPT13'UTRwt	pEGFP-N1 vector with removed EGFP open reading frame and containing a *Kpn*I/*Not*I digested L-GFPT1 100bp 3'UTR wt fragment	this study
pCMVL-c*22C>A	pEGFP-N1 vector with removed EGFP open reading frame and containing a *Kpn*I/*Not*I digested L-GFPT1 100bp 3'UTR c*22C>A fragment	this study
pCMVGFPT13'UTRwt	pEGFP-N1 vector with removed EGFP open reading frame and containing a *Kpn*I/*Not*I digested GFPT1 100bp 3'UTR wt fragment	this study
pCMVc*22C>A	pEGFP-N1 vector with removed EGFP open reading frame and containing a *Kpn*I/*Not*I digested GFPT1 100bp 3'UTR c*22C>A fragment	this study
pRLTK	1. *E. coli* origin of replication for plasmid propagation in *E. coli* 2. ampicillin resistance marker for selection of *E. coli* transformants 3. mammalian expression vector (HSV-TK promoter) 4. encodes the *Renilla* luciferase enzyme	Promega
pRL-1xG wt	pRLTK vector containing a *Xba*I digested 1xG wt fragment in the 3'UTR region of the *Renilla* luciferase enzyme	this study
pRL-1xA mut	pRLTK vector containing a *Xba*I digested 1xA mut fragment in the 3'UTR region of the *Renilla* luciferase enzyme	this study
pRL-4xG wt	pRLTK vector containing a *Xba*I digested 4xG wt fragment in the 3'UTR region of the *Renilla* luciferase enzyme	this study
pRL-4xA mut	pRLTK vector containing a *Xba*I digested 4xA mut fragment in the 3'UTR region of the *Renilla* luciferase enzyme	this study
pGL4.26	1. *E. coli* origin of replication for plasmid propagation in *E. coli* 2. ampicillin resistance marker for selection of *E. coli* transformants 3. mammalian expression vector (minP promoter) 4. encodes the Firefly luciferase enzyme	Promega
pENTR-EF1-mir155	1. E. coli origin of replication for plasmid propagation in E. coli 2. kanamycin resistance marker for selection of E. coli transformants 3. mammalian expression vector 4. the pre-miRNA cloning site is flanked on either side with sequences from murine miR-155 to allow proper processing of the engineered pre-miRNA sequence	Sirion
pEF1-miR-600	pENTR-EF1-mir155 vector containing ds miR-600 oligo wihtin the *AaR*I site	this study

Table 2: Overview of plasmids

1.5 Antibodies

1.5.1 Primary antibodies

Primary antibody	Supplier	Host	Dilution
anti-RL2 O-linked N-Acetylglucosamine IgM	Abcam	mouse	WB: 1:1000
anti-GFPT1 IgG	ProteinTech Group, Inc	rabbit	WB: 1:1000
anti-GFP IgG	Abcam	rabbit	WB: 1:10000
anti-alpha-tubulin IgG	Cell Signaling	rabbit	WB: 1:1000
anti-beta-actin IgG	Santa Cruz	goat	WB: 1:200
anti-c-Myc IgM	Clontech	mouse	WB: 1:100 IF: 1:100
anti-GAPDH IgM	Millipore	mouse	WB: 1:5000

Table 3: Overview of primary antibodies

1.5.2 Secondary antibodies

Secondary antibody	Conjugate	Supplier	Host	Dilution
anti-rabbit	HRP	Jackson ImmunoResearch	goat	1:10000
anti-goat	HRP	Sigma	rabbit	1:10000
anti-mouse	HRP	DAKO	rabbit	1:10000
anti-mouse IgG	Alexa Fluor 488	Invitrogen	goat	1:500

Table 4: Overview of secondary antibodies

1.6 *E.coli* strains

Strain	Genotype	Supplier
TOP10	F- mcrA Δ(mrr-hsdRMS-mcrBC) φ80lacZΔM15 ΔlacX74 recA1 araD139 Δ(ara-leu) 7697 galU galK rpsL (StrR) endA1 nupG λ-	Invitrogen
DH5α	F– Φ80*lac*ZΔM15 Δ(*lac*ZYA-*arg*F) U169 *rec*A1 *end*A1 *hsd*R17 (rK–, mK+) *pho*A *sup*E44 λ– *thi*-1 *gyr*A96 *rel*A1	Invitrogen

Table 5: Overview of strains

1.7 Nucleic acids

1.7.1 Solution

Real-time PCR reaction mix:
QuantiTect SYBR Green PCR Master Mix (Qiagen, Hilden, Germany)
SYBR Green PCR Master Mix (Applied Biosystems, Carlsbad, USA)

1.7.2 Size standards

1 kb ladder: GeneRuler™ 1 kb DNA ladder (Fermentas)
100 bp ladder: GeneRuler™ 100 bp DNA ladder (Fermentas)

1.7.3 Oligonucleotides for molecular genetic analysis of putative *GFPT1* patients

Oligonucleotide primer	Sequence
GFAT1s	5'-GAGGGAGTCGTGTCGGC-3'
GFAT1as	5'-CATCACCCAGACTTCGCAC-3'
GFAT2s	5'-TGAAATGTTTGAAAGACAGAATCTAAC-3'
GFAT2as	5'-GCAATACTCCACATAAATGGTAACAC-3'
GFAT3s	5'-TATCCTGGTTCTTGACACACAATAG-3'
GFAT3as	5'-TTTCTTTCCTCCCTTCAATGTTAC-3'
GFAT4s	5'-GTATATTCCAAGAGAGCAGCATTG-3'
GFAT4as	5'-TGCTCTCTACTACTTCTGAATGTTTG-3'
GFAT5s	5'-ACTGTTTGCTTCAGCTATGCCAC-3'
GFAT5as	5'-TATGGTGTTTGTTGCACATCCC-3'
GFAT6s	5'-TTTGAATAATGGGATATGGTGTTC-3'
GFAT6as	5'-CTAATCCTCCATCGTGTGTACTGTG-3'
GFAT7s	5'-AAGCCAGTATGTTCTAGGCATTTC-3'
GFAT7as	5'-TAAATGGAAGAGTGGTAAGCAACAG-3'
GFAT8s	5'-TCTTATATCTGAAGTTGAGCTTGGG-3'
GFAT8as	5'-ATCTGACCAAAGAGCCATCTATTC-3'
GFAT9s	5'-CATGGAAATAAGGTGATCTACTTGG-3'
GFAT9as	5'-AGACTGATACACAATGACTTCTTGG-3'
GFAT10s	5'-TCTGAGATACTGCAGAGTGATAGAG-3'
GFAT10as	5'-CTAGCGTTGTCCCTTCACTAATC-3'
GFAT11s	5'-TTTAGGCAGTCATGTCTATTGC-3'

GFAT11as	5'-AGTTGTTCTACAAGGCTATTAAGGG-3'
GFAT12s	5'-ATTGCCTAGTTCACATGGTTCTTTG-3'
GFAT12as	5'-CCATGGATAAATAATTCCAAGCAG-3'
GFAT13s	5'-AAGTCCGATGAAAGAGTATTTGAAG-3'
GFAT13as	5'-AATCTGTATTCGTCAAGTCATCTGC-3'
GFAT14s	5'-AGGAAGAGAGATCCTGACAAGCC-3'
GFAT14as	5'-TTAAACTCTATCAGGAAGAGGGAG-3'
GFAT15s	5'-ACAGGGTCTCACTCTGTCCCAG-3'
GFAT15as	5'-CTAAATAGCTACAAGCCACAGCTTC-3'
GFAT16s	5'-ACCCATACTGATTGATAGCACAGAG-3'
GFAT16as	5'-CAATGCATAAATACAGAAGCACTTTC-3'
GFAT17s	5'-TTTGGATAGATAGACAGTGGCTTG-3'
GFAT17as	5'-ATGTAAACCTCAAAGGCTGTATTCC-3'
GFAT18s	5'-CCTGGTATTTCTTAGTTGCATGAG-3'
GFAT18as	5'-GTGATGTAACCTACAAATTGGGC-3'
GFAT19s	5'-CTCTTTCTGTGTGAACTGGCAC-3'
GFAT19as	5'-TAGATTCCATTATTCAAAGTCCTCC-3'
GFAT8Amss	5'-GGAATAGATGGCTCTTTGGTCAG-3'
GFAT8Amsas	5'-GCACATTCATTCACTCCAAGAAC-3'

Table 6: Overview of *GFPT1* exon oligonucleotides

1.7.4 Oligonucleotides for cDNA amplification

Oligonucleotide primer	Sequence
KpnIGFPT1_for	5'-TATTAGGTACCCGCCACCATGTGTGGTATATTTGCTTACTTAAAC-3'
EcoRIGFPT1_for	5'-GCGAATTCTGATGTGTGGTATATTTGCTTACTTAAAC-3'
NotIGFPT1_rev	5'-GCGGCCGCTCACTCTACAGTCACAGATTTGG-3'
NotIGFPT13UTR_rev	5'-TTGATGCGGCCGCGTCCTCCACAAATTACTGGGAAAATG-3'

Table 7: Overview of cDNA amplification oligonucleotides

1.7.5 Oligonucleotides for site-directed mutagenesis PCR

Oligonucleotide primer	Sequence
GFAT1_R111C sense	5'-GTCAATAGCCACCCCCAG**T**GCTCTGATAAAAATAATGA-3'
GFAT1_R111C antisense	5'-TCATTATTTTTATCAGAGC**A**CTGGGGGTGGCTATTGAC-3'
GFAT1_T15A sense	5'-AACTACCATGTTCCTCGA**G**CGAGACGAGAAATCCT-3'
GFAT1_T15A antisense	5'-AGGATTTCTCGTCTCG**C**TCGAGGAACATGGTAGTT-3'
GFAT1_D43V sense	5'-TCTGCTGGTGTGGGATTTG**T**TGGAGGCAATGATAA-3'
GFAT1_D43V antisense	5'-TTATCATTGCCTCCA**A**CAAATCCCACACCAGCAGA-3'
GFAT1_I121T sense	5'-AGCGCTCTGATAAAAATAATGAATTTATCGTTA**C**TCACAATGGAATCATCA-3'
GFAT1_I121T antisense	5'-TGATGATTCCATTGTGA**G**TAACGATAAATTCATTATTTTTATCAGAGCGCT-3'
GFAT1_ D348Y sense	5'-ATGAGAGGAAGAGTCAACTTTGAT**T**ACTATACTGTGAATTTGGG-3'
GFAT1_ D348Y antisense	5'-CCCAAATTCACAGTATAGT**A**ATCAAAGTTGACTCTTCCTCTCAT-3'
GFAT1_ R434H sense	5'-GATACTTTGATGGGTCTTC**A**TTACTGTAAGGAGAGAGGA-3'
GFAT1_ R434H antisense	5'-TCCTCTCTCCTTACAGTAA**T**GAAGACCCATCAAAGTATC-3'
GFAT1_ M492T sense	5'-TGATGTTTGCCCTTATGA**C**GTGTGATGATCGGATCTC-3'
GFAT1_M492T antisense	5'-GAGATCCGATCATCACACG**T**CATAAGGGCAAACATCA-3'
GFAT1_R385H sense	5'-ATCATGAAGGGCAACTTCAGTTCATTTATA**C**AGAAGGAAATATTTG-3'
GFAT1_ R385H antisense	5'-CAAATATTTCCTTCTG**T**ATAAATGAACTGAAGTTGCCCTTCATGAT-3'
GFAT1_c.*22 sense	5'-GTGAGGAATATCTATACAAAATGTA**A**GAAACTGTATGATTAAGCAACACAA-3'
GFAT1_c.*22 antisense	5'-TTGTGTTGCTTAATCATACAGTTTC**T**TACATTTTGTATAGATATTCCTCAC-3'

Table 8: Overview of mutagenesis oligonucleotides

1.7.6 Oligonucleotides for plasmid sequencing

Oligonucleotide primer	Sequence
pCMVs	5'-ACTTTCCAAAATGTCGTAACAACTC-3'
pCMVas	5'-ACCACAACTAGAATGCAGTGAAAA-3'
GFAT1_600bp_for	5'-ATTGGTGTACGGAGTGAACATAAAC-3'
pCMVmyc_for	5'-GATCCGGTACTAGAGGAACTGAAAAAC-3'
pCMVmyc_rev	5'-ATAGCATCACAAATTTCACAAATAAAG-3'
pENTRs	5'-CCTACGTCGAGCAGCACGAGATG-3'
pRLTKs	5'-GGTCTTCATTTTTCGCAAGAAG-3'

Table 9: Overview of plasmid sequencing oligonucleotides

1.7.7 Oligonucleotides for cloning of the miR-600 expression plasmid

miR single strand nucleotides	sequence
miR-600_top	5'-TGCTGACTTACAGACAAGAGCCTTGCTCGTTTTGGCCACTGACTGA CTAGGAAGGCTCTTGTCTGTCAGG-3'
miR-600_bottom	5'-CCTGCCTGACAGACAAGAGCCTTCCTAGTCAGTCAGTGGCCAAAAC GAGCAAGGCTCTTGTCTGTAAGTC-3'

Table 10: Overview of miR-600 oligonucleotides

1.7.8 Oligonucleotides for qRT-PCR

Oligonucleotide primer	Sequence
GFPT1 for	5'-AACACAGTTGGCAGTTCCAT-3'
GFPT1 rev	5'-GCATGATCTCTTTGCGTCTT-3'
hH4 for	5'-GGTGACTTACACGGAGCAC-3'
hH4 rev	5'-ACCGCCGAAACCATAAAG-3'

Table 11: Overview of qRT-PCR oligonucleotides

All primers were designed with Primer3 program, synthesized and ordered at Metabion (Martinsried, Germany). The miScript Primer Assays for real-time PCR in order to detect the mature miRNAs hsa-miR-600 and oan-miR-206* were ordered at Qiagen (Hilden, Germany).

1.7.9 Mature siRNAs/miRNAs/inhibitors and control miRNA

Oligonucleotide		Supplier
hsa-miR-600-MSY0003268	5`-ACUUACAGACAAGAGCCUUGCUC-3`	Qiagen
anti-hsa-miR-600-MIN0003268		Qiagen
oan-miR-206*-MSY0006994	5`-ACAUGCUUCUUUAUAUCCCCA-3`	Qiagen
siRNA *Gfpt1*-MSS204659	5`-UAUCCAAGAAGUCACUGGCAAGCUC-3`	Invitrogen
miRNA control-1027280		Qiagen

Table 12: Overview of miRNAs, inhibitors, controls and siRNAs

As hsa-miR-206* was not annotated, assays were performed using oan-miR-206* after checking sequence homology using http://www.mirbase.org/.

1.8 Patients

1.8.1 Collection of genomic DNA samples

Venous blood samples were obtained from the patients as well as from their unaffected relatives, if available. All studies were carried out with informed consent of the patients or their parents. All samples that were collected were assigned an identification number.

2 Methods

2.1 Patient selection

The patients were selected for the molecular genetic analysis of *GFPT1* according their clinical picture and – for linkage studies – according to the pedigree structure. This subgroup of CMS patients is characterized by proximal muscle weakness and fatigue. The majority showed tubular aggregates in muscle biopsies but additional CMS patients without tubular aggregates, and patients with non-fatigable weakness but with tubular aggregates were included as well. A common feature was a beneficial response to acetylcholinesterase inhibitor treatment, while the patients showed only minimal ocular and facial involvement [65, 66]. Most of the patients had been tested negative for *DOK7* mutations.

2.2 Microbiology methods

2.2.1 Preparation of competent cells

E. coli bacteria from glycerol stocks were streaked out on LB plates and incubated o.n. at 37°C. One single colony was used to grow a 5 ml LB preculture o.n. at 37°C. About 16 h later, 2 ml of the preculture was transferred into 1 l LB medium and grown to an OD_{600} of 0.5 (about 2-3 h). The culture was cooled on ice for 10 min and centrifuged (10 min, 4000 rpm, 4°C). After centrifugation, the supernatant was discarded and the cell pellet was resuspended in 300 ml ice cold TFBI. Cells were incubated on ice for 30 min and centrifuged at 4000 rpm for 5 min (4°C).

The pelleted cells were gently resuspended in 40 ml ice cold TFBII. Aliquots of 200 µl were stored at -80°C.

Luria-Bertani (LB) medium

1.0 % bacto-tryptone
1.0 % NaCl
0.5 % bacto-yeast extract
pH 7.0 with 10 M NaOH

The medium was autoclaved and after cooling down to 60°C the appropriate antibiotics were added. For preparing plates the LB medium was mixed with 1.5 % agar.

TFBI

30 mM KAcetate
100 mM KCl
50 mM $MnCl_2$
15 % glycerol
pH 5.8
filter 0.2 µm, keep at 4°C

TFBII

10 mM MOPS/NaOH pH 7
75 mM $CaCl_2$
10 mM KCl
15 % glycerol
filter 0.2 µm, keep at 4°C

2.2.2 Plasmid transformation

Chemically competent cells were thawed on ice and plasmid DNA or ligation product was added. The cell suspension was incubated on ice for 30 min, heat-shocked for 30 sec at 42°C and immediately chilled on ice for 2 min. 250 µl of SOB medium was added and the cells were incubated for 1 h at 37°C. The transformed cells were plated on LB agar plates supplemented with the appropriate antibiotic and incubated for 12 to 16 h at 37°C.

Super Optimal Broth (SOB) medium

2 % bacto-tryptone

0.5 % bacto-yeast extract

8.56 mM NaCl

2.5 mM KCl

0.01 mM $MgCl_2$

pH 7.0 with 10 M NaOH

The medium was sterilized in an autoclave.

2.2.3 Culturing of *E. coli*

E. coli cells were grown in LB medium, supplemented with appropriate antibiotic if indicated, at 37°C with constant shaking at 200 rpm. In order to isolate single colonies, cells were plated onto LB agar plates containing appropriate antibiotic if indicated.

2.2.4 Isolation of plasmid DNA from *E. coli*

2.2.4.1 Miniprep

LB medium (5 ml) supplemented with the appropriate antibiotic was inoculated with a single colony picked from an agar plate of transformed bacteria. The cultures were grown at 37°C and shaking at 200 rpm o.n. 4 ml of each o.n. culture were transferred into a tube and centrifuged (5 min, 14000 rpm). The pelleted bacteria were resuspended in 250 µl P1 to destabilize the bacterial membrane. The bacterial suspension is lysed by adding 250 µl P2. To mix the components, the tubes were immediately inverted several times and incubated at rt for 3 min. The lysis was stopped by adding 350 µl P3 immediately followed by inverting the tube again several times and incubating on ice for at least 10 min. Chromosomal DNA and precipitated proteins were sedimented by centrifugation (10 min, 14000 rpm). The supernatant was transferred in a 1.5 ml tube. Isopropanol (600 µl) was added and the sample was centrifuged 30 min at 14000 rpm (4°C). The pelleted plasmid DNA was washed twice with 70 % ethanol and centrifuged (5 min, 13000 rpm, 4°C). The supernatant was discarded and the pellet air dried. The dried DNA was rehydrated in an appropriate volume of TE buffer.

P1

50 mM Tris pH 8.0

10 mM EDTA

100 µg/ml RNase A

P2

200 mM NaOH

1 % SDS

P3

3 M KAcetate pH 5

TE buffer

10 mM Tris-HCl

1 mM EDTA

pH 8.0

2.2.4.2 Maxiprep

In order to obtain larger amounts of plasmid DNA, 250 ml of LB medium including the appropriate antibiotic were inoculated with 150 µl of a single colony preculture. The culture was incubated at 37°C at 200 rpm in a shaker (o.n.). The bacterial suspension was transferred into a corning tube and the bacteria were pelleted by centrifugation (15 min, 3500 rpm, 4°C). The further isolation of the plasmid DNA was done with the NucleoBond PC 500 kit according to the manufacturer`s instructions.

2.3 Nucleic acid methods

2.3.1 Genomic DNA isolation from whole blood samples

Total genomic DNA was isolated from leukocytes of whole blood samples by means of a salting-out method using a blood and tissue culture DNA extraction kit (Wizard Genomic DNA Purification Kit, Promega) according to the manufacturer's recommendations.

2.3.2 Agarose gel electrophoresis

For qualitative as well as quantitative analysis, the DNA was separated by size on an agarose gel containing ethidium bromide. The percentage of agarose solution ranged from 1 to 4 % in 1x TAE buffer. For high percentage gels (4 %) 10 % ethanol (80 %) was added to the 1x TAE buffer. The agarose solutions were boiled and allowed to cool down to approximately 50°C. Afterwards ethidium bromide was added to a final concentration of 0.1 µg/ml.
Before loading the samples onto the gel they were mixed with 6x loading dye. Gel electorphoresis was performed with 10 V/cm gel length. 1 kb or 100 bp ladder were used as a size standard. The DNA was visualized by UV light. Gels were documented with the help of a gel documentation system.

1x TAE
0.049 M Tris
2 mM EDTA
Acetic acid glacial pH 8.5

6x loading dye
10 mM Tris-HCl pH 7.6
0.03 % Bromphenol blue
60 % Glycerol
60 mM EDTA

2.3.3 Gel purification

For DNA gel purification, the NucleoSpin Extract II Kit was used. In brief, the desired DNA band was excised from the gel and the gel slice was dissolved in appropriate buffer at 50°C. The DNA was supplied onto the column, provided with the kit. After a washing step, the DNA was eluted in an appropriate volume of TE buffer and stored at -20°C.

2.3.4 Quantification and purity analysis of DNA

The concentration and the purity of solutions of plasmid DNA, PCR products after purification via agarose gels or isolated DNA from blood samples were determined with a NanoDrop ND-1000 spectrophotometer by measuring the absorption at 260 nm.

2.3.5 Cloning of the miRNA expression plasmid

The pENTR-EF1-mir155 (SIRION BIOTECH, Martinsried, Germany) vector was used to create the pEF1-miR-600 expression plasmid. The pre-miRNA cloning site is flanked on either side with sequences from murine miR-155 to allow proper processing of the engineered pre-miRNA sequence. Two complementary single-stranded DNA oligonucleotides encoding the hsa-miR-600 were designed containing a 5' overhang (TGCT or CAGG) (Table 10) complementary to the vector and required for directional cloning. The synthetic oligonucleotides were synthesized and purchased at Metabion (Martinsried, Germany). After annealing, the double-stranded (ds) oligos were directly cloned into the *Aar*I site of the pENTR-EF1-mir155 vector. Orientation of the insert was verified by sequencing.

2.3.6 Polymerase Chain Reaction (PCR)

2.3.6.1 Exon-specific PCR

After isolation of total DNA from blood of putative CMS patients, PCR was used to amplify known coding exons, the adjacent intronic regions as well as the promoter region of CMS genes.

Standard reaction:

Component	Amount per reaction
ddH_2O	ad 50 µl
10xThermoPol buffer	5 µl
dNTPs	0.25 mM each
Forward primer	50 pmol
Reverse primer	50 pmol
gDNA template	100-500 ng
Taq	2.5 U
Total reaction volume	50 µl

Temperature	Time	Cycles
95°C	2 min	
95°C	15 sec	
59°C	1 min	40x
72°C	2 min	
72°C	7 min	

The calculation of the melting temperature (T_m) according to the nearest neighbor method was done as described by [106] but using the values published by [107]. For this purpose the Oligonucleotide Properties Calculator OligoCalc by [108] available at http://www.basic.northwestern.edu/biotools/oligocalc.html was used.
The PCR products were analysed on an agarose gel in order to control the amplification of the DNA fragments by agarose gel electrophoresis. The required band was excised from the gel, purified and sequenced.

2.3.6.2 cDNA amplification PCR

Human *GFPT1* cDNA was amplified from human skeletal muscle cDNA and inserted into the *EcoR*I and *Not*I sites of the pCMV-Myc vector allowing expression of human GFPT1 with an N-terminal Myc-tag. For enzyme activity assays, the *GFPT1* constructs were cloned into the pEGFP-N1 plasmid. Simultaneously the EGFP open reading frame was removed to obtain untagged GFPT1. For expression studies, the human *GFPT1* coding region and additional 100 bp of the 3' – UTR was amplified from human skeletal muscle cDNA and inserted into the *Kpn*I and *Not*I sites of the pEGFP-N1 plasmid (Clonetech, Mountain View, CA). The EGFP open reading frame was removed to obtain untagged GFPT1.

Standard reaction:

Component	**Amount per reaction**
ddH_2O	Ad 50 µl
10xPfuUltra HF reaction buffer	5 µl
dNTPs	0.25 mM each
Forward primer	50 pmol
Reverse primer	50 pmol
DNA template (500ng/µl)	1 µl
PfuUltra HF DNA Polymerase	1 µl
Total reaction volume	50 µl

Temperature	Time	Cycles
95°C	2 min	
95°C	30 sec	
49°C	30 sec	5x
72°C	1-3 min	
95°C	30 sec	
53°C	30 sec	20x
72°C	1-3 min	
72°C	7 min	

All PCR samples were analysed on an agarose gel. The required band was excised from the gel, purified, digested and ligated in the appropriate digested vector. Ligated plasmid DNA was directly transformed into *Escherichia coli* cells. Correct orientation of the inserts and absence of PCR-induced mutations were verified by sequencing.

2.3.6.3 Site-directed mutagenesis PCR

The *GFPT1* mutants T15A, D348Y, R434H, D43V, M492T, I121T, R385H, R111C and *22C>A were generated by site directed mutagenesis [109] with mismatch primers (Table 8). In brief, two mutant fragments were amplified and purified. In the following steps the fragments were annealed and extended. After purification of the extended mutant fragment it was digested and ligated into the appropriate digested vector. Ligated plasmid DNA was directly transformed into *Escherichia coli* cells. Correct orientation of the inserts and absence of PCR-induced mutations were verified by sequencing.

2.3.6.4 Colony PCR

Colony PCR was used to screen single bacterial colonies by PCR in order to determine if they have inserted the transformed plasmid DNA.

Standard reaction:

Component	Amount per reaction
ddH_2O	ad 50 µl
10xThermoPol buffer	5 µl
dNTPs	0.25 mM each
Forward primer	50 pmol
Reverse primer	50 pmol
Bacterial suspension	2 µl
Taq	2.5 U
Total reaction volume	50 µl

Temperature	Time	Cycles
95°C	6 min	
95°C	30 sec	
55°C	30 sec	40x
72°C	1-3 min	
72°C	7 min	

All PCR samples were analysed on an agarose gel and plasmid DNA from positive colonies was isolated by miniprep. The orientation of the insert and absence of polymerase chain reaction-induced mutations were verified by sequencing.

2.3.6.5 Reverse transcription (RT)-PCR

Total RNA was extracted from cells or human muscle using RNeasy kit according to the manufacturer‘s manual. In case of human muscle, the protocol was adjusted. The tissue (about 30 mg) was pestled under liquid nitrogen at least 15 min prior to the homogenization step in QIAzol. To avoid DNA contamination, on column DNaseI digestion was performed. The cDNA was dissolved in RNase-free water. RNA concentration was quantified using a spectrophotometer.

Standard reaction for total and large RNA:

Component	Amount per reaction
RNase free H_2O	ad 20 µl
RNA	500 ng
5x reaction buffer	4 µl
RiboLock RNase inhibitor	20 U
dNTPs	1 mM
Reverse transcriptase	20 U
Random hexamer primers	1 µl
Total reaction volume	20 µl

Temperature	Time
25°C	10 min
37°C	60 min
70°C	10 min
4°C	hold

The cDNA was used for qRT-PCR, amplification of specific genes (end-point PCR) or stored at -20°C.

In order to extract and separate into small (miRNA) and large RNA (mRNA), the miRNeasy Kit was combined with the RNeasy MinElute Cleanup Kit according to the manufacturer‘s manual. RNA was dissolved in RNase-free water (small RNA in 14 µl; large RNA in 45 µl) and the concentration of the large RNA fraction was quantified using a spectrophotometer.

Standard reaction for small RNA using the miScript PCR Kit:

Component	Amount per reaction
RNase free H_2O	3.5 µl
RNA (MinElut)	3 µl
5x reaction buffer	2 µl
Nucleic mix	1 µl
Reverse transcriptase mix	0.5 µl
Total reaction volume	10 µl

Temperature	Time
37°C	60 min
95°C	5 min
4°C	hold

The cDNA was used for qRT-PCR or stored at -20°C.

2.3.6.6 Quantitative real-time PCR (qRT-PCR)

For mRNA, the desired target cDNA species were amplified using specific primers. The primer pairs for mRNA expression (Table 11) were designed using published sequences (*GFPT1*: NM_002056.3; hH4: NM_175054.2). They were ordered and synthesized at Metabion (Martinsried, Germany). To correct for sample to sample variation, an endogenous control, hH4, was amplified with the target and served as an internal reference to normalize the data. The expression levels of *GFPT1* relative to those of hH4 were calculated using the $2^{-\Delta\Delta C}{}_T$ method [110].

Standard reaction:

Component	Amount per reaction
RNase free H_2O	ad 20 µl
cDNA	12.5 ng
2x SensiFAST SYBR no-ROX Mix	10 µl
Forward primer (10µM)	0.8 µl
Reverse primer (10µM)	0.8 µl
Total reaction volume	20 µl

The reaction plates were centrifuged for 2 min at 3000 rpm to abolish bubbles.

Temperature	Time	Cycles
95°C	2 min	
95°C	5 sec	
60°C	10 sec	40x
72°C	10 sec	
65-95°C		0.5°C steps

For miRNA, the miScript Primer Assay for specific miRNA targets were synthesized and ordered at Qiagen. MicroRNA was quantified by a two-step real-time PCR using the miScript-Reverse

Transcripton kit combined with the miRNA-SYBR Green PCR kit. Cellular miRNA levels were normalized using U6 snRNA (RNU6) as reference RNA. The amount of miR-600, miR-206 and miR-206* relative to RNU6 was calculated using the $2^{-\Delta\Delta C}{}_T$ method [110]. For the qRT-PCR 96-Well Optical Reaction Plates (BioRad) were used.

Standard reaction using the miScript PCR system:

Component	**Amount per reaction**
RNase free H_2O	5 µl
cDNA	16.7 ng
2x QuantiTec SYBR Green	10 µl
10x UP primer	2 µl
10x primer assay primer	2 µl
Total reaction volume	20 µl

The reaction plates were centrifuged for 2 min at 3000 rpm to remove bubbles.

Temperature	**Time**	**Cycles**
95°C	15 min	
94°C	15 sec	
55°C	30 sec	40x
70°C	30 sec	
65-95°C		0.5°C steps

All PCR samples were analysed on a 4 % agarose gel.

2.3.7 Restriction digest

For analytic restriction, about 400 ng of DNA were digested using 5 U of each restriction enzyme in a total volume of 20 µl. Double digests were performed using the appropriate NEB buffer to achieve the highest possible activity for the combination of both enzymes. Bovine serum albumin (BSA) was added if required. Restriction digest was performed for 2 h at 37°C.
For cloning purposes, 2 µg of DNA were digested using 10 U of enzyme for 2 h at 37°C. BSA was added if required. The linearized plasmid was dephosphorylated with 1 U Calf Intestine Alkaline Phosohatase (CIAP) in CIAP buffer for 30 min at 37°C to prevent re-ligation. Afterwards the

phosphatase was inactivated for 10 min at 65°C. The sample was purified via NucleoSpin Extract II Kit according to the manufacturer´s protocol.

2.3.8 Ligation

Ligation of digested plasmids and PCR fragments was performed with T4 DNA ligase. Reaction mixtures contained plasmid and PCR fragment (insert) in a molar ration of 1:3. Usually 100 ng of plasmid were used. The mass of insert to be used was calculated according to the following equation:

$$\text{mass (insert)} = 3 \cdot \text{mass (plasmid)} \cdot \frac{\textbf{number of bp (insert)}}{\textbf{number of bp (plasmid)}}$$

Component	Amount per reaction
ddH_2O	ad 10 µl
Plasmid	100 ng
Insert 3-fold molar amount of plasmid	
T4 DNA ligase	1 µl
T4 DNA reaction buffer (10x)	1 µl
Total reaction volume	10 µl

The reaction mix was pipetted at rt and incubated o.n. in an isolating box in the cold room (4°C).

2.3.9 Sequencing of DNA

The sequencing of purified DNA premixed with primer was performed by Eurofins MWG Operon (Ebersberg, Germany).

2.3.10 Genome-wide linkage analysis

Homozygosity mapping [111] was performed by genome-wide genotyping of SNP for family LGM3 using the Illumina 300 K chip (Illumina, San Diego, CA). Multipoint linkage analysis was performed with MERLIN [112]. DNA samples from families LGM1, LGM2, LGM5, LGM6, LGM7, LGM8, LGM10, LGM11, and LGM12 were analyzed with short tandem repeat (STR) markers.

Twenty-three markers were retrieved from the National Center for Biotechnology Information UniSTS database, and four new polymorphisms were identified by using the Repeat-Masker program. PCR primers for new STRs were designed by the Primer3 program. The sense primers were labeled with FAM fluorophores (MWG Biotech, Ebersberg, Germany) for detection on an ABI 377 DNA sequencer (Applied Biosystems, Foster City, CA). Multipoint LOD scores were calculated with the GeneHunter v2.1r5 program [113] in the EasyLinkage software package [114]. The genomic localization of the markers was derived from the Marshfield map and the University of California Santa Cruz (UCSC) human genome assembly. Linkage analysis was performed in collaboration with Prof. Dr. Jan Senderek (Aachen, Germany) and Dr. Tim-Matthias Strom (Munich, Germany).

2.3.11 Linkage analysis

In some CMS index patients we used a linkage approach with DNA marker sets of the known CMS genes [115] in order to reduce the number of candidate genes prior to subsequent mutation analysis. In order to use the patients for linkage analysis, they have to derive from families with more than one affected patient or several unaffected siblings and possibly parental consanguinity. The microsatellite marker set included the gene loci of the known CMS genes *CHRNA1*, *CHRNB1*, *CHRNE*, *CHRND, CHAT*, *COLQ*, *RAPSN*, *DOK7*, *MUSK*, *SCN4A, AGRN* and *GFPT1.* The linkage analysis was performed in collaboration with Prof. Dr. Angela Hübner (Dresden, Germany).

2.4 Tissue culture methods

Five different adherent cell lines were used in this study: human embryonic kidney 293 cells (HEK293), skeletal mouse myoblasts C2C12, the human adrenal carcinoma cell line SW13, the african green monkey kidney fibroblast cell line COS-7 and human myoblasts. All cell lines were obtained from the American Type Culture Collection (ATCC, Manassas, VA, USA) except for human myoblasts (Muscle Tissue Culture Collection, Friedrich-Baur-Institute, Munich, Germany).

2.4.1 General information

HEK293, C2C12, SW13 and COS-7 cells were cultured in Dulbecco's Modified Eagle's medium (DMEM) supplemented with 10 % fetal calf serum, 2 mM Glutamine and penicillin/ streptomycin

(40 U/mL penicillin and 0.04 mg/mL streptomycin). Primary human myoblasts were isolated as previously described [116]. Myoblasts from patients with *GFPT1* mutations and control myoblasts were obtained from the Medical Research Council (MRC) Centre for Neuromuscular Diseases Biobank, Newcastle, UK, and the Muscle Tissue Culture Collection, Friedrich-Baur-Institut, Munich, Germany. Human myoblasts were grown in skeletal muscle growth medium (SGM PromoCell, Heidelberg, Germany) supplemented with SupplementalMix (Provitro), 10 % FCS, 1.5 % 100 x Glutamax (Gibco) and 50 µg/ml gentamycin. For maturation into multinucleated myotubes, the human myoblasts were grown in SGM on culture dishes coated with laminin (Sigma) to near confluency. They were induced to fuse and differentiate by replacing SGM with DMEM supplemented with 5 % horse serum (fusion medium) for 7 d. All cell lines were kept in a 37°C incubator with a humidified atmosphere of 5 % CO_2.

2.4.2 Passage of cells

The cells were grown in 10 cm or 16 cm tissue culture dishes and washed once with PBS before digestion with 0.05 % trypsin-EDTA for about 5 min at 37°C. The trypsin digest was terminated by adding supplemented DMEM or SGM medium.

2.4.3 Transfection of HEK293, SW13, COS-7 or C2C12 cells

Cells were plated in 10 cm tissue culture dishes, 6-well plates, 24-well plates or on cover slips the day before transfection and grown to 60-90 % confluency. HEK293 cells were transfected with 3–6 mg of wild-type and mutated *GFPT1* plasmid DNA (with and without N-terminal Myc tag) with Polyplus jetPEI transfection reagent (Biomol, Hamburg, Germany) according to the manufacturer's recommendations. Transfection of SW13 cells was carried out with FuGene6 transfection reagent (Roche Diagnostics, Mannheim, Germany). C2C12 cells were transfected with 3 µg of GFPT1-3'-UTR wt or mutant (c.*22C>A) constructs. The cells were co-transfected with 0.3 µg pEGFP-N1 (Clontech, Mountain View, CA) in order to use the expression of the green fluorescent protein (GFP) as a transfection efficiency control. Lipofectamine (Invitrogen, Carlsbad, CA) was used according to manufacturer's instructions. Cells were analyzed 24-48 h after transfection by immunoblot, immunofluorescence staining or GFPT1 activity assay.

2.4.4 siRNA experiments

C2C12 cells were plated in 6-well plates the day before transfection and grown to a confluency of 50 %. The siRNA duplex oligonucleotides (100 pmol) (Table 12) were diluted in Lipofectamine according to manufacturer's instructions. The mixture was added drop by drop to the cells and they were analyzed 24 h after transfection by immunoblot.

2.4.5 Harvesting of cells

Growth medium was removed using a vacuum pump and cells were washed with sterile PBS. The cells were mechanically scraped in ice cold 1xPBS buffer and transferred to a 1.5 ml tube. After centrifugation at 14000 rpm at 4°C (5 min) the supernatant was removed and the cell pellet was used for protein isolation or stored at -80°C.

2.4.6 Storage of cells

Cells were grown to 80-90 % confluency in 10 cm tissue culture dishes and washed once with PBS before digestion with 0.05 % trypsin-EDTA for about 5 min at 37°C. The trypsin digest was terminated by adding supplemented DMEM medium. The cell suspension was transferred to a 50 ml falcon tube and centrifuged for 3 min at 1200 rpm (RT). The cell pellet was resuspended in 2 ml freezing medium, transferred to a 2 ml freezing vials and gently cooled down to -80°C. The frozen cells were stored in liquid nitrogen.
To utilize cells in culture, they were quickly thawed, washed with medium (3 min, 1200 rpm, RT) and seeded in a 10 cm dish for further culturing.

Freezing medium
DMEM medium
10 % DMSO
30 % FCS

2.5 Protein methods

2.5.1 Protein isolation

For Western blot analysis, protein extracts from different cell lines were used. Cells were harvested 24 or 48 h after transfection. The cells were washed once with 1xPBS buffer, mechanically scraped in 1x PBS buffer and transferred to a 1.5 ml tube. After centrifugation at 14,000 rpm at 4°C for 5 min the supernatant was removed and the cell pellet was homogenized in lysis buffer. Homogenized cell samples were then incubated at 95°C for 5min. Debris was removed by 5 min centrifugation at 14,000 rpm and supernatants were used for immunoblot analysis.

Lysis buffer
10 mM Tris-HCl pH 7.4
1 % SDS

2.5.2 Protein quantification

Protein concentrations were determined using the BCA Protein Assay (Pierce) or the BioRad Protein Assay according to the manufacturer`s instruction. BSA (Bovine serum albumin) was used as a protein standard [117].

2.5.3 SDS-Polyacrylamid-Gelelectrophoresis (SDS-PAGE)

Discontinuous electrophoresis was used to separate protein mixtures. The gel consists of an 8 % separating and a 3.3 % stacking gel that were poured sequentially. After complete polymerization of the gel it was placed into a chamber filled with SDS running buffer. The protein samples were mixed with SDS loading dye and denatured for 5 min at 95°C before applying on the gel. Protein markers were used to determine the molecular weight of the samples. Proteins were separated at 120 V.
Afterwards the gel was further processed by Western blotting.

Lower Tris (4x)

36.34 g Tris base

8 ml 10 % SDS

ad 200 ml H_2O

pH 8.8

Upper Tris (4x)

6.06 g Tris base

4 ml 10 % SDS

ad 100 ml H_2O

pH 6.8

Separating gel (8 %)

4.83 ml H_2O

2.67 ml acrylamid mix (30/0.8)

2.5 ml Lower Tris

50 µl 10 % APS

10 µl TEMED

Stacking gel (3.3 %)

3.25 ml H_2O

0.55 ml acrylamid mix (30/0.8)

1.25 ml Upper Tris

20 µl 10 % APS

10 µl TEMED

Running buffer

25 mM Tris

192 mM glycine

0.1 % SDS

SDS loading dye (6x)

20 mM Tris-HCl pH 6.8

6 % SDS

30 % glycerol

0.03 % bromphenol blue

5 % β-Mercaptoethanol

2.5.4 Western blotting

A nitrocellulose membrane (BioTrace™ NT Nitrocellulose Transfer Membrane; 9 cm x 6 cm; 0.20 µm pore size; PALL) as well as two filter papers and two fiber pads were pre-wet in transfer buffer. The gel was removed from the electrophoresis apparatus and the blotting sandwich was assembled in the following order: gel holder cassette (white side; facing the positive electrode), 1 fiber pad, 1 piece of filter paper, membrane, gel, 1 piece of filter paper, 1 fiber pad, gel holder cassette (black side; facing the negative electrode). The assembly was transferred to the blotting apparatus, which was filled with 1 x transfer buffer and an ice block for cooling. The proteins were transferred to the membrane by electrophoresis at 110 V for 2 h at 4°C.

In order to determine the blotting efficiency the membrane was Ponceau S stained after the transfer and washed in 1xTBS-T for 20 min. The membrane was blocked in 5 % milk/BSA in 1x TBS-T for 1 h at rt on a shaker. Subsequently it was incubated with the primary antibody in 5 % milk/BSA in TBS-T o.n. at 4°C on a shaker followed by five washing steps (5 min each) in TBS-T. Afterwards the membrane was incubated with the appropriate HRP conjugated secondary antibody for 1 h at 4°C while shaking. The blot was washed again five times and the immunoreactive bands were visualised with the ECL system (ECL Advance Western Blotting Detection Kit, Amersham) using the ChemoCam Imager of INTAS.

Ponceau S staining solution

0.1 % Ponceau S

5 % acetic acid

1x TBS-T

10 mM Tris-HCl pH 7.4

140 mM NaCl

0.1 % Tween-20

Transfer buffer
25 mM Tris
192 mM glycine
0.02 % SDS
15 % methanol

2.5.5 Immunofluorescence

For immunofluorescence analysis, cells were grown on glass coverslips and transfected as described above. Fortyeight hours after transfection, coverslips were washed in PBS, fixed in 3.7 % formaldehyde (freshly prepared from paraformaldehyde) in 1x CSK buffer for 10 min at room temperature, and permeabilized with 0.1 % Triton X-100 in 1x CSK buffer for 15 min. After three washes in PBS, nonspecific binding sites were blocked with PBS containing 5 % horse serum for 1 h, followed by overnight incubation at 4°C with the appropriate primary antibody in PBS with 5 % horse serum. After three washes in PBS, cells were incubated with the secondary antibody, for 1 h at room temperature. Nuclei were visualized with bisbenzimide H 33258 (40 mg/ml). Digital images were captured with a Zeiss Axiovert 200 M fluorescence microscope and a Zeiss AxioCam HR photo camera.

1x CSK buffer
100 mM NaCl
300 mM sucrose
3 mM $MgCl_2$
1 mM EGTA
10 mM PIPES
pH 6.8

2.5.6 GFPT1 enzyme activity assay

The enzymatic activity of untagged wild-type and mutant GFPT1 was measured with the glutamate dehydrogenase method [118, 119]. HEK293 cells transfected with GFPT1 expression constructs were lysed in GFPT buffer, and 100 ml aliquots of the lysates were mixed with an equal volume of the reaction buffer and incubated at 37°C for 45 min. Glutamate was used as a standard. The change in absorbance was monitored at 370 nm with a Spectra Max 250 microplate reader. The enzymatic activity of each mutant was normalized to GFPT1 expression

levels determined by immunoblot analysis of cell lysates used for enzyme activity measurements. All transfections and measurements were done in triplicates.

GFPT buffer

50 mM KH_2PO_4

10 mM EDTA

5 mM reduced L-glutathione

12 mM D-glucose-6-phosphate Na_2

1 mM PMSF

pH 7.6

freshly prepared

Reaction buffer

100 mM KH_2PO_4

10 mM D-fructose 6-phosphate

6.0 mM L-glutamine

0.3 mM 3-acetylpyridine adenine dinucleotide

50 mM KCl

6 U L-glutamate dehydrogenase from bovine liver

pH 7.6

freshly prepared

2.5.7 Dual Luciferase reporter assay

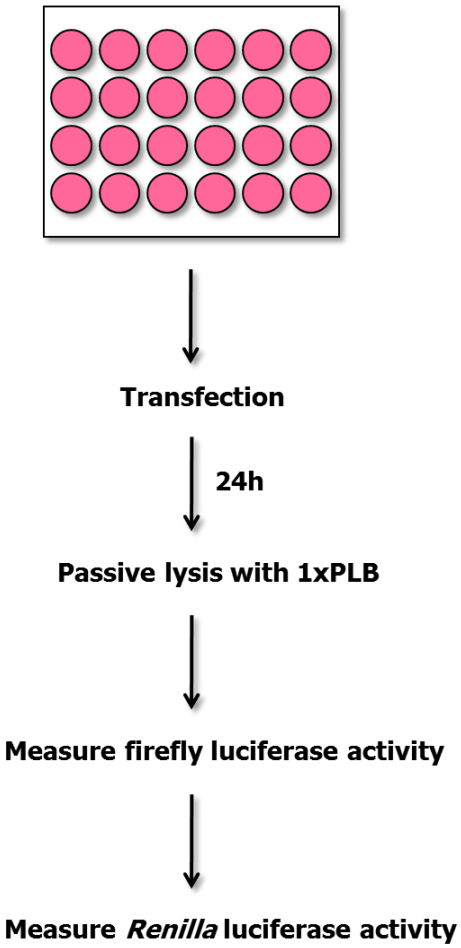

Figure 4: Schematic view of the transfection of COS-7 cells followed by the Dual-Luciferase reporter assay

The pRL-TK (Promega, Madison, WI) reporter vector containing a wt and mutant (c.*22C>A) 80 bp fragment of the *GFPT1* 3'-UTR or multimers of it (Figure 28) was used as reporter assay in COS-7 cells. The four tandem repeats of an 80 bp sequence (GeneArt, Carlsbad, CA) encompassing wt or mutant c.*22C>A predicted miRNA binding site were cloned into the *Xba*I restriction site downstream from the Renilla luciferase (RLuc) gene. An empty Firefly luciferase reporter vector (pGL4, Promega) was used as control. 0.8 x 10^5 cells per well in 24-well plates were transfected using Polyplus jetPEI transfection reagent (Biomol, Hamburg, Germany) following manufacturer's recommendations with a mixture comprising 200 ng of pRL-TK construct, 2 ng of pGL4 control vector and the appropriate mature miRNA mimic (hsa-miR-600, oan-miR-206*; Qiagen, Hilden, Germany) or control miRNA (100 nM; Qiagen, Hilden, Germany). For blocking experiments 300 nM αmiRNA-600 (Qiagen, Hilden, Germany) were included. 24 h after transfection, luciferase expression was analysed using the dual-luciferase reporter assay system (Promega, Madison, WI). In brief, cells were rinsed once with 1xPBS and lysed with 1xPLB. In order to assure complete lysis, cell lysates were incubated on a shaker at 200 rpm for 15 min. The Firefly reporter is measured first by adding Luciferase Assay Reagent II to generate a luminescent signal. After quantifying this luminescence, the reaction is quenched, and the Renilla luciferase reaction is simultaneously initiated by adding Stop & Glo Reagent. In order to correct for vector-dependent unspecific effects and to correct for differences in the transfection efficiency, relative reporter activity was obtained by normalization to Firefly luciferase activity (ratio of Renilla luciferase to Firefly luciferase). Each experimental condition was measured in triplicates and each assay was performed three times. Dual luciferase assay was performed on white 96-well plates using 20 µl lysate and 100 µl of both substrates per well. Luciferase expression was detected on a Berthold Technologies TriStar LB 941 reader. As hsa-

miR-206* was not annotated, assays were performed using oan-miR-206* after checking sequence homology using http://www.mirbase.org/.

2.6 Statistical analysis

The data show the mean ± SD. Statistical significance was determined with two-tailed Student's t-test. Significance was set at $p < 0.05$ (*), $p < 0.01$ (**), or $p < 0.001$ (***).

G Results

1 Identification of *GFPT1* mutations in LG-CMS families

LG-CMS patients, characterized by weakness of limb muscles, sparing of ocular or facial muscles, good treatment response to acetylcholinesterase inhibitors and tubular aggregates (TA) in muscle biopsy samples were analysed by a genome-wide linkage screen in order to identify the molecular defect causing this condition.

1.1 Selection of LG-CMS families for molecular genetic studies

Using direct sequencing or haplotype analysis we had previously excluded all known genes and loci known to be involved in CMS (*CHRNA1*, *CHRNB1*, *CHRND*, *CHRNE*, *CHAT*, *COLQ*, *DOK7*, *RAPSN*, *MUSK*, *SCN4A*, *LAMB2*, *AGRN* as well as two functional candidate genes *CNTN1* and *AChE*) in the 16 LG-CMS families analysed in this study.

1.1.1 Clinical features of LG-CMS families

Sixteen LG-CMS families (comprising 23 patients) of various ethnic origins were selected for molecular genetic studies.

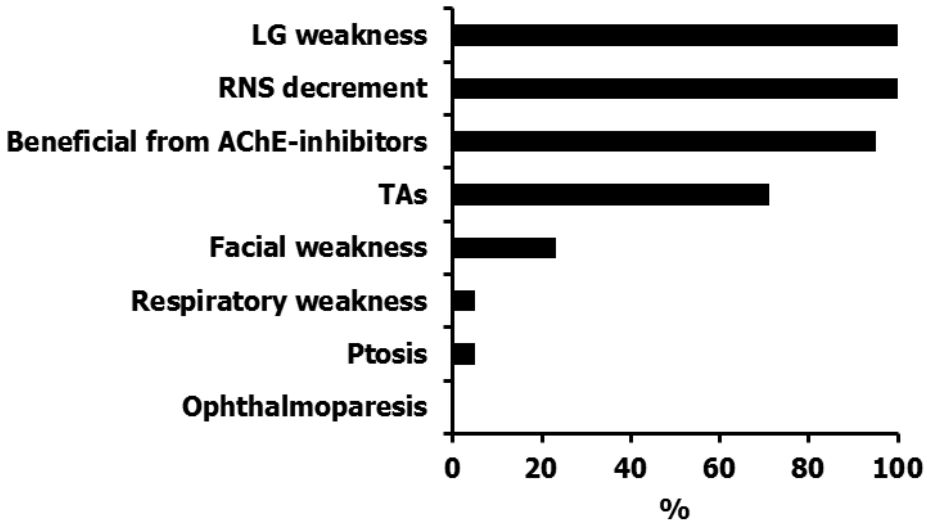

Figure 5: Summary of the clinical features of 23 LG-CMS patients.

LG: limb-girdle; RNS: repetitive nerve stimulation; AChE: acetylcholine esterase; TA: tubular aggregate

All patients presented with limb-girdle weakness and patients who had a neurophysiological examination showed a decremental response in repetitive nerve stimulation (RNS). Almost all patients (95 %) responded well to AChE-inhibitor therapy. Tubular aggregates (TAs) were identified in the muscle biopsies of 75 % of the LG-CMS patients. Only few patients had facial weakness (23 %) and only 5 % of the patients showed respiratory weakness. Ocular muscles were generally spared: None of the patients showed involvement of the external eye muscles (ophthalmoparesis) and only 5 % exhibited ptosis.

1.1.2 Pedigree analysis

Pedigrees of the LG-CMS families included in the study:

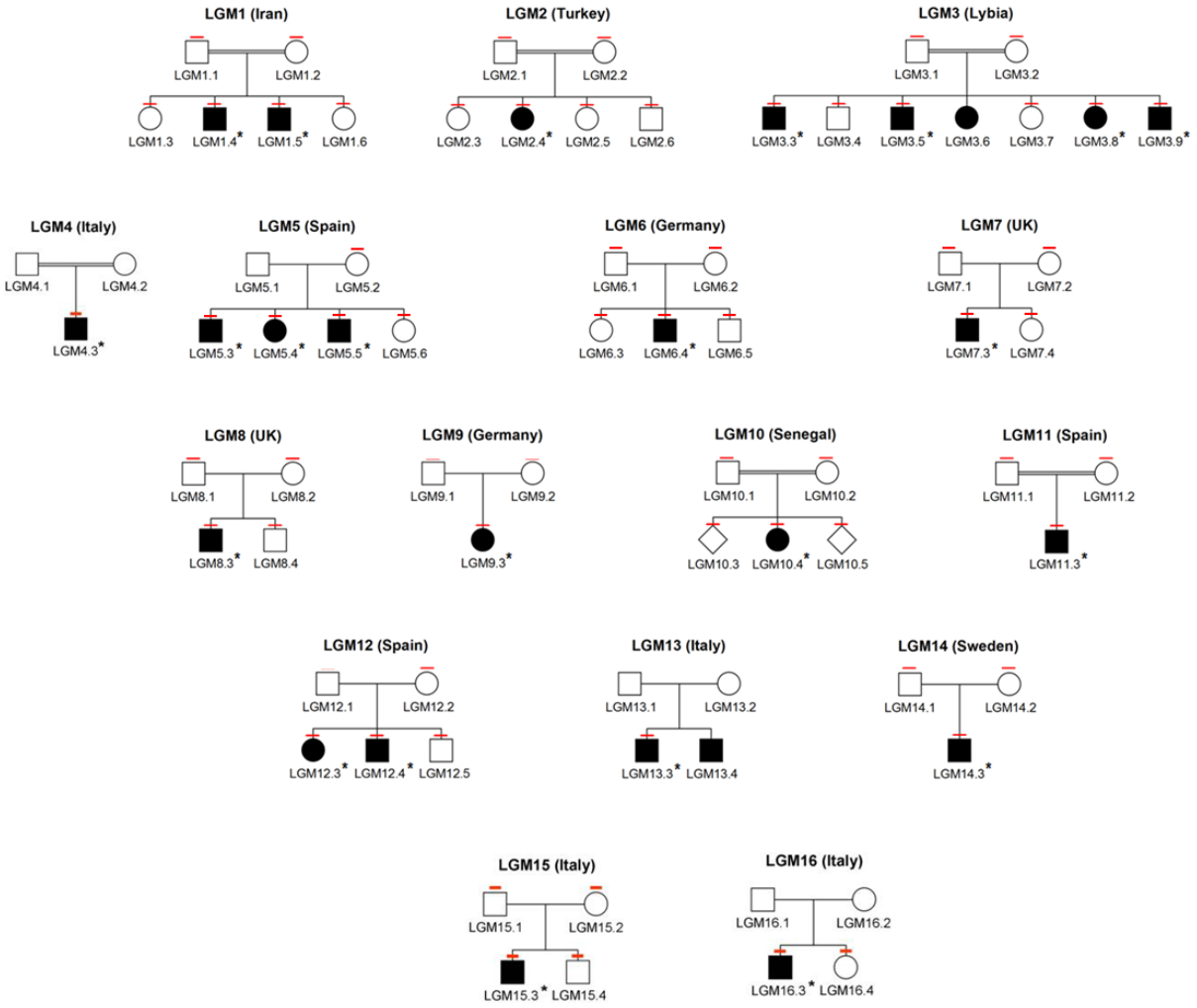

Figure 6: Pedigrees of the limb-girdle myasthenia (LGM) families included in the study.
Circles represent females, squares males and diamonds were used when the information on the gender was unknown. A double line indicates a consanguineous marriage. Filled symbols represent affected family members. Red bars indicate the individuals of whom genomic DNA was obtained and used for genotyping. Asterisks indicate patients whose clinical data were available.

Family	Ethnic origin	Consanguinity
LGM1	Iran	+
LGM2	Turkey	+
LGM3	Libya	+
LGM4, 13, 15, 16	Italy	4: +; 13, 15, 16: -
LGM5	Spain	-
LGM6	Germany	-
LGM7	UK	-
LGM8	UK	-
LGM9	Germany	-
LGM10	Senegal	+
LGM11	Spain	+
LGM12	Spain	-
LGM13	Italy	-
LGM14	Sweden	-
LGM15	Italy	-
LGM16	Italy	-

Table 13: Summary of the ethnic origin and the marriages of the 16 limb-girdle myasthenia (LGM) families. +: yes; -: no

The families are of various ethnic origins from nine different countries (Table 13). There is almost equal frequency of the disease in both sexes (female and male). LGM families LGM1-4, LGM10 and LGM11 are consanguineous (Figure 6 and Table 13). All parents of the patients are healthy. In total, the genomic DNA of 62 individuals was used for genotyping, of whom 23 were affected and clinical data was available (Figure 6).
All in all, the genetic evaluation of the LG-CMS families revealed pedigrees typical of an autosomal recessive trait of the disease (Figure 6).

1.2 Genome-wide homozygosity mapping

Genome-wide homozygosity mapping in an extended pedigree of a consanguineous Libyan family (LGM3, Figure 6) with five affected children allowed to identify the genetic locus for LG-CMS. The homozygosity mapping in this family defined a single candidate region on chromosome 2 (2p12-p15) with a maximum LOD score (logarithm (base 10) of odds) of 3.24. A LOD score >3 is usually considered sufficient for establishing genetic linkage to a chromosomal region. Using

linkage and homozygosity data from additional, smaller pedigrees (LGM1, 2, 5, 6, 7, 8, 10, 11, 12) the critical interval was narrowed down to a region of interest of 5.92 Mb. The genes in this region (46 genes) were prioritized on the basis of expression pattern and function. They were evaluated and ranked with respect to neuromuscular endplate and skeletal muscle biology and disease or role in calcium metabolism (tubular aggregates seen in muscle biopsies of LG-CMS patients might be a consequence of calcium overload) or vesicle transport.

Gene name	GenBank	Mutation analysis
MEIS1	NM_002398	yes
ETAA1	NM_019002	no
C1D	NM_001190265	no
WDR92	NM_138458	yes
PNO1	NM_020143	no
PPP3R1	NM_000945	yes
CNRIP1	NM_001111101	no
PLEK	NM_002664	yes
FBXO48	NM_001024680	no
APLF	NM_173545	no
PROKR1	NM_138964	yes
ARHGAP25	NM_001007231	yes
BMP10	NM_014482	no
GKN2	NM_182536	no
GKN1	NM_019617	no
ANTXR1	NM_032208	no
GFPT1	NM_002056	yes
NFU1	NM_015700	yes
AAK1	NM_014911	yes
ANXA4	NM_001153	yes
GMCL1	NM_178439	no
SNRNP27	NM_006857	no
MXD1	NM_002357	yes
ASPRV1	NM_152792	no
LOC400960	NR_033872	no
PCBP1	NM_006196	no
C2orf42	NM_017880	no
TIA1	NM_022173	no
PCYOX1	NM_016297	no
SNRPG	NM_003096	no
FAM136A	NM_032822	no
TGFA	NM_003236	yes

ADD2	NM_017488	yes
FIGLA	NM_001004311	no
CLEC4F	NM_173535	no
CD207	NM_015717	no
VAX2	NM_012476	no
ATP6V1B1	NM_001692	no
ANKRD53	NM_024933	no
TEX261	NM_144582	no
NAGK	NM_017567	yes
MCEE	NM_032601	no
MPHOSPH10	NM_005791	no
PAIP2B	NM_020459	no
ZNF638	NM_014497	yes
DYSF	NM_001130981	yes

Table 14: Positional candidate genes in the defined LG-CMS candidate region (chromosome 2p12-p15; region of interest of 5.92 Mb)

None of the 46 genes had been previously associated with CMS or is exclusively expressed at the NMJ or in motor neurons or in skeletal muscle. Therefore, the entire coding region and exon-intron boundaries of 16 genes (Table 14; mutation analysis: yes) were sequenced in the index patients of three families (LGM1, 3, 10).

Fifteen genes were sequenced before different homozygous missense mutations were identified in the glutamine—fructose-6-phosphate transaminase 1 (*GFPT1*) gene in all three families. No disease-related sequence changes were identified in any of the other sequenced genes. Further evidence for a causative role of *GFPT1* mutations in LG-CMS where achieved when extending the mutation screening to additional families in our cohort. Mutations were identified in all LG-CMS families except for LGM4, 15 and 16. *GFPT1* mutations had not previously been linked to a human disease.

1.3 *GFPT1* mutation spectrum

GFPT1 is the first and rate-limiting enzyme in the hexosamine biosynthetic pathway (HBP) leading to UDP-GlcNAc production. The *GFPT1* gene is composed of 19 constitutive exons (1-19) and one alternative exon (8A) exclusively incorporated in mRNA encoding the muscle-specific GFPT1-L protein. *GFPT1* has a total length of 62 kb and is located on chromosome 2p13.

Exon	Nucleotide change	Effect on the protein	LG-CMS families with the mutation
2	c.43A>G	p.Thr15Ala	LGM13
2	c.44C>T	p.Thr15Met	LGM8
3	c.128A>T	p.Asp43Val	LGM6
4	c.222_223insA	p.Gln76fs	LGM14
4	c.331C>T	p.Arg111Cys	LGM3, LGM14
5	c.362T>C	p.Ile121Thr	LGM6
7	c.595G>T	p.Val199Phe	LGM9
8	c.621_622 del	p.Leu208fs	LGM13
8A	c.719G>A	p.Trp240X	LGM2
11	c.1042G>T	p.Asp348Tyr	LGM1
13	c.1154G>A	p.Arg385His	LGM7
14	c.1278_1281 dup	p.Asp428fs	LGM12
14	c.1301G>A	p.Asp434His	LGM7
15	c.1472T>C	p.Met491Thr	LGM11
15	c.1475T>C	p.Met492Thr	LGM5
15	c.1486C>T	pArg496Trp	LGM8
15	c.1534C>T	p.Arg512Trp	LGM10
19	c.*22C>A		LGM5, LGM9, LGM12

Table 15: *GFPT1* mutations identified in LG-CMS families.

No *GFPT1* mutations were identified in LGM families LGM4, 15 and 16. The nucleotide and amino acid numbering is according to NM_002056.2 and NP_002047.2 (exception c.719G>A (p.Trp240X): AF334737.1 and AAK15342.1).

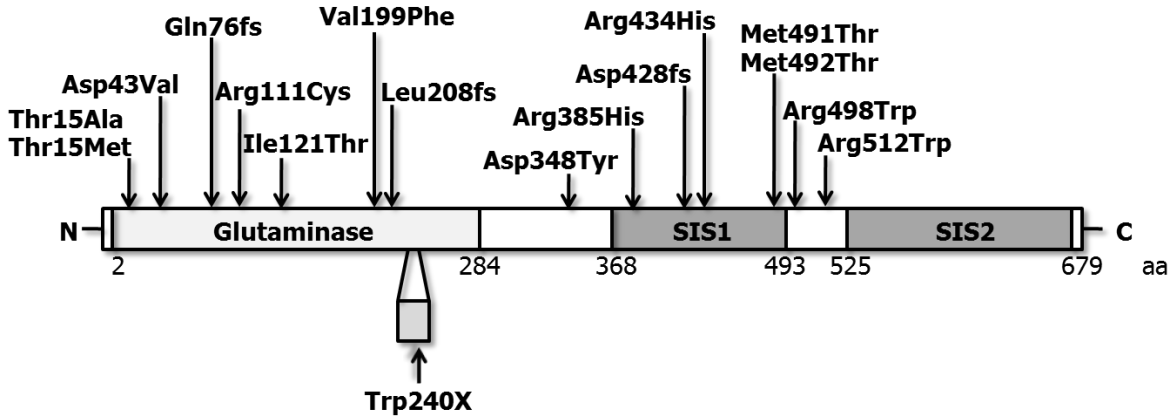

Figure 7: Schematic view of the domain structure of GFPT1 and the positions of the identified mutations in 13 LG-CMS families.

GFPT1 consists of a glutaminase and two sugar isomerase (SIS) domains. The insertion of 18 amino acids (aa) of the muscle-specific exon is indicated. Reference sequence: NM_002056.2

In total, 18 different GFPT1 mutations consisting of 13 missense mutations, three frameshift mutations (p.Gln76fs, p.Leu208fs and Asp428fs), one nonsense mutation (p.Trp204X) and one variant in the 3'-UTR (c.*22C>A) were found in 13 unrelated LG-CMS families (Table 15 and Figure 7). Mutations are distributed throughout the entire gene and affect the glutaminase as well as the sugar isomerase domain (Figure 7). There is only one LG-CMS patient with a homozygous-*GFPT1* null mutation (LGM2). However, the homozygous p.Trp240X mutation is located in the alternative exon, exclusively incorporated in the muscle-specific GFPT1-L protein (Figure 7). None of the GFPT1 patients carried two null mutations in the constitutive exons of the gene. One of the *GFPT1* mutations identified in three independent families from Spain (LGM5 and 12) and Germany (LGM9) was a nucleotide exchange 22 bp downstream of the TGA translation termination codon (c.*22C>A) in the 3'-untranslated region (UTR). In all three families, the mutation was compound heterozygous to missense or protein truncating mutations (Table 15).

2 Molecular genetic analysis of isolated LG-CMS patients

2.1 Clinical features of putative *GFPT1* patients of the Munich CMS patient cohort

Subsequent to the identification of *GFPT1* as novel CMS gene further undiagnosed patients from our cohort of about 900 CMS patients were screened for mutations in the *GFPT1* gene according to their clinical picture and/or haplotype analysis results.

We primarily selected patients with prominent limb-girdle weakness, tubular aggregates in skeletal muscle biopsies and good response to esterase inhibitor therapy.

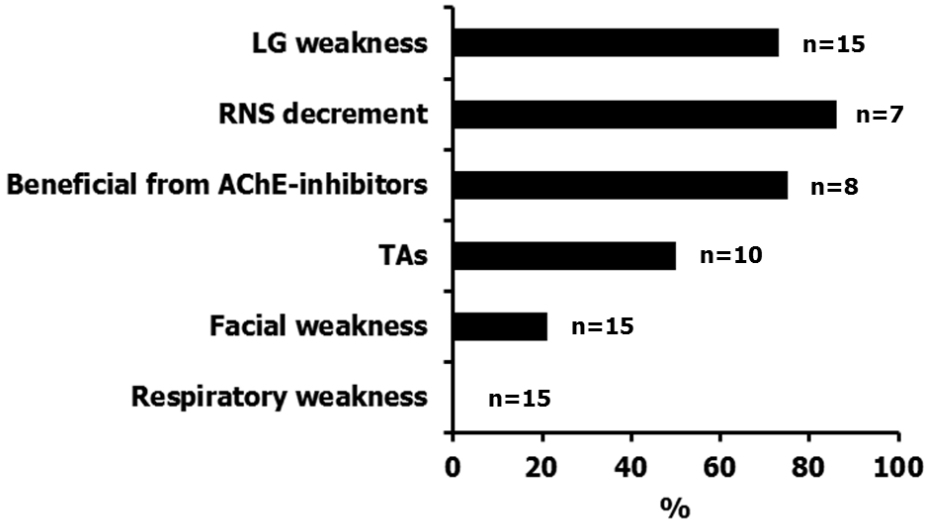

Figure 8: Summary of the clinical features of 15 CMS patients analysed in this study in order to identify the underlying molecular genetic defect.

LG: limb-girdle; RNS: repetitive nerve stimulation; AChE: acetylcholine esterase; TA: tubular aggregates

In total, 15 undiagnosed CMS patients from our CMS cohort were screened for *GFPT1* mutations. The majority of the patients (73 %) exhibited limb-girdle weakness. If limb-girdle weakness was missing, the patients showed at least tubular aggregates in their muscle biopsy and/or haplotype analysis suggested potential linkage at the *GFPT1* locus. In about 86 %, repetitive nerve stimulation (RNS) yielded a decremental response, if electrophysiology was tested (6/7). About 75 % of the patients responded well to AChE-inhibitor therapy if treated (6/8). Most muscle biopsies showed unspecific or mild myopathic changes and tubular aggregates (TAs) were identified in 50 % (5/10). Four patients showed only tubular aggregates in muscle biopsies, while additional hints for LG-CMS were missing. These patients were included in order to define whether only TAs are a sufficient inclusion criteria for LG-CMS with *GFPT1* mutations. Only a minor proportion of patients exhibited facial weakness (21 %) and none of the patients showed respiratory weakness.

2.2 Identified *GFPT1* mutations

The following results were obtained by direct sequencing of the coding exons (1-19 and the additional muscle-specific exon 8A) and the adjacent intronic regions of the *GFPT1* gene in additional patients selected as described above.

2.2.1 Polymorphisms and harmless variants

Sequencing of the *GFPT1* gene in the 15 CMS patients revealed several known and unknown single nucleotide polymorphisms (SNPs) that are unlikely to be disease-related but rather represent normal variations among individual genomes.

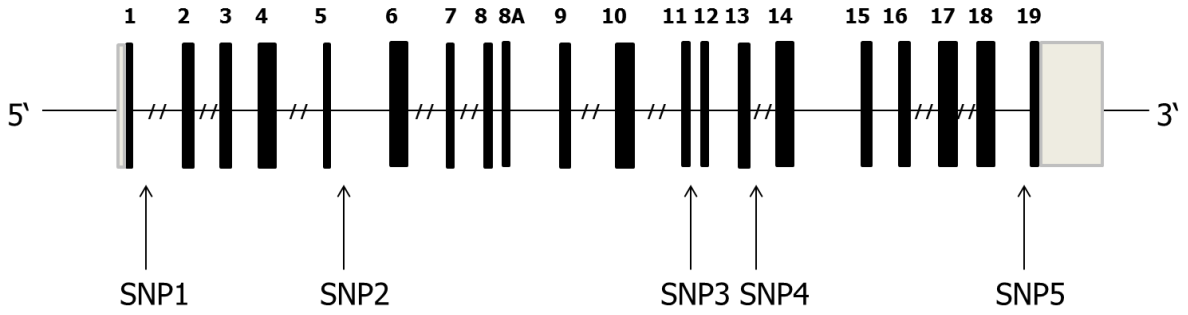

Figure 9: Map of *GFPT1* gene and the locations of the SNPs relative to the coding exons.
Dark shading indicates coding regions, light shading indicates untranslated regions and introns are shown as a line. Large introns are not shown completely (double vertical lines).

Name	Sequence variation	Location	dbSNP ID	Minor allele frequency (MAF)
SNP1	IVS1+36T>C	intron 1	rs6720415	A = 0.38
SNP2	IVS5+30T>C	intron 5	rs67760762	G = 0.26
SNP3	IVS11+7A>G	intron 11	rs6722492	T = 0.39
SNP4	IVS13+13delT	intron 13	rs113734896	- = 0.10
SNP5	IVS18-22delTT	intron 18	unknown	unknown

Table 16: Summary of the sequence variations found in 15 putative *GFPT1* patients.
Reference sequence: AC114772. IVS: intervening sequence; del: deletion; A: adenine; C: cytosine; G: guanine; T: thymine. SNP1, SNP2 and SNP3 are already published in [120, 121]. MAF source: dbSNP.

As the so far identified *GFPT1* mutations are found along the coding sequence, all exons were sequenced in this study. A total of five sequence variations were identified in 15 putative *GFPT1* patients of our Munich patient cohort (Table 16). All variations are localized in different introns of the *GFPT1* gene. They do not affect spice sites and they were found in a broad variety of patients and controls. The MutationTaster algorithm (http://www.mutationtaster.org) [122] and the

Exome Variant Server predicted all variations as polymorphisms. Therefore, they were supposed to be single nucleotide polymorphisms (SNPs).

2.2.2 Pathogenic mutations identified in GFPT1

Putative pathogenic mutations are sequence variations which are assumed to alter different protein features and are linked to a human disease. The 15 putative *GFPT1* patients were sequenced for *GFPT1* mutations according to their clinical picture and/or haplotype analysis results. The disease co-segregation with recessive inheritance of the *GFPT1* mutations was analysed if DNA from family members was available.

Exon	Nucleotide change	Effect on the protein	Patient with the mutation
7	c.572G>T	p.Ser191Ile	patient 3
8	c.639G>A	p.Ser213Asn	patient 1
12	c.1060G>C	p.Gly354Arg	patient 2
15	c.1472T>C	p.Met491Thr	patient 1
16	c.1649C>T	p.Ala550Val	patient 4
19	c.*22C>A		patient 4

Table 17: *GFPT1* mutations identified in 15 putative GFPT1 patients.
GFPT1 mutations were identified in four of 15 putative GFPT1 patients. The nucleotide and amino acid numbering is according to NM_002056.2 and NP_002047.2.

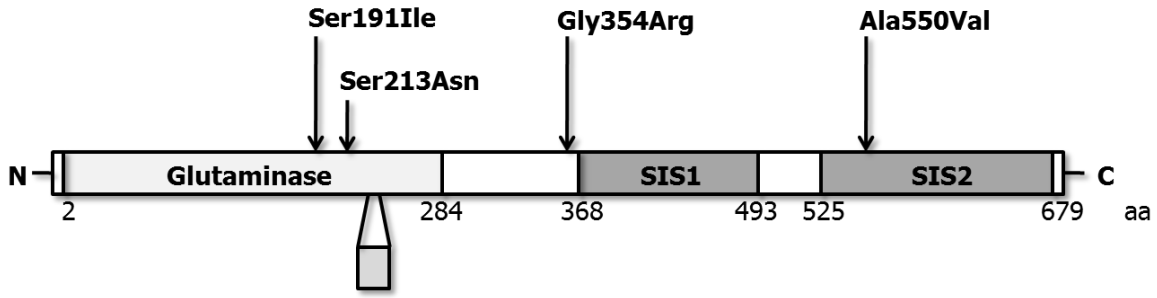

Figure 10: Schematic view of the domain structure of GFPT1 and the position of the identified mutations.
GFPT1 consists of a glutaminase and two sugar isomerase (SIS) domains. The insertion of 18 amino acids (aa) of the muscle-specific exon is indicated. Reference sequence: NM_002056.2

In total, putative pathogenic GFPT1 mutations were identified in four of 15 unsolved CMS patients (Table 17 and Figure 10).

Patient 1 showed limb-girdle weakness, decremental response to RNS and benefited from AChE-inhibitors. His muscle biopsy revealed aspecific changes without TAs. This patient carried the compound heterozygous mutations c.1472T>C (p.M491T) [65] and c.638G>A (p.S213N). To date, the p.S213N mutation localized within the glutaminase domain (Figure 10), has not been published but the MutationTaster algorithm (http://www.mutationtaster.org) predicts a "disease causing" effect of the mutation on the GFPT1 protein. In addition, the mutation is not listed in the Exome Variant Server (http://evs.gs.washington.edu/EVS/). Compound heterozygosity was confirmed by analysis of DNA samples of the parents.

Patient 2 showed limb-girdle weakness, no clear effect from AChE-inhibitor therapy and no TAs in a biopsy of the muscle. RNS was not tested. The parents of the patient are first cousins. This patient carried the homozygous *GFPT1* mutation c.1060G>C (p.G354R) which is localized between the glutaminase and the SIS1 domain (Figure 10). The MutationTaster algorithm (http://www.mutationtaster.org) also predicts a "disease causing" effect of the mutation on the GFPT1 protein. The mutation c.1060G>C (p.G354R) is not listed in the Exome Variant Server (http://evs.gs.washington.edu/EVS/).

Patient 3 showed limb-girdle weakness, a positive effect from AChE-inhibitor treatment and TAs in muscle biopsy. The RNS test revealed no decremental response. In this patient, the heterozygous variation c.572G>T (p.S191I) which is localized within the glutaminase domain was identified. The MutationTaster algorithm (http://www.mutationtaster.org) predicts a "disease causing" effect of the mutation on the GFPT1 protein but no second mutation was identified in this patient. The sequence variation c.572G>T (p.S191I) is not listed in the Exome Variant Server (http://evs.gs.washington.edu/EVS/). The healthy father of patient 3 also carried the mutation heterozygously making autosomal dominant inheritance very unlikely. In order to investigate if the patient carries a second mutation not detectable by sequencing of genomic DNA, the cDNA reverse transcribed from muscle RNA of the patient was analysed.

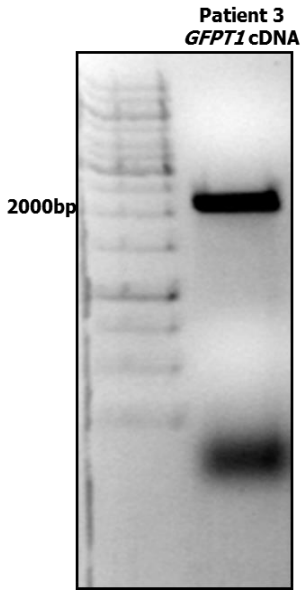

Figure 11: Gel analysis of the *GFPT1* cDNA PCR product of patient 3.

Gel electrophoresis analysis of the amplicon confirms the presence of one fragment with the expected size (~2.1 kb). An 1 kb DNA marker was used. Since the *GFPT1* and the *GFPT1-L* transcripts differ only in 54 bp and the DNA resolution of the gel (1 % agarose) is low, only one *GFPT1* cDNA band, consisting of both transcripts, was observed.

Gel analysis of the PCR product showed one *GFPT1* cDNA band at about 2.1 kb. This band consists of the muscle specific longer isoform *GFPT1-L* (2.097 kb) and the shorter isoform *GFPT1* (2.045 kb). No truncated transcripts were detected and sequencing of the RT-PCR product did not reveal any abnormal exon-exon junctions, largely excluding a second mutation which has an effect on splicing.

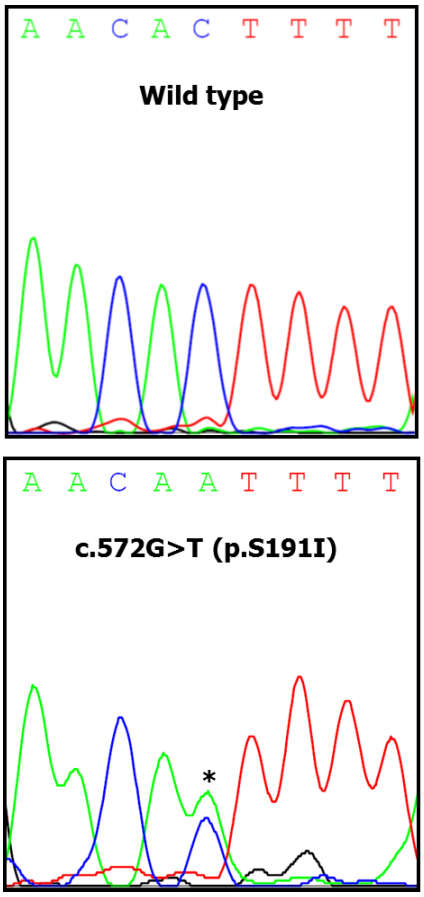

Figure 12: Sequence analysis of cDNA of a control patient (wild-type) and patient 3 carrying *GFPT1* c.572G>T (p.S191I) heterozygously.
Reverse strand chromatograms are shown.

Sequence analysis of the cDNA fragment amplified from muscle cDNA of patient 3 also showed biallelic expression of G and T alleles at position c.572. This finding largely excluded the possibility of mutations leading to instable transcripts or the existence of an mRNA that contains a premature translation-termination codon (PTC) which could lead to nonsense-mediated decay (NMD) of the mRNA. The results suggest that, patient 3 carries a putative pathogenic mutation (p.S191I) but without any effect on the patient due to the heterozygous state of the mutation and the absence of a second mutation.

Patient 4 showed limb-girdle weakness, benefited from AChE-inhibitor therapy and had no TAs in a biopsy of the deltoid muscle. A decremental response was observed in the trapezius muscle. This patient carried the compound heterozygous mutations c.*22C>A and c.1649C>T (p.A550V). The 3'-UTR mutation c.*22C>A is a recurrent change [65] while the p.A550V variant, localized within the isomerase 2 (SIS2) domain (Figure 10), has not yet been published. The MutationTaster algorithm (http://www.mutationtaster.org) predicts a "disease causing" effect of

the mutation on the GFPT1 protein. The mutation is not listed in the Exome Variant Server (http://evs.gs.washington.edu/EVS/).

No *GFPT1* mutations were identified in the patients with non-fatigable weakness but with tubular aggregates in the muscle biopsies (4/15).

3 Characterization of mutant GFPT1 species

3.1 Investigation of GFPT1 missense mutations

In total, 21 different GFPT1 mutations consisting of 16 missense mutations, three frameshift mutations, one nonsense mutation and one in the 3'-UTR were found in 16 unrelated LG-CMS families (Figure 7 and 10). GFPT1 mutations had not previously been linked to a human disease and the pathomechanism resulting in NMJ and skeletal muscle dysfunction is currently unclear. In order to investigate the role of GFPT1 in CMS pathogenesis, selected missense mutations were characterized. First of all GFPT1 protein levels were analysed in myoblast cells of GFPT1 patients. After that mutant proteins were transiently expressed in SW13 or HEK293 cells and effects on expression levels and subcellular localization were assessed. Finally the enzyme activity of GFPT1 mutants was measured *in vitro*.

3.1.1 Expression studies of mutant *GFPT1* species

3.1.1.1 Reduced GFPT1 expression in GFPT1-mutated myoblast cells from GFPT1 patients

Primary myoblasts were derived from three GFPT1 patients. The immunoblots were performed to establish the GFPT1 protein levels in the myoblast lysates using anti-GFPT1 antibody.

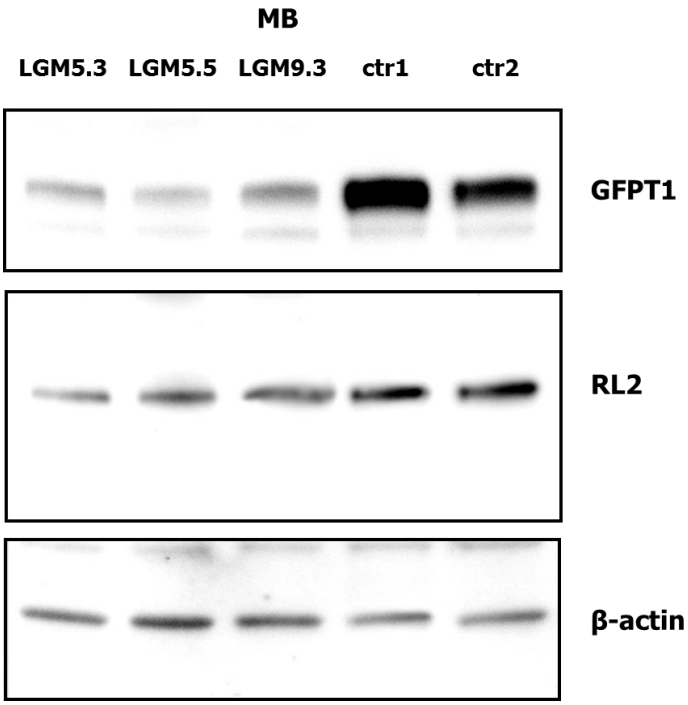

Figure 13: Western Blot of GFPT1 and *O*-GlcNAcylation in myoblast samples of *GFPT1* patients.
Immunoblot was performed on protein samples from primary human myoblasts (MB) obtained from three different GFPT1 patients (LGM5.3, 5.5 and 9.3), heterozygous for c.*22C>A, compared to two healthy control individuals (ctr1 and ctr2) with an anti-GFPT1 antibody (top). LGM5.3 and 5.5 are compound heterozygous for c.*22C>A and c.1475T>C (p.Met492Thr); LGM9.3 is compound heterozygous for c.*22C>A and c.595G>T (p.Val199Phe). The RL2 antibody detects single *N*-acetylglucosamine at serine or threonine residues [123] (middle). The anti-β-actin antibody was used to ensure equal protein loading (bottom).

Western Blot analysis of myoblasts obtained from three GFPT1 patients (LGM5.3, 5.5 and 9.3) revealed reduced expression of the mutant GFPT1 protein compared to wild-type controls. Furthermore, immunoblotting of protein extracts with the RL2 antibody, which selectively detects *O*-linked N-acetylglucosamine (*O*-GlcNAc) residues on numerous proteins [123], revealed markedly decreased band intensities in myoblasts of GFPT1 patients compared to healthy controls. The anti-β-actin antibody visualized equal protein loading (Figure 13).

3.1.1.2 Modulation of GFPT1 affects the levels of O-linked N-acetylglucosamine on proteins

O-GlcNAc, the main product of the hexosamine biosynthetic pathway (HBP) which is regulated by GFPT1, is essential for posttranslational modification of serine and threonine residues of nuclear and cytoplasmic proteins. Immunoblot analysis of myoblast lysates of GFPT1 patients and controls with the RL2 antibody, which selectively detects *O*-GlcNAc residues on proteins, showed

that *O*-GlcNAcylated proteins were markedly decreased in lysates from the patients' myoblast cells. To examine whether loss of Gfpt1 leads to impaired glycosylation of proteins in cultured myoblasts, C2C12 cells were treated with *Gfpt1* siRNA to decrease its expression.

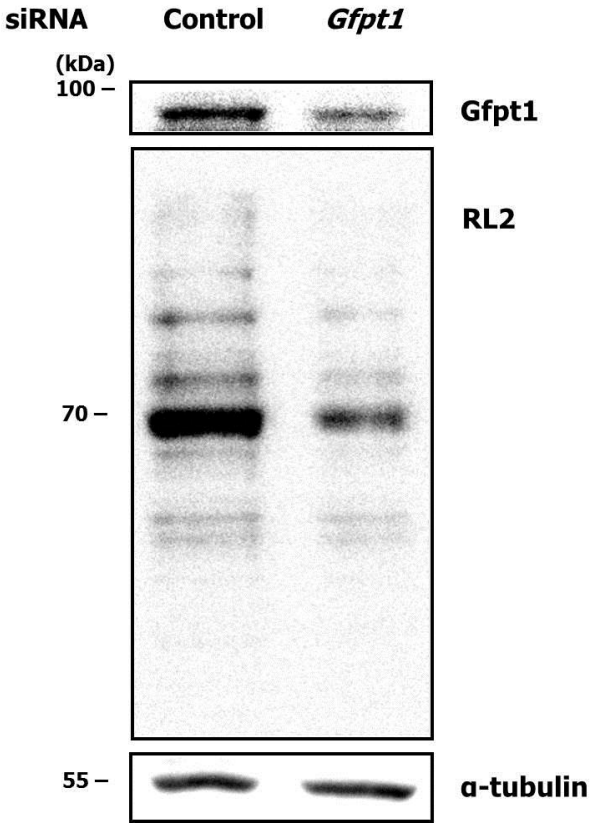

Figure 14: Western Blot of GFPT1 and *O*-GlcNAcylation in siRNA treated C2C12 cells

C2C12 cells were treated with control or *Gfpt1* siRNA and immunoblotted with an anti-GFPT1 antibody. The RL2 antibody detects single *N*-acetylglucosamine at serine or threonine residues [123]. The anti-α-tubulin antibody was used to ensure equal protein loading.

Western Blot analyses showed that *Gfpt1* siRNA down-regulated endogenous Gfpt1 protein levels (Figure 14; Gfpt1 antibody). Silencing with siRNA reduced Gfpt1 protein efficiently (85-90 %) and resulted in a reduction of the levels of *O*-linked N-acetylglucosamine on proteins compared with control siRNA (Figure 14; RL2 antibody).

This experiment also linked reduced amounts of functional Gfpt1 protein to reduced levels of *O*-linked N-acetylglucosamine on proteins.

3.1.1.3 Transfection studies of wild-type and mutant GFPT1 constructs in HEK293 cells

To study the effect of mutations on protein expression levels in a controlled experiment, plasmid constructs were generated to express wild-type and mutant myc-tagged GFPT1-L (muscle-specific variant) protein (p.Arg111Cys, p.Asp43Val, p.Met492Thr, p.Thr15Ala, p.Asp348Thr, p.Arg434His and p.Ile121Thr) in HEK293 cells. The cells were co-transfected with the different myc-tagged *GFPT1* constructs together with a pcDNA3 vector, expressing GFP to estimate transfection efficiency. Immunoblot analysis was performed to establish the levels of wild-type and mutant myc-tagged GFPT1 protein in HEK293 cells using anti-GFPT1 antibody.

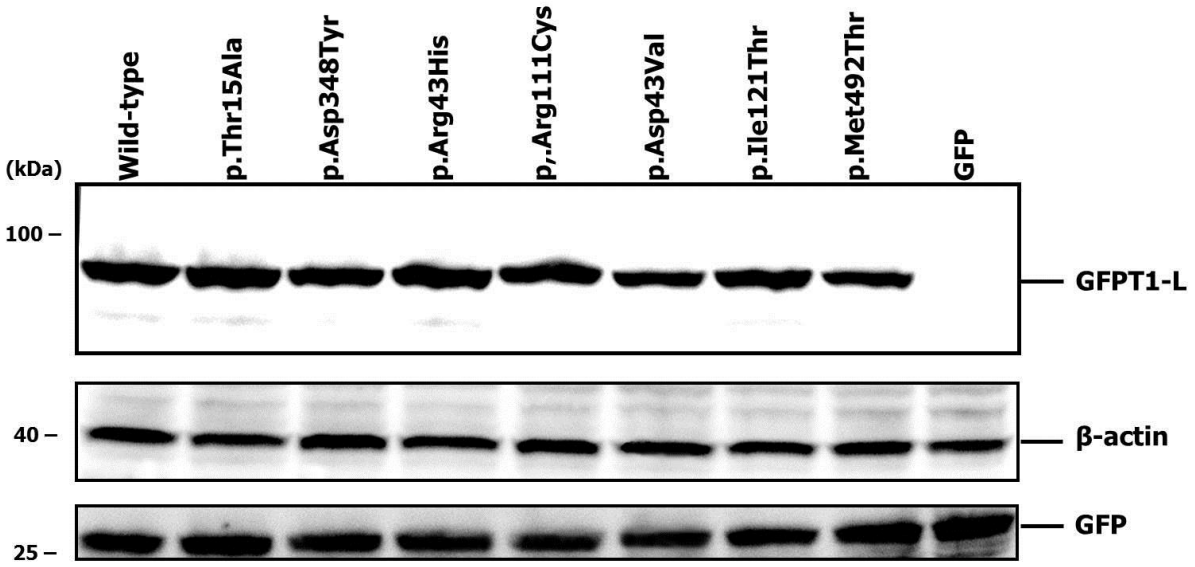

Figure 15: Western Blot of GFPT1 in HEK293 cells co-transfected with either the wild-type or mutant *GFPT1* constructs and GFP.

The cells were co-transfected with a GFP expression vector for transfection efficiency control. The cell lysates were immunoblotted with an antibody that recognizes the myc-tagged GFPT1 protein. The anti-actin antibody was used as loading control and visualized equal protein loading.

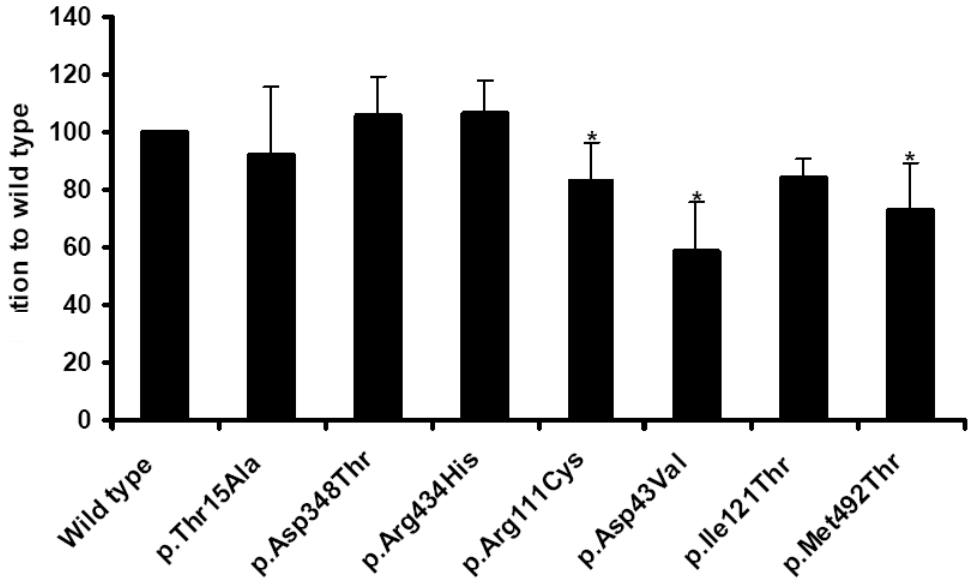

Figure 16: Expression study

HEK293 cells were transfected with either wild-type or mutant *GFPT1* constructs and GFP. Protein bands (for a representative experiment see figure 15) were quantified with the ImageJ program. GFPT1 expression levels were normalized to GFP and actin protein amounts. Expression levels of each mutant are compared to that of the wild-type. Three independent transfection experiments were performed for each mutant and lysates were measured in triplicates. Error bars indicate + SD; significant differences from wild-type $*P < 0.05$.

The amount of myc-tagged GFPT1 protein species was measured by immunoblotting in transiently transfected HEK293 cells. Comparison of total myc-tagged GFPT1 amounts in HEK293 cells transfected with either wild-type or mutant *GFPT1* constructs showed a reduction of the GFPT1 expression to 83 % for p.Arg111Cys, 58 % for p.Asp43Val and 73 % for p.Met492Thr compared to the wild-type GFPT1 amount (Figure 15 and 16). The mutants p.Thr15Ala, p.Asp348Thr, p.Arg434His and p.Ile121Thr had no effect on protein expression (Figure 15 and 16). HEK293 cells transfected only with GFP showed no expression of myc-tagged GFPT1 (Figure 15). The actin-antibody visualized equal protein loading (Figure 15).

3.1.2 Subcellular localization of mutant GFPT1 species

Glutaminase and isomerase activities have been attributed to GFPT1 but little is known about the regulation and subcellular localization of GFPT1. Mutations that alter protein folding could result in abnormal subcellular localization of the mutant protein. To characterize the subcellular localization pattern of wild-type and mutant GFPT1-L, SW13 cells were transfected with either wild-type or mutant Myc-tagged *GFPT1* constructs and investigated by indirect immunofluorescence microscopy with appropriate antibodies.

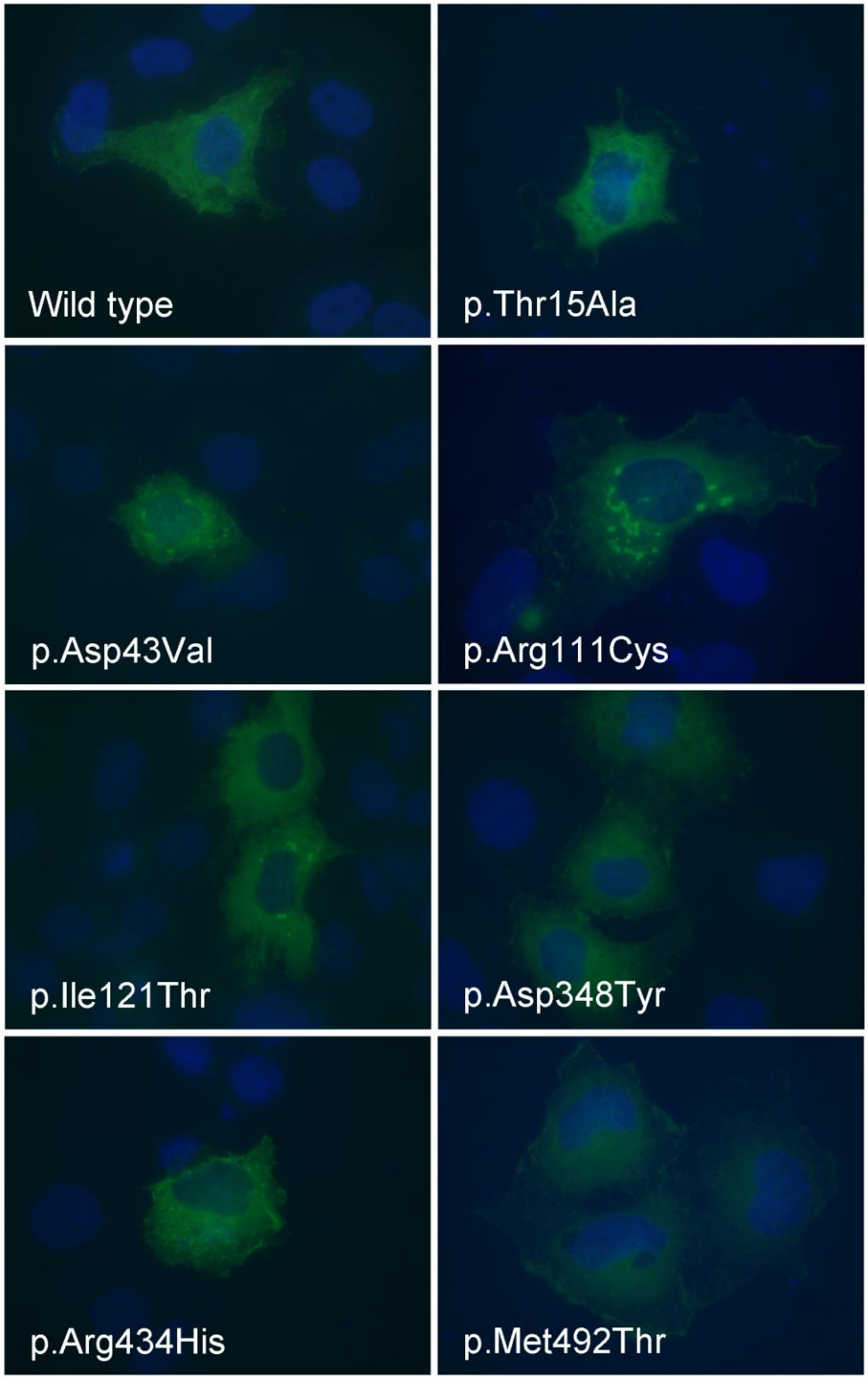

Figure 17: Subcellular localization of GFPT1 mutants.

SW13 cells were transfected with either wild-type or mutant Myc-tagged *GFPT1* constructs. Cells were stained with a mouse monoclonal antibody that recognizes the Myc-tag, followed by an anti-mouse IgG secondary antibody conjugated to a green fluorescent dye (Alexa Fluor 488).

Immunofluorescence microscopy using an antibody that recognizes the Myc-tag of the transiently expressed GFPT1 species reveals that all mutants show a diffuse cytoplasmic staining pattern similar to wild-type GFPT1 (Figure 17). GFPT1 was not detected in the nucleus. At high expression levels, some *GFPT1* constructs, including wild-type, tend to form aggregates (Figure 17). This finding is most likely non-specific and rather results from the high non-physiological expression level.

3.1.3 Enzyme activity of GFPT1 mutants

The activity of the rate-limiting enzyme of the hexosamine biosynthetic pathway (HBP), Glucosamine-fructose-6-phosphate aminotransferase 1 (GFPT1) was measured *in vitro* by the glutamate dehydrogenase (GDH) method in transiently transfected cells. HEK293 cells were transfected with either wild-type or mutant *GFPT1* constructs. For this series experiments I decided to use untagged GFPT1 as myc-tagged GFPT1 did not exhibit enzyme activity. The aim of these studies was to investigate whether GFPT1 missense mutations, observed in LG-CMS patients may cause NMJ and muscle pathology through altered enzyme activity.

Figure 18: Determination of the GFPT activity

The enzyme activity is measured by quantification of glutamate using glutamate dehydrogenase (GDH) as coupling enzyme. Reduction of the 3-acetylpyridine analogue of NAD+ (acetylpyridine adenine dinucleotide, APAD) by GDH can be followed spectrometrically by the measurement of the absorbance at 370 nm.

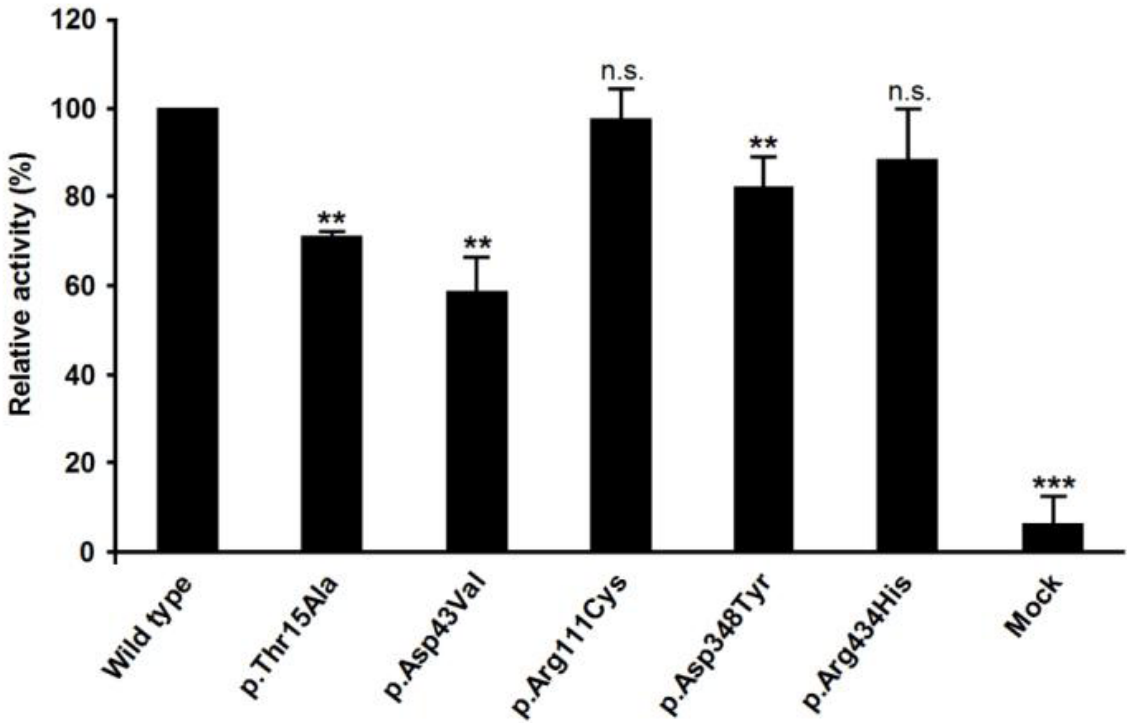

Figure 19: Analysis of the enzymatic activity of GFPT1 mutants

HEK293 cells were transfected with either wild-type or mutant untagged *GFPT1* constructs. GFPT1 enzyme activity was measured in cell lysates with the glutamate dehydrogenase method 48 h after transfection. The enzymatic activity of each mutant was normalized to GFPT1 protein amounts determined by Western blot analysis of cell lysates. Three independent transfection experiments were performed for each mutant and lysates were measured in triplicates. Error bars indicate + SD; significant differences from wild-type $^{**}P < 0.01$; $^{***}P < 0.001$. n.s., not significant.

Heterologous expression of GFPT1 mutants and analysis of the GFPT1 enzyme activity using the the GDH method revealed that the mutations p.Thr15Ala (relative activity of about 71 %), p.Asp43Val (relative activity of about 58 %) and p.Asp348Tyr (relative activity of about 82 %) had small effects on enzymatic activity. Furthermore, the mutants p.Arg111Cys (relative activity of about 97 %) and p.Arg434His (relative activity of about 88 %) had no statistically measurable effect on enzymatic activity. Mock transfected HEK293 cells showed only a low GFPT1 enzyme activity (relative activity of about 6 %). This finding correlates with the result that HEK293 cells express only low protein levels of endogenous GFPT1 compared to cells transfected with *GFPT1* constructs.

4 Investigation of the 3'-UTR mutation c.*22C>A

The c.*22C>A mutation in the 3'-UTR of the *GFPT1* gene was identified heterozygously in four independent families from Spain and Germany (LGM5, 9, 12 and patient 4). It was determined that the 3'-UTR mutation c.*22C>A is associated with reduced amounts of GFPT1 protein levels in myoblasts, myotubes and muscle tissue obtained from three patients (Figure 13) [65]. Sequence analysis of the *GFPT1* cDNA of these patients excluded major degradation of the c.*22A mRNA species relative to the mRNA amount transcribed from the 2nd allele [65]. However, no absolute quantification of *GFPT1* mRNA levels was performed in these patients. Because this variant does not alter the *GFPT1* open reading frame, its pathogenic relevance has not yet been extablished. Therefore, experiments were designed to characterize the pathomechanism related to c.*22C>A.

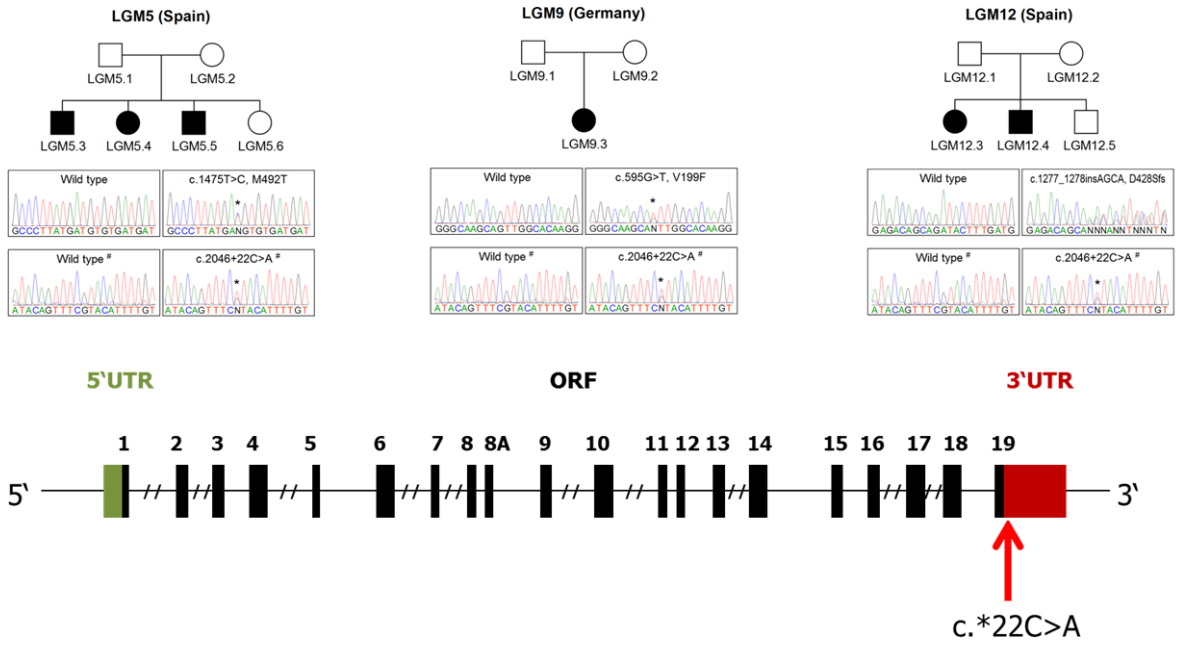

Figure 20: 3'-UTR mutation c.*22C>A in the *GFPT1* gene.

The mutation in the 3'-UTR of *GFPT1* has been identified in 3 independent families (LGM5, 9 and 12) by linkage and homozygosity data (Table 15). After the identification of *GFPT1* mutations in LG-CMS patients, this mutation has been identified in one further patient (Patient 4, Table 17). The compound heterozygous state of the mutation has been confirmed [65]. The mutation is located after the open reading frame (ORF) of *GFPT1*, 22 bp downstream of the translation termination codon (TGA) in the 3'-UTR (red arrow indicates the position of the mutation). Dark shading indicates coding regions, green and red shading indicates untranslated regions and introns are shown as a line. Large introns are not shown completely (double vertical lines).

4.1 Relative quantification of *GFPT1* mRNA in myoblast and muscle lysates

As a first experiment, *GFPT1* mRNA levels were quantified in total RNA derived from the myoblast and muscle samples of *GFPT1* patients carrying the c.*22C>A mutation and a missense change on the 2nd allele, and control individuals. The mRNA levels were analysed and quantified by real-time qRT-PCR.

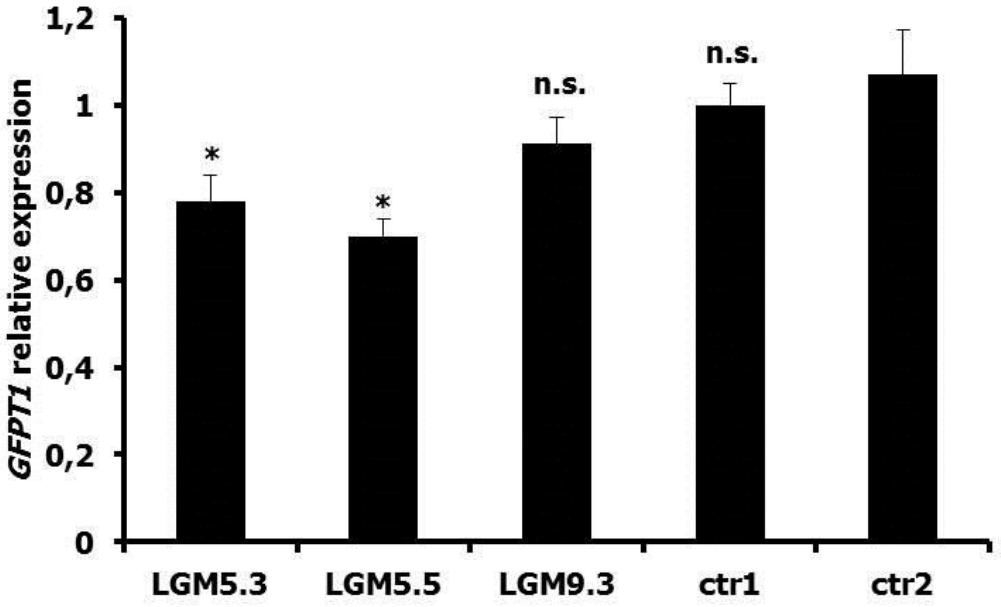

Figure 21: *GFPT1* relative expression in myoblasts.

Relative expression of *GFPT1* mRNA in myoblast samples obtained from GFPT1 patient (LGM5.3, 5.5 and 9.3) compound heterozygous for c.*22C>A and two healthy control individuals (ctr1 and 2). LGM 5.3 and 5.5 are compound heterozygous for c.*22C>A and c.1475T>C (p.Met492Thr); LGM9.3 is compound heterozygous for c.*22C>A and c.595G>T (p.Val199Phe). Transcript levels were analysed by qRT-PCR and normalized to histone hH4. Error bars indicate + SD; significant differences from control 2 (ctr2) $*P < 0.05$. n.s., not significant.

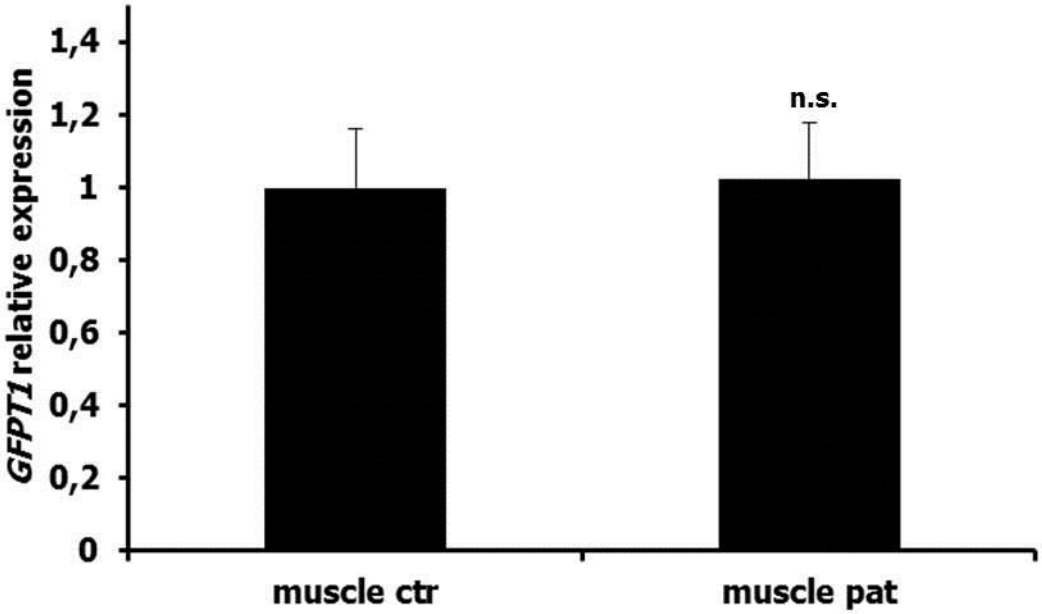

Figure 22: *GFPT1* relative expression in muscle.

Relative expression of *GFPT1* mRNA in muscle biopsy samples obtained from a control individual (wt) and a GFPT1 patient (patient 4 of this study), compound heterozygous for c.*22C>A and c.1649C>T (p.A550V). Transcript levels were analysed by qRT-PCR and normalized to histone hH4. Error bars indicate + SD; n.s., not significant.

The quantification of the *GFPT1* mRNA levels in total RNA derived from myoblasts of patients with the c.*22C>A mutation (LGM5.3, 5.5 and 9.3) by real-time qRT-PCR revealed no gross changes in the *GFPT1* mRNA level compared to control individuals (ctr 1 and ctr 2) (Figure 21). Consistently, the real-time qRT-PCR analysis revealed almost identical *GFPT1* relative expression in skeletal muscle of a *GFPT1* patient (1.02), compound heterozygous for c.*22C>A and c.1649C>T (p.A550V), and a control individual (ctr) (1.0) (Figure 22). A significant difference between the *GFPT1* transcript level of patients (LGM5.3 and LGM5.5) compared to a healthy control individual (ctr2) was observed only in myoblast cells from one family (LGM5) (Figure 21). There was no significant difference in all other analysed patients (Figure 21 and figure 22). This result indicates that the reduced amounts of GFPT1 protein levels in muscle and myoblast lysates (Figure 13) of *GFPT1* patients [65] resulted from repression of translation rather than altered mRNA stability.

4.2 Expression analysis of the 3'-UTR mutation c.*22C>A

To confirm the association of the 3'-UTR mutation c.*22C>A with lower amounts of GFPT1 protein directly in a controlled experiment, C2C12 myoblasts were transfected with either wild-type or mutant *GFPT1* constructs. The constructs used here contained the *GFPT1-L* coding region and about 100 bp of its endogenous 3'-UTR downstream of the TGA stop codon in wild-type or mutant c.*22C>A state.

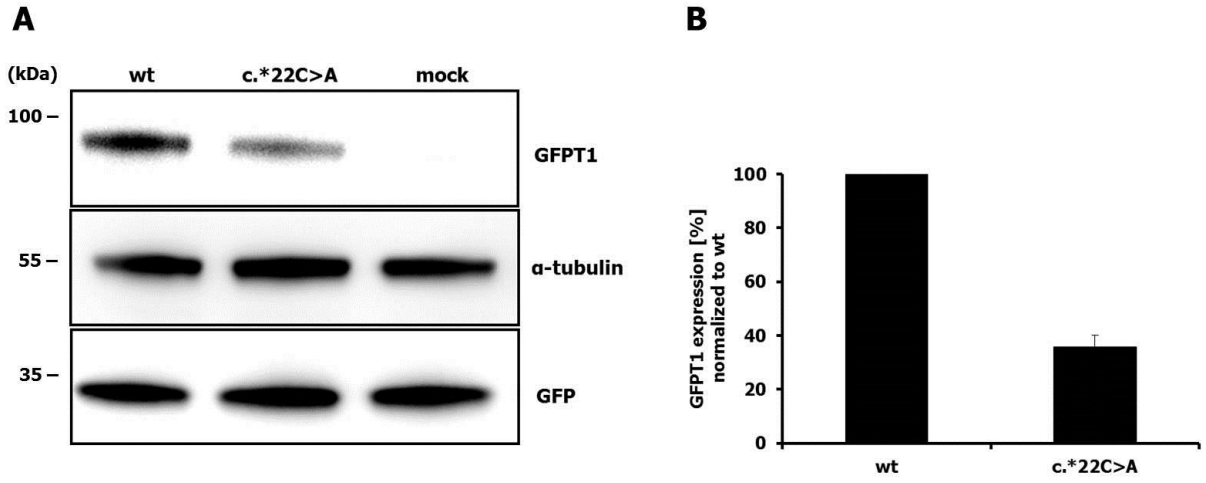

Figure 23: Western Blot of GFPT1 in C2C12 cells transiently transfected with *GFPT1*-3'-UTR wt or mutant (c.*22C>A) constructs.

The cells were co-transfected with a GFP expression vector for transfection efficiency control. The intensities of the bands were measured and GFPT1 expression was normalized to the GFP and α-tubulin levels. Each bar represents the average GFPT1 protein levels observed in n=3 independent experiments in C2C12 cells. Data are shown relative to the wt GFPT1 level.

Western Blot analysis of C2C12 cells transfected with either *GFPT1* wild-type or mutant constructs revealed that the 3'-UTR mutation leads to a significant decrease in GFPT1 expression levels compared to wild-type (Figure 23 A, top) confirming the association of *GFPT1* c.*22C>A with reduced GFPT1 protein levels in a controlled assay. Co-transfection of a GFP expression vector shows equal transfection efficiency for both constructs (Figure 23 A, bottom). The experiment revealed a reduction in the expression of the mutated construct to 36 % (Figure 23 B) compared to wild-type (wt). This result confirms the association of *GFPT1* c.*22C>A with reduced GFPT1 protein levels.

4.3 The mutation c.*22C>A creates a miR-600 and miR-206* binding site in the *GFPT1* 3'-UTR

It has been shown that endogenous GFPT1 protein amounts are reduced in myoblasts, myotubes and muscle tissue samples of patients with the c.*22C>A mutation [65] and the findings from the expression analysis of transfected cells in this study support this observation (Figure 23). On the other hand, *GFPT1* mRNA levels seemed largely unchanged in a muscle biopsy and myoblast samples of patients with the 3'-UTR variant. Thus the pathogenic effect of the 3'-UTR mutation may be mediated through downregulation of GFPT1 protein translation. One mechanism of expression regulation is miRNA binding to its target mRNA. The binding results in translational repression through either the degradation of the mRNA or its translational inhibition. Considering the possibility that the 3'-UTR variant may have an effect on the regulation of *GFPT1* expression, *in silico* analyses were undertaken and revealed two potential miRNA binding sites.

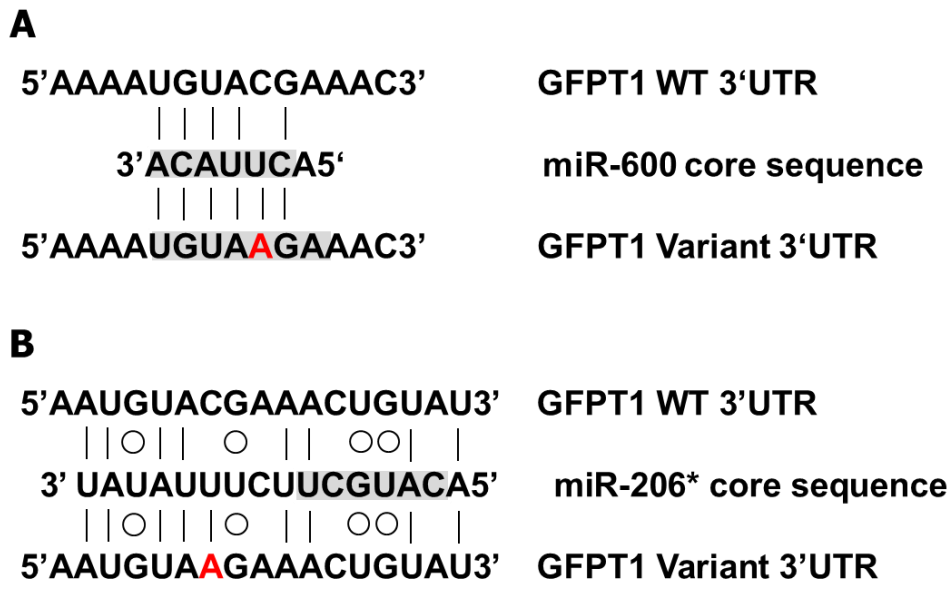

Figure 24: Schematic representation of the sequence alignment of the hsa-miR-600 and the miR-206* with wild-type (wt) and the variant (c.*22C>A) *GFPT1* mRNA.

Bioinformatics tools on http://bioinfo.uni-plovdiv.bg/microinspector/ and http://www.mirbase.org/search.shtml revealed that the 3'-UTR mutation c.*22C>A may result in a gain of a putative binding site in the 3'-UTR for both the miR-600 and miR-206* miRNA. (A) miR-600 alignment [MIMAT0003268]. The mutation creates a 7mer-A1 site which is highlighted in grey. The *GFPT1* 3'-UTR c.*22C>A mutation is shown in red. (B) miR-206* [MIMAT0006994] alignment shows imperfect seed pairing, but compensatory pairing in the 3'-region of the miRNA. The *GFPT1* 3'-UTR c.*22C>A mutation is shown in red. Cycles indicate wobble base pairing (G:U), while lines indicate Watson-Crick base pairing. The seed region is highlighted in grey.

In silico analysis revealed that the c.*22C>A variant results in a sequence matching the seed of mature hsa-miR-600 (5'CUUACA3'; Figure 24 A). The predicted hsa-miR-600 site in the variant *GFPT1* 3'-UTR is a 7mer-A1 seed match type, which comprises the exact seed match (position 2-7 of the mature miRNA) supplemented by an A across from miRNA nucleotide 1 (Figure 24 A). The mutation c.*22C>A changes the 3'-UTR sequence from 5'UGUACG3' (wild-type) to 5'UGUAAG3' (mutant c.*22C>A) generating a perfect match to the seed of hsa-miR-600 (Figure 24 A).

In addition, the *GFPT1* variant also leads to the gain of a putative binding site on its 3'-UTR for miR-206*. There is no perfect seed matching but there seems to be a compensatory base pairing site in the 3'-region of the miR-206*. The c.*22C>A variant lies within the compensatory site and the C>A change results in an additional Watson-Crick base pairing (A:U) (Figure 24 B).

4.3.1 Hsa-miR-600 controls the expression of mutant *GFPT1*

In order to test the interaction between mutant *GFPT1* and miR-600, co-expression studies were performed. HEK293 cells were transfected with *GFPT1*-3'-UTR wt or mutant (c.*22C>A) constructs together with the empty pENTR vector or with the miR-600 expression vector pEF1-miR-600. The GFPT1 protein amounts were investigated 24 or 48 h after transfection by Western blot analysis with appropriate antibodies. To investigate potential downstream effects of altered GFPT1 levels, I made use of the RL2 antibody which recognises single *O*-GlcNAc modifucations of proteins [123].

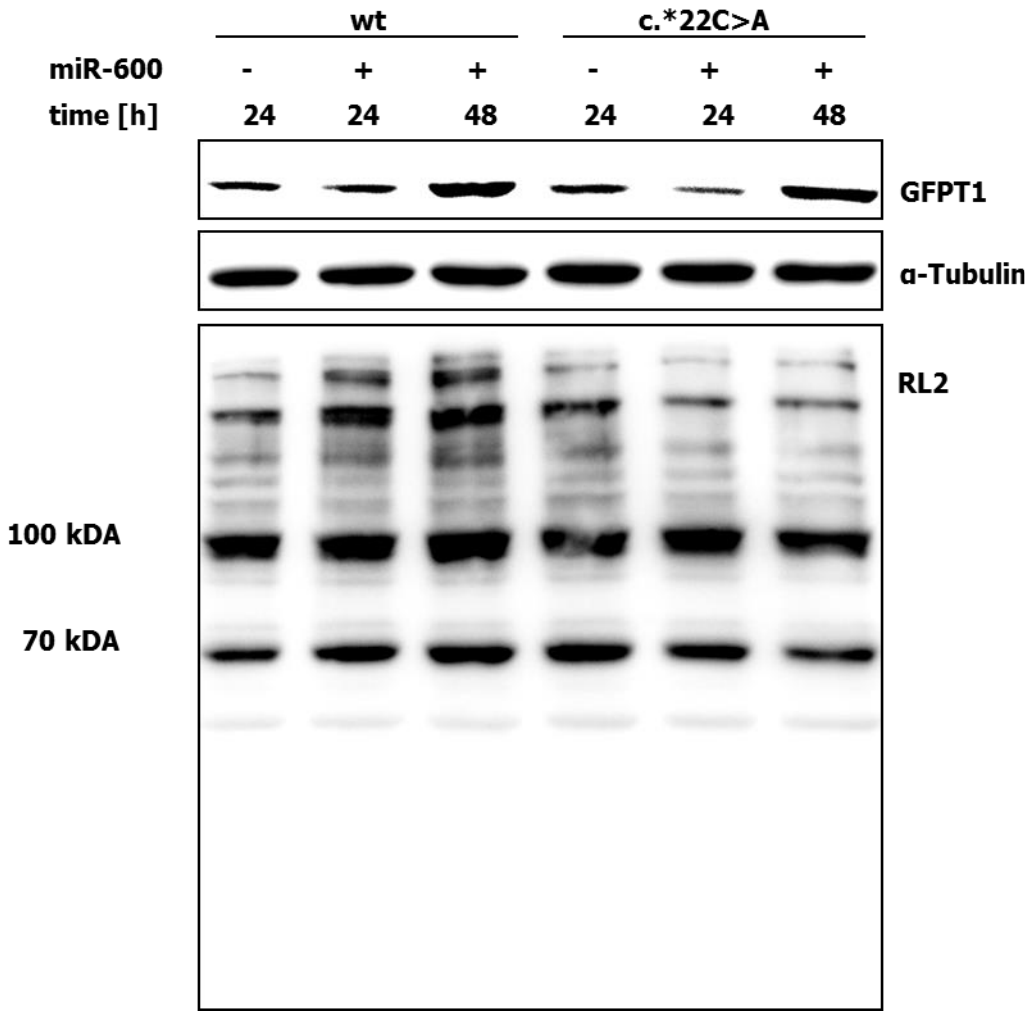

Figure 25: Western Blot of GFPT1 and *O*-GlcNAcylation in HEK293 cells transfected with *GFPT1*-3'-UTR wt or mutant (c.*22C>A) constructs.

The cells were co-transfected with either an empty pENTR vector or a pENTR vector expressing the hsa-miR-600. Cells were lysed either 24 or 48 h after transfection. The RL2 antibody detects single N-acetylglucosamine modifications at serine or threonine residues [123].

The microRNA miR-600 downregulates the expression of mutant *GFPT1.* Co-transfection of the mutant *GFPT1*-3'-UTR construct with the miR-600 expression vector pEF1-miR-600 led to a reduction of the mutant GFPT1 protein amount compared with the amount of mutant GFPT1 co-trasfected with the empty pENTR vector (Figure 25) after 24 hours. Due to the limited lifetime of the small microRNA miR-600, no reduction of the mutant GFPT1 protein was observed 48 hours after transfection. In contrast, the protein amount of wild-type GFPT1 co-transfected with the miR-600 expression vector was almost the same as co-transfected with the empty vector after 24 and 48 hours. Furthermore, immunoblotting of lysates from co-transfected HEK293 cells with the RL2 antibody, which selectively detects *O*-linked N-acetylglucosamine (*O*-GlcNAc) residues on numerous proteins [123], revealed markedly decreased band intensities when the mutant

construct was co-transfected with the miR-600 expression vector. In contrast, compared to the band intensities detected with the RL2 antibody after 24 hours (+/- miR-600), the intensities were markedly increased after 48 hours when co-transfecting the wild-type construct together with the miR-600 expression vector. This result correlates with the higher expression level of GFPT1 after 48 hours compared to the expression level after 24 hours (+/- miR-600) and confirms that the expression of the miR-600 has no influence on the expression of wild-type GFPT1 (Figure 25).

4.3.2 Expression profile of the microRNAs miR-206* and miR-600

As the expression of microRNAs is spatially and temporally controlled, the expression profile of miR-206* and miR-600 was investigated. It is known that miR-206 is highly expressed in human skeletal muscle and may play a potential role in myogenesis [124-128]. Its expression is robustly induced during the myoblast-myotube transition in primary human myoblasts [129]. However, there is no information on the abundance of its star-form miR-206*. Concerning miR-600, there is only one publication on the expression of this microRNA in human colorectal cells [130].
The microRNAs were quantified by a two-step real-time PCR using the miScript-Reverse Transcription kit and the miRNA-SYBR Green PCR Kit. The first step includes polyandenylation and reverse transcription of total RNA, followed by real-time PCR. In addition to dissociation curve analysis, the PCR products were run on an agarose gel to verify specificity of the amplification.

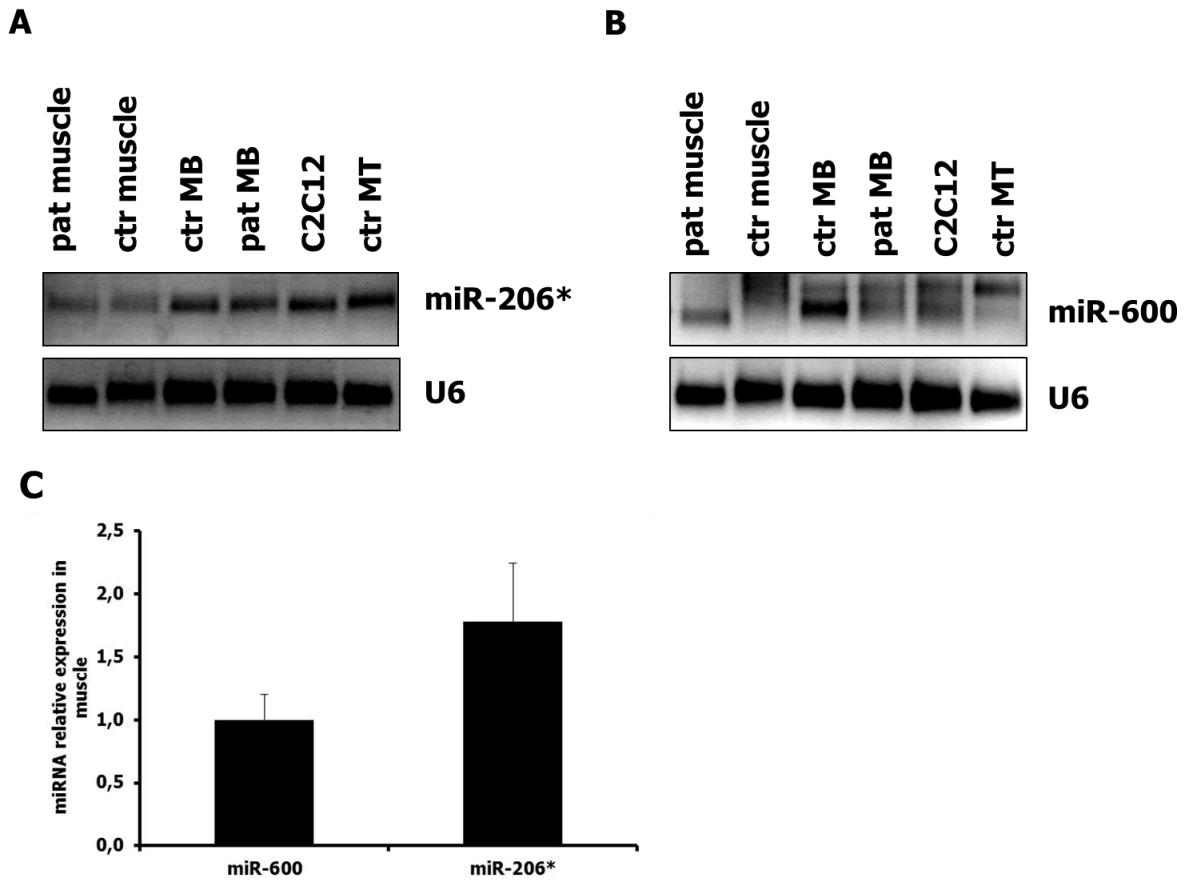

Figure 26: Expression profile of miR-206* (A) and miR-600 (B).

qRT-PCR to detect miR-206* and miR-600 was performed on cDNA samples from muscle biopsies and myoblasts (MB) obtained from GFPT1 patients (pat), heterozygous for c.*22C>A, compared to control (ctr) muscle, human myoblasts (MB), myotubes (MT) and C2C12 cells. MB pat (LGM9): compound heterozygous for c.*22C>A and c.595G>T (p.V199F); muscle pat (patient 4 of this study): compound heterozygous for c.*22C>A and c.1649C>T (p.A550V). PCR products were run on an agarose gel to verify specificity. U6 snRNA was used as normalization control. (**C**) Relative expression of the microRNA miR-600 and miR-206* in muscle samples of the patient. miRNAs were detected by qRT-PCR and normalized to U6 snRNA. miScript PCR control primers for U6 snRNA show relatively constant expression levels across the different samples.

To determine the abundance of miR-206*, real-time qRT-PCR was performed on RNA samples from muscle, myoblasts and myotubes (Figure 26 A). The expression of the miRNAs was analysed in samples obtained from GFPT1 patients compound heterozygous for the mutation c.*22C>A and control individuals. The miR-206* is robustly expressed in muscle and myoblast cells of GFPT1 patients and controls. The star-form is also abundant in C2C12 cells and myotubes of controls. Gel electrophoresis analysis of the amplicon confirms the presence of a single specific fragment of the expected size (~ 90 base pairs).

The microRNA miR-600 is also detectable in RNA samples obtained from human muscle biopsies and myoblast samples of GFPT1 patients as well as in C2C12 cells (Figure 26 B). Gel

electrophoresis analysis of the PCR products revealed the presence of a single specific fragment of the expected size (~ 90 base pairs) in the patient muscle biopsy sample, but there was a second, non-specific fragment of approximately 110 base pairs in human myoblasts and C2C12 cells (Figure 26 B).

The relative quantification by real-time qRT-PCR of the miRNA samples derived from human muscle samples showed that the miR-206* is more abundant (~2x) in patients' muscle biopsies than the miR-600 (Figure 26 C).

4.3.3 Relative expression profile of the microRNAs miR-206 and 206*

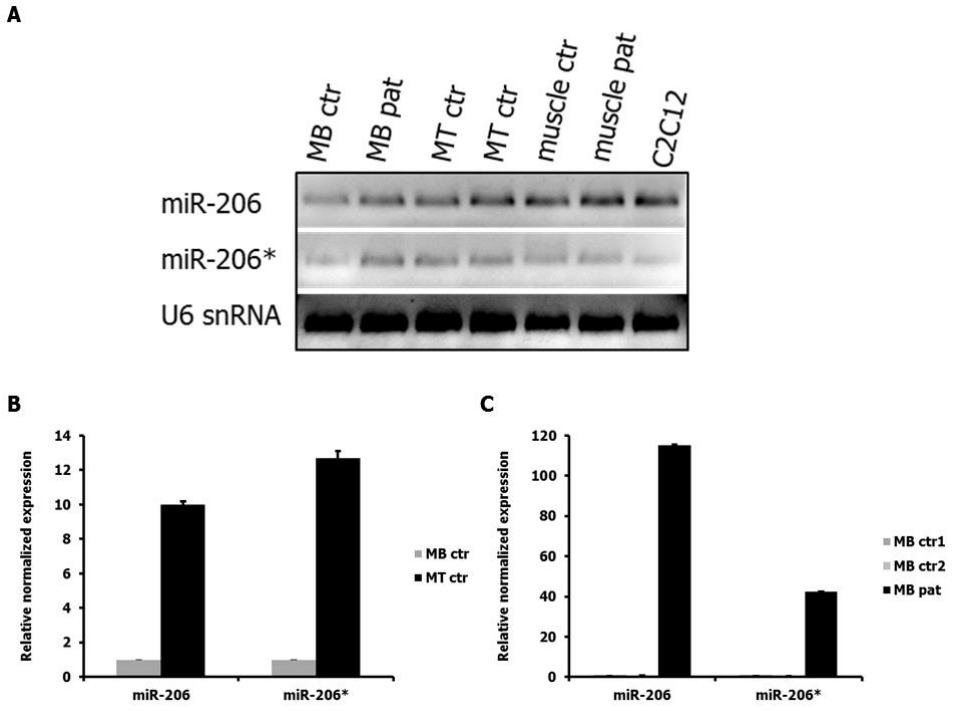

Figure 27: Expression profile of hsa-miR-206 and miR-206*.

Detection of miRNAs hsa-miR-206 and miR-206* in muscle, myoblasts and myotubes. The miRNAs were isolated with the miRNeasy Kit. RT-PCR was performed using the miScript SYBR Green PCR Kit containing QuantiTec Primer sets specific for hsa-miR-206, oan-miR-206* or U6 snRNA. U6 snRNA was used as an internal control. qRT-PCR was performed on cDNA samples from muscle and myoblasts (MB) obtained from two different *GFPT1* patients (pat), heterozygous for c.*22C>A, compared to control (ctr) muscle, human myoblasts (MB), myotubes (MT) and C2C12 cells. **(A)** The PCR products were confirmed by 4 % agarose gel electrophoresis. **(B)** Relative expression of the microRNAs miR-206 and miR-206* in myoblast (MB) and myotube (MT) samples of controls (ctr). **(C)** Relative expression of the microRNAs miR-206 and miR-206* in myoblast (MB) samples of a *GFPT1* patient (pat) and two controls (ctr). MB pat: compound heterozygous for c.*22C>A and c.595G>T (p.V199F); muscle pat: compound heterozygous for c.*22C>A and c.1649C>T (p.A550V).

The miR-206 is known to be robustly induced during the myoblast-myotube transition in primary human myoblasts [129, 131]. Consistent with this, qRT-PCR analysis of myoblast and myotube samples of a healthy control individual showed that the miR-206 is more abundant in myotubes than in myoblasts (Figure 27 A and B). Furthermore, the qRT-PCR assay revealed also that star-form miR-206* is detectable in myoblasts and is further upregulated upon differentiation (Figure 27 A and B) like known from the miR-206.
In addition, relative quantification showed that both miR-206 and miR-206* are more abundant in myoblast (MB) samples of a *GFPT1* patient (pat) than in two controls (ctr) (Figure 27 C).
Gel electrophoresis of qRT-PCR products (miR-206 and miR-206*) confirmed the presence of a specific fragment (~ 90 base pairs). No non-specific fragments were observed. miScript PCR control primers for U6 snRNA show relatively constant expression levels across the different samples (Figure 27 A).

4.3.4 Reporter assay testing the interaction between putative regulatory miRNAs and mutant *GFPT1*

In order to test the hypothesis that the *GFPT1* 3'-UTR mutation c.*22C>A leads to the gain of a miRNA binding site, a reporter gene assay was performed. This assay offers the opportunity to test the interaction between the mutant 3'-UTR and microRNAs directly.

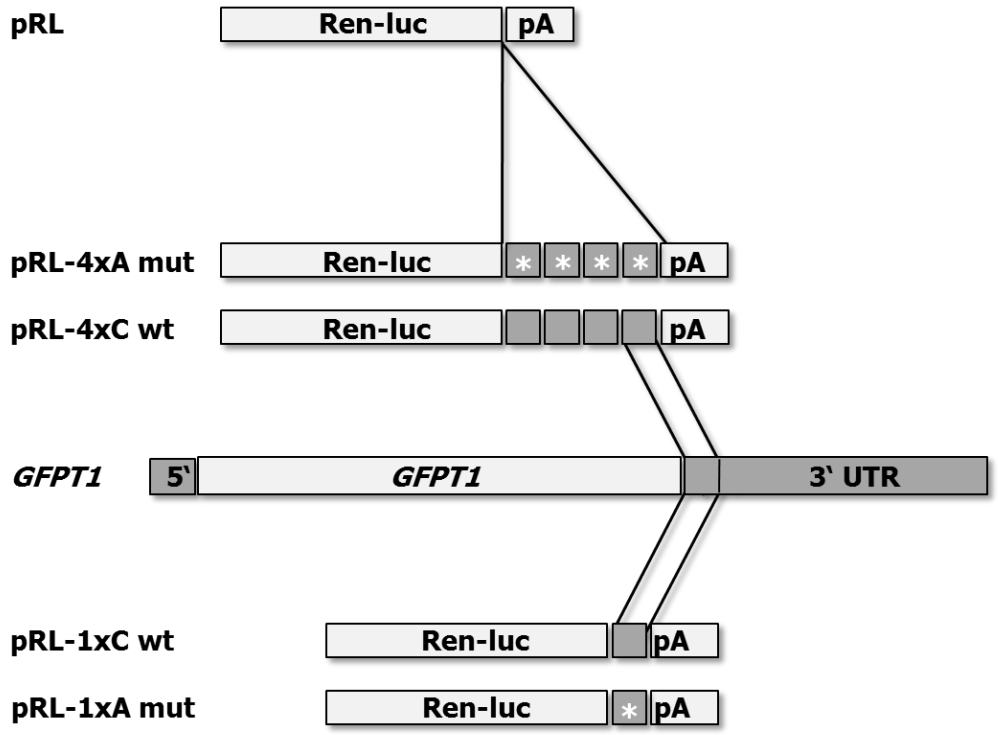

Figure 28: Schematic representation of the *Renilla* luciferase (Ren-luc) expression vectors and the *GFPT1* gene.

Four tandem repeats (4xA or 4xC) or a single unit (1xA or 1xC) of an 80 bp sequence around *GFPT1* c.*22 with C (wild-type; wt) or A (c.*22C>A; mutant; mut) were subcloned downstream of the Ren-luc gene. * indicates the position of the mutation (c.*22C>A); (pA): poly(A) signal

Either four tandem repeats (to increase the effect) or a single unit of an 80 bp sequence around *GFPT1* c.*22 with C (wt) or A (c.*22C>A; mut) were subcloned downstream of the luciferase gene (Figure 28). RNAfold programme was used to avoid the occurrence of secondary RNA structures that might interfere with miRNA binding due to secondary structures of the tandem repeats.

4.3.4.1 Reporter assay for testing the interaction between putative regulatory miRNA miR-600 and mutant GFPT1

Reporter gene assays are widely used to study gene expression. The dual-luciferase reporter assay enables the simultaneous expression of the *Renilla* and firefly luciferase. While the partial *GFPT1* 3'-UTR (wt and c.*22C>A) was cloned downstream of the *Renilla* luciferase gene (Figure 24), an empty firefly luciferase reporter vector was used as control. After cell lysis, the firefly luminescent signal is measured first by adding the appropriate reagent. After quantifying this luminescence, the reaction is quenched, and the *Renilla* luciferase reaction is initiated. In order to

correct for vector-dependent unspecific effects relative reporter activity was obtained by normalization to firefly luciferase activity. MiR-mimics are double-stranded miRNA-like RNA fragments. Once introduced into the cell, this small RNA fragment mimics an endogenous miRNA, binds to its target gene and leads to posttranscriptonal repression of the gene [132, 133].
Reporter gene vectors and the appropriate miR-mimic (or control) were transiently transfected into COS-7 cells and the *Renilla* luciferase relative to the firefly luciferase activity was measured. Since COS-7 cells do not express miR-206 endogenously, miR-206 levels can be easily titrated by transfection with a cognate miRNA expression vector, and this cell line was chosen for reporter assay experiments [134]. Likewise, the microRNA miR-600 is not abundant in COS cells either.

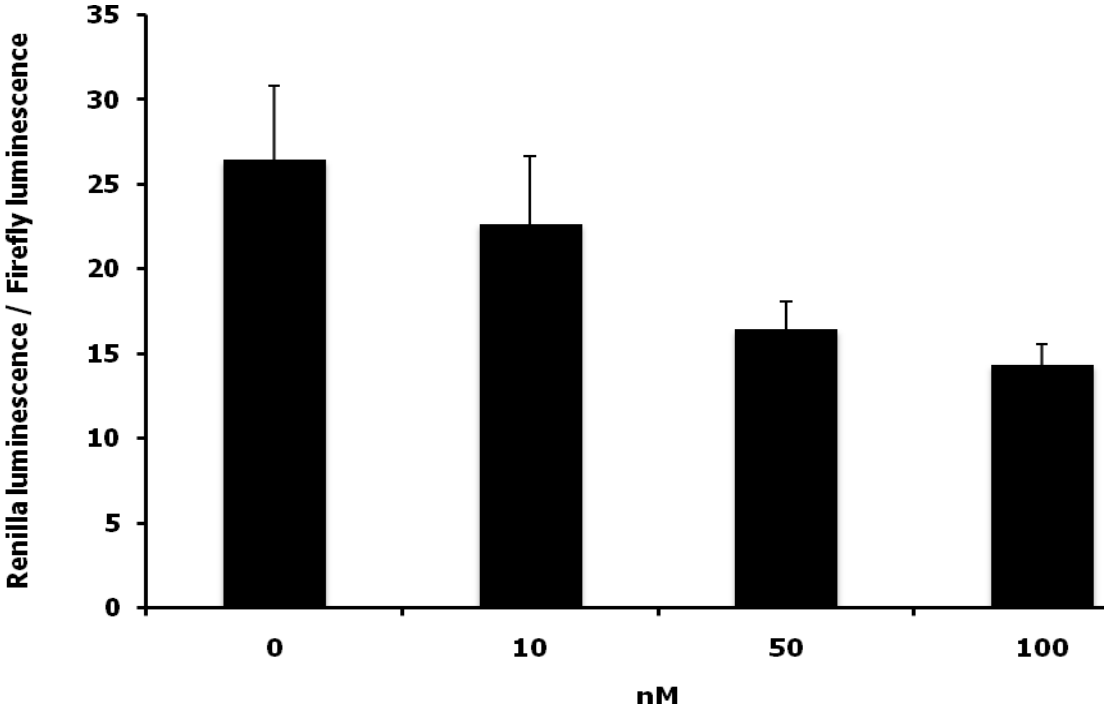

Figure 29: Renilla-to-firefly luminescence ratios
Renilla-to-firefly luminescence ratios observed when co-transfecting COS-7 cells with the luciferase reporter pRL-4xA (mut) with either 0, 10, 50 or 100 nM miR-600. Error bars indicate +SD obtained from three replicates.

In order to find the right miR-600 concentration for further experiments, dose-response experiments of the pRL-4xA (mut) construct and the miR-600 (either 0, 10, 50 or 100 nM) were performed. The highest effect (reduction of the signal to ~ 50 %) was achieved with 100 nM miR-600 (Figure 29).

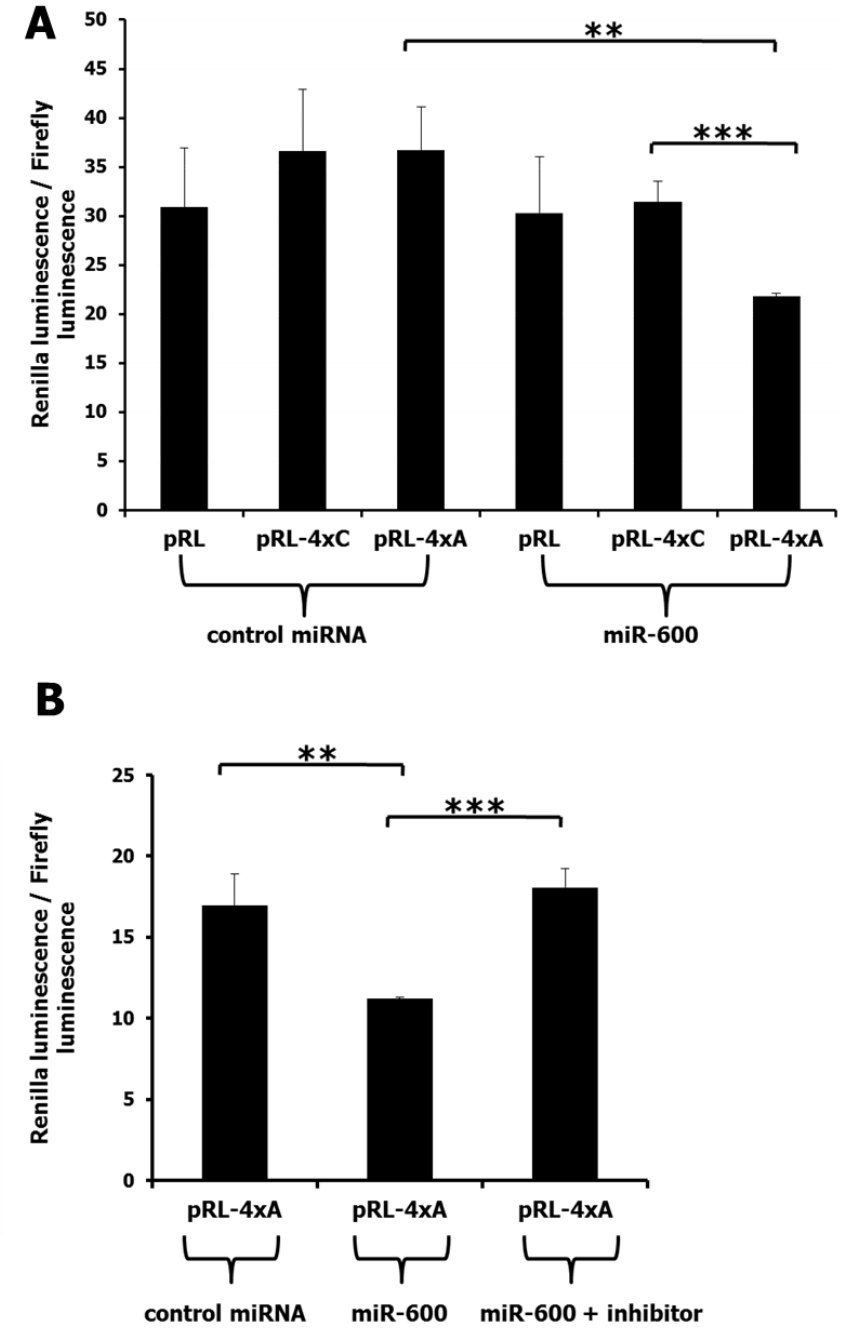

Figure 30: Renilla-to-firefly luminescene ratios

Renilla-to-firefly luminescence ratios observed when co-transfecting COS-7 cells with the indicated luciferase reporter (pRL, pRL4xC or pRL4xA) and either 100 nM control miRNA, 100 nM miR-600 (A) or 300 nM miR-600 inhibitor (B). Error bars indicate +SD obtained from three replicates. *: $P < 0.05$; ***: $P < 0.001$; **: $P < 0.01$.

In agreement with the prediction that miRNA miR-600 downregulates the expression of *GFPT1* c.22*C>A, co-transfection of the reporter constructs (pRL, pRL4xC or pRL4xA) with the miR-600 led to a highly significant reduction of the pRL-4xA (mut) signal to ~ 66 % of the signal obtained with pRL-4xC (wt) or the unmodified pRL (Figure 30 A). On the other hand, when co-transfecting

the same reporter constructs with a control miRNA, there was no significant difference between luminescence obtained with pRL-4xC, pRL-4xA or unmodified pRL. The pRL-4xA (mut) signal co-transfected with the miR-600 was significantly decreased to ~ 57 % of the signal obtained with the pRL-4xA (mut) construct co-transfected with the control miRNA. As opposed to this, co-transfection of miR-600 had no significant effect on the pRL-4xC (wt) signal compared to control miRNA.

Addition of a miR-600 inhibitor to cells co-transfected with the pRL-4xA (mut) construct and miR-600 restored the signal to the level obtained with the pRL-4xA (mut) construct co-transfected with the control miRNA (Figure 30 B).

These results indicate that miR-600 specifically repressed luciferase activity of mutant constructs containing the c.*22C>A but had no effect on the wild-type sequence. Moreover, derepression was obtained with an inhibitor against miR-600.

The experiments were repeated with luciferase vectors into which a single transcript unit of an 80bp sequence around *GFPT1* c.*22 with either C (wt) or A (c.*22C>A; mut) was subcloned, creating constructs pRL-1xC (wt) and pRL-1xA (mut) respectively (Figure 28).

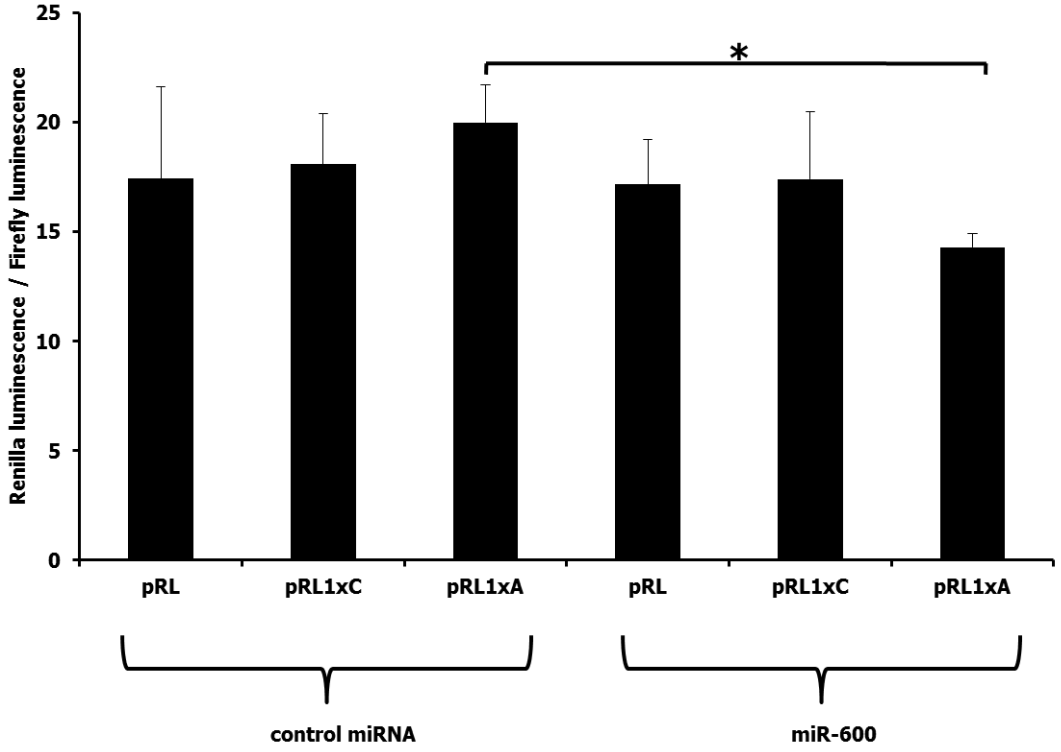

Figure 31: Renilla-to-firely luminescence ratios

Renilla-to-firefly luminescence ratios observed when co-transfecting COS-7 cells with the indicated luciferase reporter (pRL, pRL1xC or pRL1xA) and either 100 nM control miRNA or miR-600. Error bars indicate +SD obtained from three replicates. *: $P < 0.05$.

The signal obtained from pRL-1xC (wild-type) did not change when COS7 cells were co-transfected with control miRNA and miR-600, whereas a significant reduction of the pRL-1xA (mutant) signal was obtained in cells co-transfected with miR-600 compared to cells cotransfected with control miRNA (decrease to ~ 70 %) (Figure 31). However, stronger effects were achieved with the tandem constructs (4xC or 4xA).

4.3.4.2 Reporter assay for testing the interaction between putative regulatory miRNA miR-206 and mutant GFPT1*

Similar to the experimental setup for the miR-600, the dose-response between the pRL-1xA (mut) reporter construct and miR-206* was determined for further experiments. The reporter gene vector pRL-1xA (mut) and the miR-206* mimic (or control) were transiently transfected into COS-7 cells and the *Renilla* luciferase relative to the Firefly luciferase activity was measured.

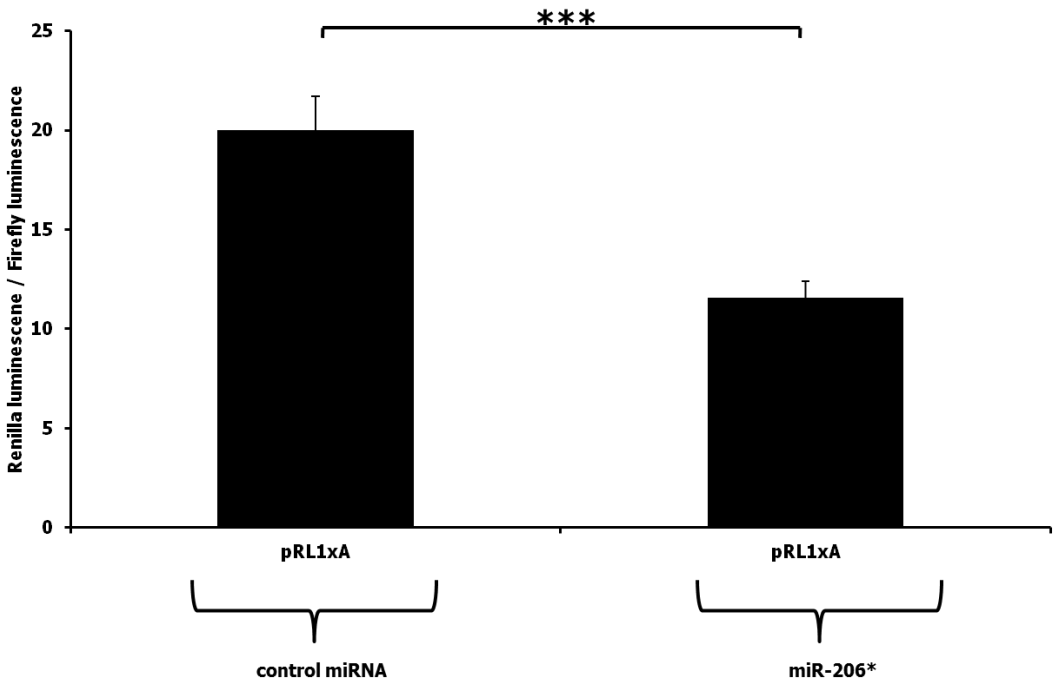

Figure 32: Renilla-to-firefly luminescence ratios

Renilla-to-firefly luminescence ratios observed when co-transfecting COS-7 cells with the luciferase reporter pRL-1xA (mut) and 100 nM miR-206*. Error bars indicate +SD obtained from three replicates.

In agreement with the prediction that miRNA miR-206* downregulates the expression of mutant *GFPT1*, co-transfection of the reporter construct pRL1xA (mut) with 100 nM miR-206* led to a highly significant reduction of the pRL-1xA (mut) signal to ~ 58 % of the signal obtained with

pRL-1xA co-transfected with the control miRNA (Figure 32). This miR-206* concentration was kept for the following experiments.

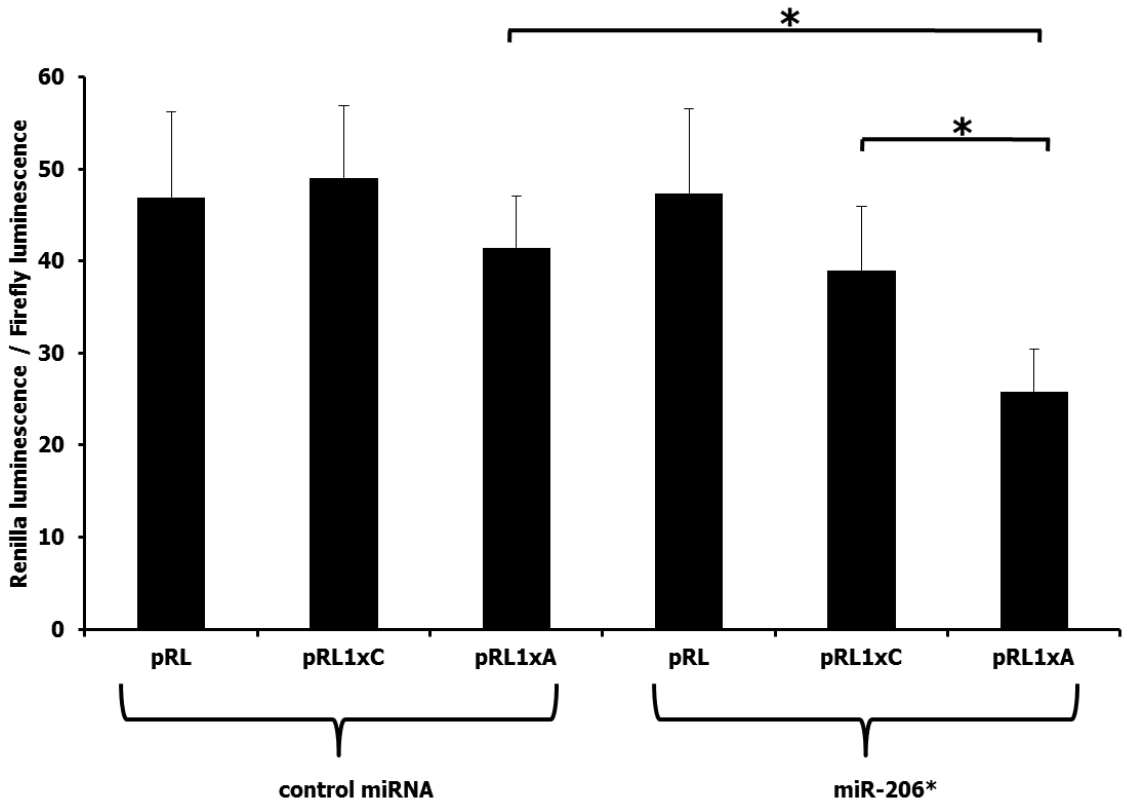

Figure 33: Renilla-to-firefly luminescence ratios

Renilla-to-firefly luminescence ratios observed when co-transfecting COS-7 cells with the indicated luciferase reporter (pRL, pRL1xC or pRL1xA) and either 100 nM control miRNA or miR-206* oligonucleotide. Error bars indicate +SD obtained from three replicates. *: $P < 0.05$; ***: $P < 0.001$; **: $P < 0.01$.

When co-transfecting the reporter constructs (pRL, pRL1xC or pRL1xA) with miR-206*, a significant reduction of pRL-1xA (mut) signal to ~66 % of the signal obtained with pRL-1xC (wt) was observed (Figure 33). On the other hand, when the same reporter constructs were co-transfected with a control miRNA, no significant difference between luminescence was obtained for pRL-1xC or pRL-1xA. Co-transfection of pRL1xA (mut) and miR-206* yielded ~61 % of the signal obtained with the pRL-1xA (mut) construct co-transfected with the control miRNA. As opposed to that, pRL-1xC (wt) showed similar signals when expressed together with miR-206* or control miRNA. Altogether, the results indicate that miR-206* repressed luciferase activity only in case of mutant constructs containing the c.*22C>A site.

H Discussion

1 Identification of mutations in the *GFPT1* gene in LG-CMS patients

Limb-girdle congenital myasthenic syndrome (LG-CMS) is an autosomal recessively inherited subform of CMS and a long-recognized entity in the clinical literature [135]. This type of CMS is characterized by prominent proximal muscle weakness. Over the past years it became apparent that LG-CMS is a less homogeneous entity than previously thought. At least two subgroups of LG-CMS patients have now been recognized. Mutations in the *DOK7* gene were identified as underlying genetic defect in one subgroup of LG-CMS patients who do not show tubular aggregates in muscle biopsies and do not benefit from acetylcholinesterase (AChE) inhibitor treatment [49, 136-138]. The other subgroup responds well to AChE inhibitors and muscle biopsies are characterized by the presence of tubular aggregates. Although the identification of the molecular defect is of paramount importance as it has direct impact on the clinical management of CMS patients, the genetic basis for AChE inhibitor-responsive LG-CMS with tubular aggregates has remained unidentified until now.

In order to identify the underlying genetic defect, we made use of our collection of LG-CMS families and performed genome-wide linkage analysis. The genome scan mapped the LG-CMS locus on chromosome 2 (2p12-p15) and sequencing of different genes at this locus in selected index patients revealed mutations in the *GFPT1* gene. In total, 18 different *GFPT1* mutations consisting of 13 missense mutations, three frameshift mutations, one nonsense mutation and one in the 3'-UTR were found in 13 out of the 16 LG-CMS families included in the initial study that lead to the identification of *GFPT1* as a new CMS gene (Table 15 and figure 7) [65].

In addition, *GFPT1* mutation screening in 15 isolated CMS patients yielded three additional novel GFPT1 missense mutations (p.S213N, p.G354R, p.S191I; Figure 10) in three LG-CMS patients. The disease causing effect of these mutations on the GFPT1 protein was predicted by the MutationTaster algorithm (http://www.mutationtaster.org) [122]. The mutations are not listed in the Exome Variant Server (http://evs.gs.washington.edu/EVS/). The parents of these patients carried mutations in the heterozygous state. One further missense change (p.S191I) was identified heterozygously in a patient without second mutation. Autosomal dominant inheritance was excluded since the healthy father of this patient (patient 3) carried the mutation heterozygously, too. This change might still be a polymorphism or the second mutation was not detectable by standard exon sequencing of genomic DNA. The analysis of the cDNA reverse

transcribed from muscle RNA of this patient (Figure 11) revealed no second mutation. Sequencing of the entire UTRs of the *GFPT1* gene might be necessary to further clarify the genetic defect of this patient (patient 3).

Up to now, the identified *GFPT1* missense or frameshift mutations are spread over the whole gene and affect the glutaminase as well as the sugar isomerase domain (Figure 7 and figure 10). There seems to be no mutation hot-spot in the *GFPT1* gene. In contrast, common mutations are well known in other CMS genes. For instance, the overwhelming majority of *DOK7* patients harbor the common frame-shift mutation c.1124_1127dupTGCC; p.Pro376ProfsX30 in exon 7 on at least one allele [19]. Common mutations are also known for the CMS genes *CHRNE* (c.1267delG; exon 12, founder mutation in South-Eastern Europe) [139] and *RAPSN* (p.Asn88Lys; exon 2, founder mutation in patients from Central Europe) [140].

1.1 Novel pathomechanism in CMS characterized by the defect in glycosylation due to GFPT1 mutations

The GFPT1 enzyme is extremely well conserved among species. It catalyses the first and rate-limiting step of the hexosamine synthesis pathway (Figure 3), transferring an amino group from glutamine to fructose-6-phosphate, to produce glucosamine-6-phosphate and glutamate. Glucosamine-6-phosphate is subsequently used to synthesise uridine diphospho-N-acetylglucosamine (UDP-GlcNAc), UDP-N-acetylgalactosamine, and cytidine monophospho (CMP)-sialic acid. These molecules are essential components for the glycosylation of proteins and lipids.
The enzyme GFPT1 and the HBP are known to be implicated in signaling pathways that may become deregulated in diseases of the immune system, cancer, diabetes mellitus, cardiovascular disease and neurodegenerative diseases [97, 141]. However, GFPT1 mutations had not previously been linked to a human disease and implicate a novel pathomechanism (impaired glycosylation) for NMJ disorders. Many key proteins of the NMJ are glycosylated [142] including AChR subunits, agrin, MuSK, dystroglycan and integrins. Furthermore, several proteins are known to be *O*-GlcNAc-modified in skeletal muscle including contractile proteins such as actin and myosin [143], but also glycolytic enzymes, signal transduction proteins and heat-shock proteins [144, 145]. In addition, it is assumed that *O*-GlcNAc variations could control the muscle protein homeostasis and could be implicated in the regulation of muscular atrophy [145].
Interestingly, a missense mutation in the epsilon subunit of the AChR (p.S143L) is located at one of the *N*-glycosylation sites of this protein and causes CMS by preventing AChR expression at the cell surface [146]. Besides, the treatment with an inhibitor of protein glycosylation (tunicamycin)

as well as *in vitro* mutations of AChR subunits that prevent glycosylation reduce the cell surface expression of AChR either through a failure in efficient assembly of the pentameric AChR or through a decrease of metabolic stability [147]. Indicating that aberrant glycosylation of NMJ proteins may lead to loss of expression of the respective protein.

In skeletal and heart muscle, the predominant splice variant is called *GFPT1-L* or muscle-specific variant. These variant has a 54 bp insertion compared to the shorter ubiquitous splice variant *GFPT1* [73].

As glycosylation is essential for cell survival, complete loss of the GFPT1 protein would likely be detrimental for organs like kidney, pancreas and liver where GFPT1 is the only or predominant isoform [73]. For that reason, *GFPT1* germline mutations causing LG-CMS are expected to create hypomorphic alleles with a residual function of the enzyme rather than resulting in complete loss-of-function. This is in line with the observation that none of the *GFPT1* patients (LGM1-16 and patient 1-4) carried two null mutations in the exons 1-19 (constitutive exons) of the *GFPT1* gene (Figure 7 and Figure 10). The homozygous p.Trp240X mutation (likely to result in severely truncated GFPT1 or no protein at all) occurs in an alternative exon (exon 8A; Figure 7), exclusively incorporated in the predominant GFPT1 species in striated muscle (GFPT1-L), and is therefore supposed to lead to decreased GFPT1 levels only in heart and skeletal muscle.

Something similar is known from CMS patients with mutations in the subunits of the AChR which account for about 50 % of CMS in a cohort of 295 patients [15], indicating that there is a correlation between the expression profile of a gene and the severity of mutations in this gene. Patients harboring null mutations in both alleles of the α-, β-, or δ-AChR subunits are rare and they have a very severe course of the disease with high fatality [15, 17]. In contrast, patients harboring null mutations in both alleles of the AChR ε-subunit generally have only mild symptoms. An explanation might be that the expression of the fetal γ-subunit partially compensates for the absence of the ε-subunit and rescues the phenotype [37, 148].

1.2 Genotype-phenotype correlations

GFPT1 mutations are associated with a myasthenic syndrome (which can be confirmed by repetitive nerve stimulation (RNS)), limb-girdle weakness, response to AChE-inhibitor therapy and tubular aggregates (TAs) in muscle biopsies whereas facial weakness, respiratory difficulties, ophthalmoparesis and ptosis are usually absent. TAs in muscle biopsies are not an obligatory finding in patients with GFPT1 mutations. The present data also confirm earlier observations, that the genetic causes of TAs are heterogeneous: Sequencing of the three patients with LG-CMS and tubular aggregates (families LGM4, 15 and 16 described in [149]; Figure 6) did not reveal *GFPT1*

mutations. Moreover, four patients without a myasthenic syndrome but with TAs in muscle biopsies did not reveal *GFPT1* mutations either. This finding is in line with the fact that the functional significance of TAs in skeletal muscle has not yet been fully understood. It is unknown whether they represent pathological structures or compensatory reactions to diverse pathogenic events such as periodic paralysis, dyskalaemia, intoxication, inflammatory myopathies, cramps and myalgias, myotonia congenita, familial myopathies, and several other myopathies of uncertain etiology [68, 69]. TAs were initially thought to originate from mitochondria. However, work of several groups has shown that TAs rather arise from the sarcoplasmatic reticulum [70]. Patients with TAs but without *GFPT1* mutations may still carry cryptic mutations in *GFPT1* which are not detectable by standard exon sequencing of genomic DNA, or they may carry mutations in other, yet unknown genes. Genes encoding enzymes of the HBP pathway downstream of GFPT1 might be novel candidates for *GFPT1*-negative LG-CMS patients (LGM4, 15 and 16) or cases with TA myopathy.

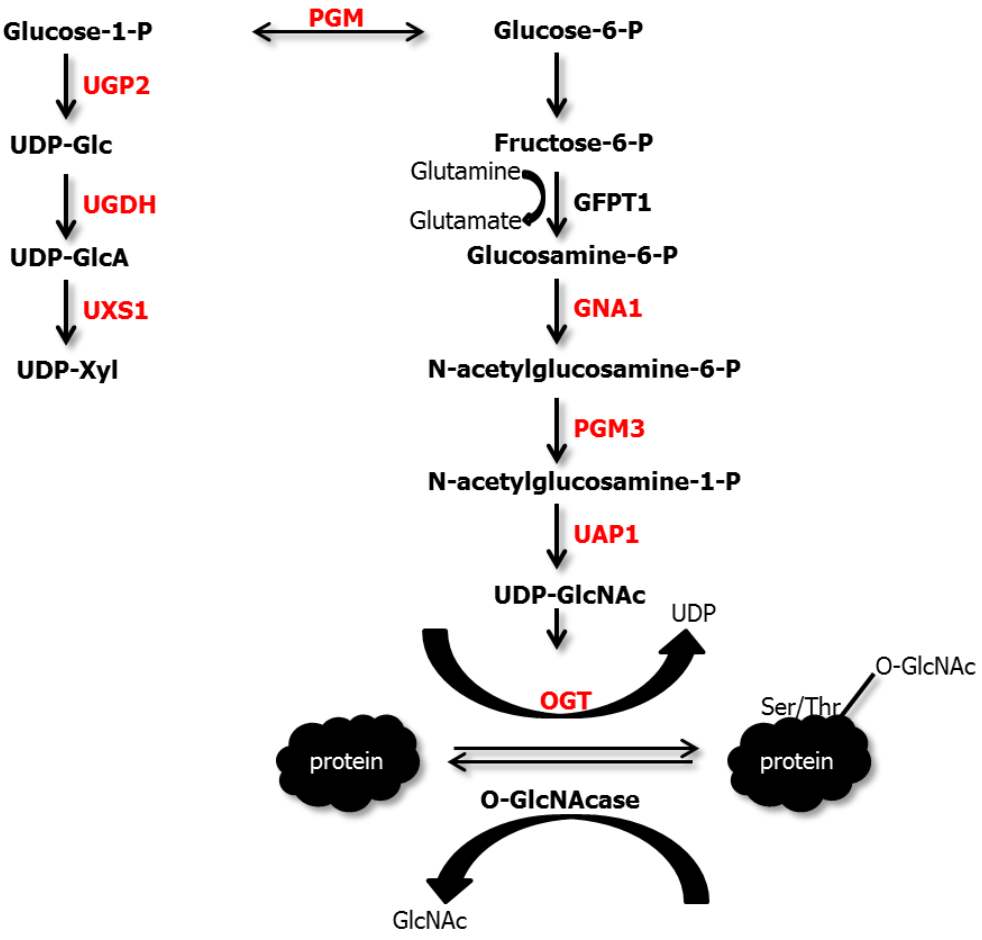

Figure 34: Synthesis pathways for the formation of UDP-sugars

Potential candidate genes for CMS are in red. The figure was adapted and modified from [85, 150].

GFPT1 is the key and rate-limiting enzyme for UDP-GlcNAc biosynthesis, the end product of hexosamine biosynthesis pathway. This pathway involves other enzymes which might be potential candidate genes for CMS. The genes coding for the HBP enzymes Glucosamine-6-phosphate N-acetyltransferase 1 (GNA1, location of the gene: 14q22.1), phosphoglucomutase 3 (PGM3, location of the gene: 6q14.1-q15), UDP-N-acteylglucosamine pyrophosphorylase 1 (UAP1, location of the gene: 1q23.3) and O-linked GlcNAc transferase (OGT, location of the gene: Xq13) might be putative novel CMS candidates (Figure 34).
On the other hand, potential candidate genes might emerge from a second synthesis pathway for formation of UDP-sugars which are also needed for the synthesis of proteoglycans. The end product of this pathway is UDP-xylose (UDP-Xyl) which is a sugar donor for the synthesis of proteoglycans in mammals [151, 152]. Candidates might be genes coding for enzymes like UDP-glucose pyrophosphorylase 2 (UGP2, location of the gene: 2p14-p13), UDP-glucose 6-dehydrogenase (UGDH, location of the gene: 4p15.1) and UDP-glucuronate decarboxylase 1 (UXS1, location of the gene: 2q12.2).

2 Effects of GFPT1 missense mutations on different protein features

2.1 Mutant GFPT1 expression and localization

Analysis of GFPT1 expression in cultured primary myoblasts and in a muscle biopsy, from GFPT1 patients revealed reduced GFPT1 protein levels compared to controls (Figure 13) [65]. To study the effect of the mutations at the protein level in a controlled experiment, plasmid constructs were generated to express wild-type and mutant myc-tagged GFPT1-L (muscle-specific variant) protein (p.Arg111Cys, p.Asp43Val, p.Met492Thr, p.Thr15Ala, p.Asp348Thr, p.Arg434His and p.Ile121Thr) in HEK293 cells. Immunoblot analysis was performed of the myc-tagged GFPT1-L protein. HEK293 cells also express endogeneous GFPT1 but its effect was negligible due to the overexpression of transfected *GFPT1* and use of an anti-myc antibody which only detects GFPT1 derived from the transfected constructs. Comparison of total GFPT1 amounts in HEK293 cells transfected with either wild-type or mutant *GFPT1* constructs showed a reduction of GFPT1 expression to 83 % of p.Arg111Cys, 58 % of p.Asp43Val and 73 % of p.Met492Thr compared to the wild-type GFPT1 amount (Figure 15 and 16). The mutants p.Thr15Ala, p.Asp348Thr, p.Arg434His and p.Ile121Thr had no effect on protein expression (Figure 15 and16). In contrast to the analysis of the GFPT1 expression in LG-CMS patients, the *in vitro* transfection studies (Figure 15 and 16) revealed only a small effect of the missense mutations p.Arg111Cys,

p.Asp43Val and p.Met492Thr on protein expression. Compared to the wild-type, the protein levels of the mutants were not reduced below 50 %. One explanation might be that for transfection studies, the human cytomegalovirus immediate-early gene (CMV) promoter was used instead of the endogenous eukaryotic *GFPT1* promoter. The CMV promoter induces high-level expression in a variety of mammalian cell lines and is probably the most widely used promoter for mammalian expression [153]. The artificial high-level expression of the GFPT1 mutants might be the reason for the small effect of the missense mutations on the GFPT1 protein levels observed by the transfection studies. The use of a promoter region derived from the human skeletal α-actin (HSA) gene which is specifically expressed in striated muscles, heart and skeletal muscle and which allows low-level expression [154, 155] might overcome this artificial situation.
The subcellular localization of mutant GFPT1 species (p.Thr15Ala, p.Asp43Val, p.Arg111Cys, p.Ile121Thr, p.Asp348Tyr, p.Arg434His and p.Met492Thr), transiently expressed in SW13 cells was almost identical to that of wild-type GFPT1 (Figure 17). Altogether, reduced expression of mutant GFPT1 protein species is a likely molecular pathomechanism although I could not confirm these data in *in vitro* transfection studies.

2.1.1 Reduced GFPT1 amounts result in reduced *O*-GlcNAc modification

Two experimental approaches link reduced amounts of functional GFPT1 protein to reduced levels of *O*-GlcNAc modified proteins. Immunoblot analysis of muscle and myoblast lysates of *GFPT1* patients and controls with the RL2 antibody, which selectively detects *O*-GlcNAc residues on proteins, showed that *O*-GlcNAcylated proteins were markedly decreased in lysates from the patients' myoblasts and muscle biopsies (Figure 13) [65]. In addition, knockdown of *Gfpt1* expression in C2C12 cells treated with *Gfpt1* siRNA also resulted in a reduction of the levels of *O*-linked N-acetylglucosamine on proteins (Figure 14). This is in line with earlier observations of others: blockage of GFPT using pharmacological and antisense strategies resulted in a decreased RL2 signal on intracellular proteins in Rat aortic smooth muscle (RASM) cells [156]. The prominent protein band that is differentially *O*-GlcNAcylated in immunoblots in both experiments (Figure 13 and Figure 14) is most likely heat shock protein 70 (Hsp70). Hsp70 has been shown to be *O*-GlcNAcylated in L6 myotubes (a model of skeletal muscle) [157].

Altered protein glycosylation is a new potential pathomechanism underlying defects of NMJ transmission in LG-CMS patients. It is likely that GFPT1 deficiency does not only influence *O*-GlcNAcylation of intracellular proteins but may also directly affect clustering of the ACh receptor (AChR) and the structure of the NMJ. It has been shown that correct glycosylation of agrin and MuSK is necessary to induce clustering of AChRs at the NMJ [158-160]. Furthermore, a mutation

in the ε-subunit of the AChR (p.S143L) is located at one of its *N*-glycosylation sites [146]. It could be shown that this mutation causes CMS by preventing AChR expression at the cell surface which indicates that aberrant glycosylation of NMJ proteins may lead to loss of expression of the respective protein and thereby to a neuromuscular disorder.

Defects in *O*-GlcNAcylation have also been described in other pathologies, including Alzheimer's disease. Several proteins that have been thought to be involved in this neurodegenerative disease (e.g. tau and the β-amyloid precursor protein) are modified by *O*-GlcNAc and there is some evidence that reduced *O*-GlcNAc levels are associated with the disease [161].

2.2 Mutant GFPT1 enzyme activity

GFPT1 catalyses the first step in *de novo* biosynthesis of hexosamines. To analyse the impact of mutations on GFPT1 enzymatic activity, the wild-type long isoform GFPT1-L containing a striated muscle-specific 18 amino acid insert was cloned into an expression vectors. Different *GFPT1* mutants were generated by site directed mutagenesis. Heterologous protein expression of the GFPT1 mutants p.Thr15Ala, p.Asp43Val and p.Asp348Tyr in HEK293 cells had only small effects on enzymatic activity and the mutations p.Arg111Cys and p.Arg43His had no effect at all (Figure 19). Based on the structural model of the *Escherichia coli* ortholog for GFPT1 (GlmS) and the crystal structure of the isomerase domain of human GFPT1 [80], no functional consequences can be predicted for the GFPT1 missense mutations analysed in this study. Consistently, no gross changes in enzyme activity were observed for GFPT1 mutants by the glutamate dehydrogenase (GDH) assay (Figure 19).

It is still conceivable that use of an alternative enzymatic assay might reveal activity changes of GFPT1 mutants. Three methods have been developed to measure the GFPT1 enzyme activity. In the present study, the glutamate dehydrogenase (GDH) method has been used. This method allows continuous determination of the GFPT1 activity with limited effort but also with less specificity. As the glutamate production is not always coupled to the amidotransferase activity of GFPT1, the GDH method has its limitations in screening inhibitors of the fructose-6-phosphate binding site of GFPT1 [162]. This method has been used since our laboratory was fully equipped with all required facilities.

The most frequently used assay is the highly specific and relatively sensitive Elson-Morgan method [163, 164]. It is based on *N*-acetylation of the amino sugar phosphate, incubation in alkaline potassium tetraborate solution and condensation with *p*-dimethylaminobenzaldeyde. The third step leads to the formation of a purple product which has the absorption maximum at 595 nm. The third method is the most sensitive one and based on a radiometric assay [165] which

allows the determination of picomolar amounts of GFPT1. However, this assay is very laborious and technically demanding.

3 A 3'-UTR mutation creates a microRNA target site in the *GFPT1* gene of LG-CMS patients

3'-untranslated regions (UTRs) are involved in diverse regulatory roles at multiple levels. They play an important role in gene expression regulation by determination of mRNA stability/degradation, subcellular localization, nuclear export and translation efficiency [166-168]. The analysis of 3'-UTRs of some 17,700 human genes identified about 100 highly conserved motifs in human 3'-UTRs by comparison of several mammals. Many of them (about one-half) turned out to be microRNA target sites and the results suggested that at least 20 % of human genes are regulated by miRNAs [169]. Currently, mutations within proximal gene regulatory regions comprises only approximately 1.7 % of known mutations associated with human inherited disease [170]. However, this might be an underestimation as 3'-UTRs are less likely to be sequenced for mutations in research testing or routine diagnostic procedures especially if they are large.

One of the identified *GFPT1* mutations in four independent families from Spain (LGM5 and 12) and Germany (LGM9 and patient 4) was a 3'-UTR mutation c.*22C>A. In all four families, the mutation was compound heterozygous to missense or protein truncating mutations. The c.*22C>A variant lies 22 bp after the TGA translation termination codon in the 3'-UTR of the *GFPT1* gene. Western blot analysis revealed that GFPT1 mutations generally lead to reduced GFPT1 protein levels in patient muscle and cultured muscle cells [65] and this was observed for patients of LGM5 and LGM9 with the c.*22C>A mutation as well (Figure 13). Nevertheless, the pathogenic mechanism of the c.*22C>A mutation which is located after the open reading frame (ORF) (Figure 20) of *GFPT1* remained unclear. Transfection experiments in C2C12 cells linked the 3'-UTR mutation directly to a reduced GFPT1 protein level in a controlled experiment (Figure 23 A). Compared to wild-type, the expression level of the mutant construct was reduced to 36 % (Figure 23 B). Several expression regulation mechanisms have to be taken into account in order to further clarify the pathomechanism of the 3'-UTR mutation.

One mechanism of expression regulation is based on miRNA binding to its target mRNA. These small non-coding RNAs participate in post-transcriptional regulation through imperfect sequence complementarity to the 3'-untranslated regions of the target mRNAs. The binding results in translational repression through the degradation of the mRNA or translational inhibition [171]. Encoded by nuclear DNA, primary miRNAs (pri-miRNAs) are processed to precursor miRNA (pre-

miRNA) hairpins and transported to the cytoplasm where they are cleaved by Dicer, resulting in miRNA duplexes of about 21-23 nucleotides. Subsequently, the strands are selectively loaded into the RNA-induced silencing complex (RISC) [171, 172]. Strand selection correlates with the thermodynamic stability of each end of the duplex [173-175]. The more abundant and biologically active strand is called miRNA, whereas its less abundant partner and inactive strand is known as the star-form miRNA (miRNA*) [172, 176]. Since the star-form is rarely expressed, the functions of the miRNA* have not been taken into account [177]. However, recent studies revealed that some miRNA* species are relatively abundant in total RNA and that the star-form miRNAs may also have an important regulatory function [176-178]. In addition, miRNA/miRNA* ratios seems to vary dramatically among developmental stages [174, 179, 180].
In this study, the pathogenic effects of the c.*22C>A mutation in the 3'-UTR of the *GFPT1* gene was investigated and the hypothesis that this mutation might interfere with microRNA-mediated gene regulation was confirmed.

3.1 The *GFPT1* 3'-UTR mutation leads to the gain of a putative binding site for microRNAs

Computer algorithms predicted that miR-600 and miR-206* would bind to the mutant *GFPT1* mRNA. The predicted microRNA binding site is present in the *GFPT1* 3'-UTR and alignments of the 3'-UTR of *GFPT1* mRNA and the predicted microRNAs confirmed increased probability for miRNA binding to the mutant mRNA (Figure 24). The predicted miR-600 site in *GFPT1* mutant 3'-UTR is a 7mer-A1 seed match type (an exact match to positions 2-7 of the mature miRNA followed by an Adenine; Figure 24). Four types of seed-matched sites are known to be selectively conserved [181]: 6mer, 7mer-m8, 7mer-A1 and the 8mer site with the following hierarchy of site efficacy: 8mer > 7mer-m8 > 7mer-A1 > 6mer [182, 183]. Although there is no perfect miR-206*:mutant *GFPT1* mRNA seed matching (position 2-7 of the mature miRNA) there seems to be a compensatory base pairing site in the 3' region of the miR-206* (Figure 24). Perfect miRNA seed matches are often necessary and sufficient for target regulation [184-187] and they are the basis of most of the genome wide predictions of miRNA binding sites [188-190]. However, recent studies presented 3'-supplementary, 3'-compensatory pairing and "centered sites" as new classes of microRNA target sites [182, 191]. The 5' region of the microRNA, containing the seed region, is the most highly conserved region of the mature miRNA and it is therefore the most important site for target recognition [188, 192]. The next most highly conserved region spans from nucleotides 13 to 16. It is the region most important for 3'-supplementary and 3'-compensatory

pairing [182]. Centered sites lack both, perfect seed pairing and 3'-compensatory pairing, and instead have 11–12 contiguous Watson–Crick pairs to the center of the microRNA [191].

3.1.1 Dual-luciferase reporter assays support the hypothesis that the *GFPT1* 3'-UTR mutation c.*22C>A leads to reduced GFPT1 protein amounts

In order to test the interaction between the mutant *GFPT1* transcript and the microRNAs directly, dual-luciferase reporter assays were performed. COS-7 cells were co-transfected with control miRNA, miR-600 or miR-206* mimics and reporter constructs containing wild-type or mutant *GFPT1* 3'-UTR sequences downstream of a luciferase reporter gene. In agreement with the predictions the mutant reporter constructs co-transfected with either miR-600 or miR-206* yielded significantly diminished reporter signals compared to the signal obtained by co-transfection with the control miRNA (Figure 30 A and 33). Therefore, the results support a model in which the point mutation c.*22C>A in the *GFPT1* 3'-UTR creates a target site for two miRNAs, miR-600 and miR-206*, which influence *GFPT1* expression.

Up to now, there are only a few examples which link gene expression regulation through miRNAs and human diseases. A mutation in the 3'-UTR of the *HDAC6* gene located in the seed region of hsa-mir-433 has been shown to abolish post-transcriptional regulation in a patient with X-linked chondrodysplasia [193]. In patients with Tourette syndrome, a variant in the 3'-UTR of the *SLITRK1* gene was found to create a hsa-miR-189 binding site with higher affinity leading to repression of *SLITRK1* expression [194]. Furthermore, miRNAs (miR-140 and miR-691) might be involved in the pathogenesis of hereditary spastic paraplegia (HSP) as they regulate expression of the HSP gene *REEP1* [195, 196]. In the future, the identification of functional miRNA targets could greatly benefit from new assays based on crosslinking immunoprecipitation (HITS-CLIP). Recently, sequence analysis of RNAs isolated by HITS-CLIP has led to the identification of functional interaction sites [197].

3.2 Repression of translation results in reduced GFPT1 protein amounts in LG-CMS patients

Quantification of *GFPT1* mRNA levels in total RNA samples derived from myoblast and muscle samples of *GFPT1* patients compound heterozygous for c.*22C>A, and control individuals (Figure 21 and 22) indicates that the reduced amounts of GFPT1 protein levels in myoblast and muscle

lysates reported in the study (Figure 13) [65] resulted from repression of translation rather than altered mRNA stability. Compared to immunoblot results which revealed markedly reduced GFPT1 protein level in *GFPT1* patients (Figure 13), the effects on *GFPT1* mRNA level are less distinct (Figure 21 and 22). Therefore, control of translation might be rather the pathogenic effect of the mutation than degradation of the target mRNA. It has been shown that destabilization of target mRNA by microRNAs account for most (>/=84 %) of the reduced protein expression. This study indicates that altered mRNA levels might reflect the impact of miRNAs on gene expression [198]. Reduced GFPT1 protein levels seem to result from repression of translation rather than degradation of the mRNA. Although most miRNAs act through destabilization of target mRNA, other miRNAs have been shown to affect translation. In a recent study about 16 % of the analysed miRNAs decrease translational efficiency of the target mRNAs [198]. Furthermore, it has to be taken into account that the *GFPT1* patients (LGM 5 and 9) carry a 2nd *GFPT1* mutation on the other allele (Table 15) and that the reduced GFPT1 protein amounts (Figure 13) [65] and the effects on the mRNA level in myoblast (Figure 21) und muscle lysates (Figure 22) reflect the impact of both mutations.

3.3 c.*22C>A mutation allows for illegitimate binding of miRNA

Several results confirm that the c.*22C>A mutation in the 3'-UTR is a causative mutation resulting in reduced protein expression. First of all, the mutation (LGM5 and LGM9) was associated with reduced amounts of GFPT1 in lysates of patients' myoblast cells (Figure 13). Secondly, the mutation was found in four unrelated families (LGM5, 9, 12 and patient 4) and the c.*22C>A mutation was absent in a large number of control chromosomes [65]. Furthermore, experiments with expression constructs revealed a link between the 3'-UTR mutation and reduced GFPT1 protein amounts in C2C12 cells experimentally (Figure 23).

Impaired glycosylation due to reduced amounts of functional GFPT1 protein (observed in two experimental approaches, Figure 13 and Figure 14) is presumably the pathogenic mechanism of GFPT1 mutations. Therefore, the co-transfection studies of the mutant *GFPT1*-3'-UTR construct with the miR-600 expression vector which revealed a functional effect on protein glycosylation (Figure 25) strongly suggest that the c.*22C>A mutation is a causative mutation.

3.4 Potential role of miRNA-206* and miR-600 in skeletal muscle

MiR-206 has previously been shown to be strongly expressed in skeletal muscle and only rarely detectable in the heart [124-127, 199]. This skeletal muscle-specific expression of miR-206 sets it apart from the other myomiR (myo = muscle + miR = miRNA) family members [128]. So far, there is no information on the fate of its star-form miR-206* which I identified as a potential regulator of *GFPT1* expression from the c.22*C>A allele.

For the majority of miRNAs, only one strand (guide strand) of the double-stranded (ds) miRNA duplex is loaded into RISC while the other strand (star, *) is degraded rapidly [172, 200-202]. However, deep sequencing studies indicate that a large number of miRNA*s are loaded into the RISC and that the relative expression levels of the two strands vary widely among tissues [177, 203-206]. It was proposed that the relative instability of the duplex termini determines which strand will be loaded. If both termini of the miRNA have almost the same stability, both strands might be selected [172]. An alternative model is proposed for miRNAs for which the two selected strands do not make a perfect miRNA duplex (with 2 nt overhangs) with similar stability on both termini. In this situation, the mature miRNA sequence, especially at the 5′ end is no longer fixed [207].

To analyse the abundance of miR-206*, real-time qRT-PCR was performed of myoblast, myotube and muscle cDNA samples. Mature miR-206* is well detectable in muscle, myoblast and myotube samples obtained from *GFPT1* patients and control individuals (Figure 26 A and 27 A). MiR-206 is known to be a critical regulator of skeletal muscle differentiation and regeneration [129, 131, 208]. Recently, it has been shown that miR-206 is upregulated following muscle injury and it has been indicated that miR-206 slows progression of Duchenne muscular dystrophy [208]. The present thesis revealed that the miR-206* is also upregulated upon differentiation (Figure 27 A and B) and that both, the miR-206 and the star-form are more abundant in GFPT1 patients' myoblasts than in controls (Figure 27 A and B). One may speculate that upregulation of miR-206* is a similar generalized protective mechanism activated in diseased skeletal muscle. However, in the particular setting of the *GFPT1* 3'-UTR mutation allowing for improved binding of miR-206* this upregulation might initiate a vicious circle by further reducing the availability of functional GFPT1 in the cell instead of alleviating the disease process.

The miR-600 expression has been reported in human colorectal cells [130], but not in muscle so far. The results of the present study showed the presence of hsa-miR600 in human muscle obtained from a *GFPT1* patient heterozygous for c.*22C>A and c.1649C>T (Figure 26 B), suggesting a physiological role in the skeletal muscle. However, gel electrophoresis analysis of the PCR products revealed the presence of a second, non-specific fragment of approximately 110 base pairs in human myoblasts and C2C12 cells (Figure 26 B).

To date, several methods have been utilized for detection and quantification of miRNAs. They are largely based on cloning, northern blotting [209], or primer extension [210]. In this study, the 3'-end of the miRNAs were first tailed with a common sequence by the *E.coli* Poly(A) Polymerase (PAP) [211] and then reverse transcribed by using a universal primer consisting of an oligo(dT) sequence with an universal primer-binding sequence at its 5'-region. A qPCR assay was used to detect and quantify the specific miRNAs by a miRNA-specific and a universal primer. The qPCR products were detected by using SYBR Green. False positive signal may arise from closely related miRNAs, precursors and genomic sequences. For instance, the target sequence is present in the primary transcript and the precursor, in addition to the mature miRNA [212]. Furthermore, SYBR Green binds to all dsDNA, including unspecific products such as primer-dimers [213]. In future, the presence of the non-specific hsa-miR600 amplification product has to be elucidated by optimization of the used detection method or by the use of another method (e.g. TaqMan probes).

4 Expected consequences for human pathology diagnosis and therapy

In general, a precise molecular classification of CMS is of paramount importance for the diagnosis, counseling and therapy of a patient. The identification of the molecular defect has direct impact on the clinical management of CMS patients [214]. In this thesis, it has been shown that mutations in a gene encoding an enzyme of a glycosylation pathway (GFPT1) underlie a form of congenital myasthenia with a limb-girdle pattern of weakness. In other fields of medicine, congenital disorders of glycosylation (CDGs) have been recognized as a rapidly expanding group of inherited disorders with a large spectrum of multisystemic phenotypes that are mostly combined with severe central neurological impairment [215].

However, glycosylation defects have not been considered to be implicated in disturbed signal transmission at the neuromuscular junction. Therefore, further research into the role of glycosylation in neuromuscular transmission may help in understanding synaptic processes.

Thanks to its size and easy accessibility the NMJ is usually considered as a model synapse. Thus, understanding the correlation between inaccurate protein glycosylation and disturbed signal transmission at the neuromuscular junction might provide a helpful model for studying general aspects of glycosylation processes at central nervous system synapses. Although several findings suggest a postsynaptic origin of the neurotransmission defect in GFPT1 patients, it is important to clarify if it is indeed primarily postsynaptic or presynaptic, or a combination of pre- and postsynaptic abnormalities. This finding could be the basis for potential novel treatment options.

Traditionally, only 0.2 % of disease-associated mutations have been estimated to reside within 3'-UTR [216] but recent findings suggest a higher rate. The data of the present thesis point toward the importance of extending molecular genetic analyses to UTRs, especially when only one heterozygous mutation is found in a recessive disease. In turn, interfering with miR-600 and miR-206* activity could provide a therapeutic option for patients with the c.*22C>A mutation. Sponge constructs and/or antagomirs against miR-600 and miR-206* might be tested for recovering GFPT1 protein levels in muscle.

Administration of glucosamine might be an alternative treatment option for CMS patients with *GFPT1* mutations. Glucosamine enters the hexosamine pathway downstream of the rate-limiting step catalyzed by the GFPT1 enzyme. It has been shown that when GFPT1 is bypassed by glucosamine it is able to elevate the *O*-GlcNAc levels in 3T3-L1 adipocytes [217]. Another strategy could be the treatment with saturated fatty acids. It has been shown that *GFPT* mRNA expression in primary myotubes can be upregulated by addition of the saturated fatty acids palmitate and stearate [218].

Since the identification of the first CMS genes it has been recognized that biochemical studies of CMS-causing mutations may lead to a better understanding of the molecules involved in signal transmission at the NMJ and they may be useful to develop potential novel therapeutic approaches. This is especially true for the discovery of a defect in glycosylation as a previously unrecognized pathomechanism in a synaptic transmission disorder.

I Contributions

Declaration of contributions to "Identification of GFPT1 Mutation in LG-CMS patients"

Genome-wide linkage analysis using the Illumina 300 K chip (Illumina, San Diego, CA) was conducted by Dr. Tim-Matthias Strom (Munich, Germany) (Results 1.2). DNA sequencing of positional candidate genes was performed in collaboration with Prof. Dr. Jan Senderek's laboratory in Aachen, Germany (Results table 14; mutation analysis). I evaluated the clinical data (Results 1.1.1), analysed the pedigrees (Results 1.1.2) and performed the extended mutation screening in additional families in our cohort (Results 1.3). These data are published by Senderek *et al.*, 2011. For this publication, I also contributed the generation of the plasmid constructs used in this study (table 2), the enzyme activity assays (Results 3.1.3), the subcellular localization studies (Results 3.1.2) and the analysis of the results.

J References

1. Hughes, B.W., L.L. Kusner, and H.J. Kaminski, *Molecular architecture of the neuromuscular junction.* Muscle Nerve, 2006. **33**(4): p. 445-61.

2. Ferraro, E., F. Molinari, and L. Berghella, *Molecular control of neuromuscular junction development.* J Cachexia Sarcopenia Muscle, 2012. **3**(1): p. 13-23.

3. Barchi, R.L., J.C. Tanaka, and R.E. Furman, *Molecular characteristics and functional reconstitution of muscle voltage-sensitive sodium channels.* J Cell Biochem, 1984. **26**(3): p. 135-46.

4. Trimmer, J.S., et al., *Primary structure and functional expression of a mammalian skeletal muscle sodium channel.* Neuron, 1989. **3**(1): p. 33-49.

5. Bezakova, G. and M.A. Ruegg, *New insights into the roles of agrin.* Nat Rev Mol Cell Biol, 2003. **4**(4): p. 295-308.

6. Kim, N., et al., *Lrp4 is a receptor for Agrin and forms a complex with MuSK.* Cell, 2008. **135**(2): p. 334-42.

7. Zhang, B., et al., *LRP4 serves as a coreceptor of agrin.* Neuron, 2008. **60**(2): p. 285-97.

8. Glass, D.J., et al., *Agrin acts via a MuSK receptor complex.* Cell, 1996. **85**(4): p. 513-23.

9. Okada, K., et al., *The muscle protein Dok-7 is essential for neuromuscular synaptogenesis.* Science, 2006. **312**(5781): p. 1802-5.

10. Mittaud, P., et al., *A single pulse of agrin triggers a pathway that acts to cluster acetylcholine receptors.* Mol Cell Biol, 2004. **24**(18): p. 7841-54.

11. Borges, L.S., et al., *Identification of a motif in the acetylcholine receptor beta subunit whose phosphorylation regulates rapsyn association and postsynaptic receptor localization.* J Neurosci, 2008. **28**(45): p. 11468-76.

12. Gautam, M., et al., *Failure of postsynaptic specialization to develop at neuromuscular junctions of rapsyn-deficient mice.* Nature, 1995. **377**(6546): p. 232-6.

13. Punga, A.R. and M.A. Ruegg, *Signaling and aging at the neuromuscular synapse: lessons learnt from neuromuscular diseases.* Curr Opin Pharmacol, 2012.

14. Newsom-Davis, J., *The emerging diversity of neuromuscular junction disorders.* Acta Myol, 2007. **26**(1): p. 5-10.

15. Engel, A.G., et al., *What have we learned from the congenital myasthenic syndromes.* J Mol Neurosci, 2010. **40**(1-2): p. 143-53.

16. Muller, J.S., et al., *Congenital myasthenic syndromes: spotlight on genetic defects of neuromuscular transmission.* Expert Rev Mol Med, 2007. **9**(22): p. 1-20.

17. Engel, A.G., *Congenital myasthenic syndromes in 2012.* Curr Neurol Neurosci Rep, 2012. **12**(1): p. 92-101.

18. Parr, J.R., et al., *How common is childhood myasthenia? The UK incidence and prevalence of autoimmune and congenital myasthenia.* Arch Dis Child, 2014. **99**(6): p. 539-42.

19. Abicht, A., et al., *Congenital myasthenic syndromes: achievements and limitations of phenotype-guided gene-after-gene sequencing in diagnostic practice: a study of 680 patients.* Hum Mutat, 2012. **33**(10): p. 1474-84.

20. Engel, A.G., *Current status of the congenital myasthenic syndromes.* Neuromuscul Disord, 2012. **22**(2): p. 99-111.

21. Engel, A.G., *Congenital myasthenic syndromes.* Neurol Clin, 1994. **12**(2): p. 401-37.

22. Engel, A.G., *Morphologic and immunopathologic findings in myasthenia gravis and in congenital myasthenic syndromes.* J Neurol Neurosurg Psychiatry, 1980. **43**(7): p. 577-89.

23. Misgeld, T., et al., *Roles of neurotransmitter in synapse formation: development of neuromuscular junctions lacking choline acetyltransferase.* Neuron, 2002. **36**(4): p. 635-48.

24. Ohno, K., et al., *Choline acetyltransferase mutations cause myasthenic syndrome associated with episodic apnea in humans.* Proc Natl Acad Sci U S A, 2001. **98**(4): p. 2017-22.

25. Schara, U., et al., *Long-term follow-up in patients with congenital myasthenic syndrome due to CHAT mutations.* Eur J Paediatr Neurol, 2010. **14**(4): p. 326-33.

26. Shen, X.M., et al., *Functional consequences and structural interpretation of mutations of human choline acetyltransferase.* Hum Mutat, 2011. **32**(11): p. 1259-67.

27. Massoulie, J., et al., *Molecular and cellular biology of cholinesterases.* Prog Neurobiol, 1993. **41**(1): p. 31-91.

28. Bon, S., F. Coussen, and J. Massoulie, *Quaternary associations of acetylcholinesterase. II. The polyproline attachment domain of the collagen tail.* J Biol Chem, 1997. **272**(5): p. 3016-21.

29. Bestue-Cardiel, M., et al., *Congenital endplate acetylcholinesterase deficiency responsive to ephedrine.* Neurology, 2005. **65**(1): p. 144-6.

30. Liewluck, T., D. Selcen, and A.G. Engel, *Beneficial effects of albuterol in congenital endplate acetylcholinesterase deficiency and Dok-7 myasthenia.* Muscle Nerve, 2011. **44**(5): p. 789-94.

31. Maselli, R.A., et al., *Mutations in LAMB2 causing a severe form of synaptic congenital myasthenic syndrome.* J Med Genet, 2009. **46**(3): p. 203-8.

32. Patton, B.L., *Laminins of the neuromuscular system.* Microsc Res Tech, 2000. **51**(3): p. 247-61.

33. Sine, S.M. and A.G. Engel, *Recent advances in Cys-loop receptor structure and function.* Nature, 2006. **440**(7083): p. 448-55.

34. Vincent, A., *Unravelling the pathogenesis of myasthenia gravis.* Nat Rev Immunol, 2002. **2**(10): p. 797-804.

35. Chaouch, A., et al., *A retrospective clinical study of the treatment of slow-channel congenital myasthenic syndrome.* J Neurol, 2012. **259**(3): p. 474-81.

36. Engel, A.G. and S.M. Sine, *Current understanding of congenital myasthenic syndromes.* Curr Opin Pharmacol, 2005. **5**(3): p. 308-21.

37. Engel, A.G., K. Ohno, and S.M. Sine, *Sleuthing molecular targets for neurological diseases at the neuromuscular junction.* Nat Rev Neurosci, 2003. **4**(5): p. 339-52.

38. Froehner, S.C., et al., *The postsynaptic 43K protein clusters muscle nicotinic acetylcholine receptors in Xenopus oocytes.* Neuron, 1990. **5**(4): p. 403-10.

39. Cartaud, A., et al., *Evidence for in situ and in vitro association between beta-dystroglycan and the subsynaptic 43K rapsyn protein. Consequence for acetylcholine receptor clustering at the synapse.* J Biol Chem, 1998. **273**(18): p. 11321-6.

40. Ohno, K., et al., *Rapsyn mutations in humans cause endplate acetylcholine-receptor deficiency and myasthenic syndrome.* Am J Hum Genet, 2002. **70**(4): p. 875-85.

41. Banwell, B.L., et al., *Novel truncating RAPSN mutations causing congenital myasthenic syndrome responsive to 3,4-diaminopyridine.* Neuromuscul Disord, 2004. **14**(3): p. 202-7.

42. Maselli, R.A., et al., *Congenital myasthenic syndrome caused by two non-N88K rapsyn mutations.* Clin Genet, 2007. **72**(1): p. 63-5.

43. Huze, C., et al., *Identification of an agrin mutation that causes congenital myasthenia and affects synapse function.* Am J Hum Genet, 2009. **85**(2): p. 155-67.

44. Maselli, R.A., et al., *LG2 agrin mutation causing severe congenital myasthenic syndrome mimics functional characteristics of non-neural (z-) agrin.* Hum Genet, 2011.

45. Chevessier, F., et al., *MUSK, a new target for mutations causing congenital myasthenic syndrome.* Hum Mol Genet, 2004. **13**(24): p. 3229-40.

46. Maselli, R.A., et al., *Mutations in MUSK causing congenital myasthenic syndrome impair MuSK-Dok-7 interaction.* Hum Mol Genet, 2010. **19**(12): p. 2370-9.

47. Mihaylova, V., et al., *Refinement of the clinical phenotype in musk-related congenital myasthenic syndromes.* Neurology, 2009. **73**(22): p. 1926-8.

48. Beeson, D., et al., *Dok-7 mutations underlie a neuromuscular junction synaptopathy.* Science, 2006. **313**(5795): p. 1975-8.

49. Selcen, D., et al., *Dok-7 myasthenia: phenotypic and molecular genetic studies in 16 patients.* Ann Neurol, 2008. **64**(1): p. 71-87.

50. Slater, C.R., et al., *Pre- and post-synaptic abnormalities associated with impaired neuromuscular transmission in a group of patients with 'limb-girdle myasthenia'.* Brain, 2006. **129**(Pt 8): p. 2061-76.

51. Muller, J.S., et al., *Dok-7 promotes slow muscle integrity as well as neuromuscular junction formation in a zebrafish model of congenital myasthenic syndromes.* Hum Mol Genet, 2010. **19**(9): p. 1726-40.

52. Lashley, D., et al., *Ephedrine treatment in congenital myasthenic syndrome due to mutations in DOK7.* Neurology, 2010. **74**(19): p. 1517-23.

53. Tsujino, A., et al., *Myasthenic syndrome caused by mutation of the SCN4A sodium channel.* Proc Natl Acad Sci U S A, 2003. **100**(12): p. 7377-82.

54. Selcen, D., et al., *Myasthenic syndrome caused by plectinopathy.* Neurology, 2011. **76**(4): p. 327-36.

55. Forrest, K., et al., *Congenital muscular dystrophy, myasthenic symptoms and epidermolysis bullosa simplex (EBS) associated with mutations in the PLEC1 gene encoding plectin.* Neuromuscul Disord, 2010. **20**(11): p. 709-11.

56. Maselli, R., et al., *Congenital myasthenic syndrome associated with epidermolysis bullosa caused by homozygous mutations in PLEC1 and CHRNE.* Clin Genet, 2010.

57. Palace, J., C.M. Wiles, and J. Newsom-Davis, *3,4-Diaminopyridine in the treatment of congenital (hereditary) myasthenia.* J Neurol Neurosurg Psychiatry, 1991. **54**(12): p. 1069-72.

58. Anlar, B., et al., *3,4-diaminopyridine in childhood myasthenia: double-blind, placebo-controlled trial.* J Child Neurol, 1996. **11**(6): p. 458-61.

59. Palace, J., et al., *Clinical features in a series of fast channel congenital myasthenia syndrome.* Neuromuscul Disord, 2012. **22**(2): p. 112-7.

60. Webster, R., et al., *Fast-channel congenital myasthenic syndrome with a novel acetylcholine receptor mutation at the alpha-epsilon subunit interface.* Neuromuscul Disord, 2013.

61. Fukudome, T., et al., *Quinidine normalizes the open duration of slow-channel mutants of the acetylcholine receptor.* Neuroreport, 1998. **9**(8): p. 1907-11.

62. Harper, C.M., T. Fukodome, and A.G. Engel, *Treatment of slow-channel congenital myasthenic syndrome with fluoxetine.* Neurology, 2003. **60**(10): p. 1710-3.

63. Burke, G., et al., *Rapsyn mutations in hereditary myasthenia: distinct early- and late-onset phenotypes.* Neurology, 2003. **61**(6): p. 826-8.

64. Banwell, B.L., et al., *Myopathy, myasthenic syndrome, and epidermolysis bullosa simplex due to plectin deficiency.* J Neuropathol Exp Neurol, 1999. **58**(8): p. 832-46.

65. Senderek, J., et al., *Hexosamine biosynthetic pathway mutations cause neuromuscular transmission defect.* Am J Hum Genet, 2011. **88**(2): p. 162-72.

66. Guergueltcheva, V., et al., *Congenital myasthenic syndrome with tubular aggregates caused by GFPT1 mutations.* J Neurol, 2011.

67. Engel, W.K., *Mitochondrial Aggregates in Muscle Disease.* J Histochem Cytochem, 1964. **12**: p. 46-8.

68. Pavlovicova, M., M. Novotova, and I. Zahradnik, *Structure and composition of tubular aggregates of skeletal muscle fibres.* Gen Physiol Biophys, 2003. **22**(4): p. 425-40.

69. Engel, W.K., D.W. Bishop, and G.G. Cunningham, *Tubular aggregates in type II muscle fibers: ultrastructural and histochemical correlation.* J Ultrastruct Res, 1970. **31**(5-6): p. 507-25.

70. Salviati, G., et al., *Tubular aggregates: sarcoplasmic reticulum origin, calcium storage ability, and functional implications.* Muscle Nerve, 1985. **8**(4): p. 299-306.

71. McKnight, G.L., et al., *Molecular cloning, cDNA sequence, and bacterial expression of human glutamine:fructose-6-phosphate amidotransferase.* J Biol Chem, 1992. **267**(35): p. 25208-12.

72. Oki, T., et al., *cDNA cloning and mapping of a novel subtype of glutamine:fructose-6-phosphate amidotransferase (GFAT2) in human and mouse.* Genomics, 1999. **57**(2): p. 227-34.

73. Niimi, M., et al., *Identification of GFAT1-L, a novel splice variant of human glutamine: fructose-6-phosphate amidotransferase (GFAT1) that is expressed abundantly in skeletal muscle.* J Hum Genet, 2001. **46**(10): p. 566-71.

74. Massiere, F. and M.A. Badet-Denisot, *The mechanism of glutamine-dependent amidotransferases.* Cell Mol Life Sci, 1998. **54**(3): p. 205-22.

75. Bateman, A., *The SIS domain: a phosphosugar-binding domain.* Trends Biochem Sci, 1999. **24**(3): p. 94-5.

76. Teplyakov, A., et al., *Channeling of ammonia in glucosamine-6-phosphate synthase.* J Mol Biol, 2001. **313**(5): p. 1093-102.

77. Milewski, S., *Glucosamine-6-phosphate synthase--the multi-facets enzyme.* Biochim Biophys Acta, 2002. **1597**(2): p. 173-92.

78. Teplyakov, A., et al., *Involvement of the C terminus in intramolecular nitrogen channeling in glucosamine 6-phosphate synthase: evidence from a 1.6 A crystal structure of the isomerase domain.* Structure, 1998. **6**(8): p. 1047-55.

79. Mouilleron, S., M.A. Badet-Denisot, and B. Golinelli-Pimpaneau, *Glutamine binding opens the ammonia channel and activates glucosamine-6P synthase.* J Biol Chem, 2006. **281**(7): p. 4404-12.

80. Nakaishi, Y., et al., *Structural analysis of human glutamine:fructose-6-phosphate amidotransferase, a key regulator in type 2 diabetes.* FEBS Lett, 2009. **583**(1): p. 163-7.

81. Richez, C., et al., *Expression and purification of active human internal His(6)-tagged L-glutamine: D-Fructose-6P amidotransferase I.* Protein Expr Purif, 2007. **54**(1): p. 45-53.

82. Zeidan, Q. and G.W. Hart, *The intersections between O-GlcNAcylation and phosphorylation: implications for multiple signaling pathways.* J Cell Sci, 2010. **123**(Pt 1): p. 13-22.

83. Marshall, S., V. Bacote, and R.R. Traxinger, *Discovery of a metabolic pathway mediating glucose-induced desensitization of the glucose transport system. Role of hexosamine biosynthesis in the induction of insulin resistance.* J Biol Chem, 1991. **266**(8): p. 4706-12.

84. Copeland, R.J., J.W. Bullen, and G.W. Hart, *Cross-talk between GlcNAcylation and phosphorylation: roles in insulin resistance and glucose toxicity.* Am J Physiol Endocrinol Metab, 2008. **295**(1): p. E17-28.

85. Laczy, B., et al., *Protein O-GlcNAcylation: a new signaling paradigm for the cardiovascular system.* Am J Physiol Heart Circ Physiol, 2009. **296**(1): p. H13-28.

86. Kornfeld, R., *Studies on L-glutamine D-fructose 6-phosphate amidotransferase. I. Feedback inhibition by uridine diphosphate-N-acetylglucosamine.* J Biol Chem, 1967. **242**(13): p. 3135-41.

87. Traxinger, R.R. and S. Marshall, *Coordinated regulation of glutamine:fructose-6-phosphate amidotransferase activity by insulin, glucose, and glutamine. Role of hexosamine biosynthesis in enzyme regulation.* J Biol Chem, 1991. **266**(16): p. 10148-54.

88. DeHaven, J.E., et al., *A novel variant of glutamine: fructose-6-phosphate amidotransferase-1 (GFAT1) mRNA is selectively expressed in striated muscle.* Diabetes, 2001. **50**(11): p. 2419-24.

89. Lehle, L., S. Strahl, and W. Tanner, *Protein glycosylation, conserved from yeast to man: a model organism helps elucidate congenital human diseases.* Angew Chem Int Ed Engl, 2006. **45**(41): p. 6802-18.

90. Federici, M., et al., *Insulin-dependent activation of endothelial nitric oxide synthase is impaired by O-linked glycosylation modification of signaling proteins in human coronary endothelial cells.* Circulation, 2002. **106**(4): p. 466-72.

91. Kudlow, J.E., *Post-translational modification by O-GlcNAc: another way to change protein function.* J Cell Biochem, 2006. **98**(5): p. 1062-75.

92. Han, I., M.D. Roos, and J.E. Kudlow, *Interaction of the transcription factor Sp1 with the nuclear pore protein p62 requires the C-terminal domain of p62.* J Cell Biochem, 1998. **68**(1): p. 50-61.

93. Zhang, F., et al., *O-GlcNAc modification is an endogenous inhibitor of the proteasome.* Cell, 2003. **115**(6): p. 715-25.

94. Duverger, E., A.C. Roche, and M. Monsigny, *N-acetylglucosamine-dependent nuclear import of neoglycoproteins.* Glycobiology, 1996. **6**(4): p. 381-6.

95. Golks, A., et al., *Requirement for O-linked N-acetylglucosaminyltransferase in lymphocytes activation.* EMBO J, 2007. **26**(20): p. 4368-79.

96. Yang, X., et al., *Phosphoinositide signalling links O-GlcNAc transferase to insulin resistance.* Nature, 2008. **451**(7181): p. 964-9.

97. Hart, G.W., M.P. Housley, and C. Slawson, *Cycling of O-linked beta-N-acetylglucosamine on nucleocytoplasmic proteins.* Nature, 2007. **446**(7139): p. 1017-22.

98. Parekh, R.B. and C. Rohlff, *Post-translational modification of proteins and the discovery of new medicine.* Curr Opin Biotechnol, 1997. **8**(6): p. 718-23.

99. Apweiler, R., H. Hermjakob, and N. Sharon, *On the frequency of protein glycosylation, as deduced from analysis of the SWISS-PROT database.* Biochim Biophys Acta, 1999. **1473**(1): p. 4-8.

100. Walsh, C.T., S. Garneau-Tsodikova, and G.J. Gatto, Jr., *Protein posttranslational modifications: the chemistry of proteome diversifications.* Angew Chem Int Ed Engl, 2005. **44**(45): p. 7342-72.

101. Hang, H.C. and C.R. Bertozzi, *The chemistry and biology of mucin-type O-linked glycosylation.* Bioorg Med Chem, 2005. **13**(17): p. 5021-34.

102. Holt, G.D. and G.W. Hart, *The subcellular distribution of terminal N-acetylglucosamine moieties. Localization of a novel protein-saccharide linkage, O-linked GlcNAc.* J Biol Chem, 1986. **261**(17): p. 8049-57.

103. Torres, C.R. and G.W. Hart, *Topography and polypeptide distribution of terminal N-acetylglucosamine residues on the surfaces of intact lymphocytes. Evidence for O-linked GlcNAc.* J Biol Chem, 1984. **259**(5): p. 3308-17.

104. Zachara, N.E. and G.W. Hart, *O-GlcNAc a sensor of cellular state: the role of nucleocytoplasmic glycosylation in modulating cellular function in response to nutrition and stress.* Biochim Biophys Acta, 2004. **1673**(1-2): p. 13-28.

105. Kreppel, L.K. and G.W. Hart, *Regulation of a cytosolic and nuclear O-GlcNAc transferase. Role of the tetratricopeptide repeats.* J Biol Chem, 1999. **274**(45): p. 32015-22.

106. Breslauer, K.J., et al., *Predicting DNA duplex stability from the base sequence.* Proc Natl Acad Sci U S A, 1986. **83**(11): p. 3746-50.

107. Sugimoto, N., et al., *Improved thermodynamic parameters and helix initiation factor to predict stability of DNA duplexes.* Nucleic Acids Res, 1996. **24**(22): p. 4501-5.

108. Kibbe, W.A., *OligoCalc: an online oligonucleotide properties calculator.* Nucleic Acids Res, 2007. **35**(Web Server issue): p. W43-6.

109. Ho, S.N., et al., *Site-directed mutagenesis by overlap extension using the polymerase chain reaction.* Gene, 1989. **77**(1): p. 51-9.

110. Livak, K.J. and T.D. Schmittgen, *Analysis of relative gene expression data using real-time quantitative PCR and the 2(-Delta Delta C(T)) Method.* Methods, 2001. **25**(4): p. 402-8.

111. Lander, E.S. and D. Botstein, *Homozygosity mapping: a way to map human recessive traits with the DNA of inbred children.* Science, 1987. **236**(4808): p. 1567-70.

112. Abecasis, G.R., et al., *Merlin--rapid analysis of dense genetic maps using sparse gene flow trees.* Nat Genet, 2002. **30**(1): p. 97-101.

113. Kruglyak, L., et al., *Parametric and nonparametric linkage analysis: a unified multipoint approach.* Am J Hum Genet, 1996. **58**(6): p. 1347-63.

114. Lindner, T.H. and K. Hoffmann, *easyLINKAGE: a PERL script for easy and automated two-/multi-point linkage analyses.* Bioinformatics, 2005. **21**(3): p. 405-7.

115. von der Hagen, M., et al., *Facing the genetic heterogeneity in neuromuscular disorders: linkage analysis as an economic diagnostic approach towards the molecular diagnosis.* Neuromuscul Disord, 2006. **16**(1): p. 4-13.

116. Lochmuller, H., T. Johns, and E.A. Shoubridge, *Expression of the E6 and E7 genes of human papillomavirus (HPV16) extends the life span of human myoblasts.* Exp Cell Res, 1999. **248**(1): p. 186-93.

117. Bradford, M.M., *A rapid and sensitive method for the quantitation of microgram quantities of protein utilizing the principle of protein-dye binding.* Anal Biochem, 1976. **72**: p. 248-54.

118. Eguchi, S., et al., *AMP-activated protein kinase phosphorylates glutamine : fructose-6-phosphate amidotransferase 1 at Ser243 to modulate its enzymatic activity.* Genes Cells, 2009. **14**(2): p. 179-89.

119. Ye, F., et al., *A simple and sensitive method for glutamine:fructose-6-phosphate amidotransferase assay.* J Biochem Biophys Methods, 2004. **59**(3): p. 201-8.

120. Ng, D.P., et al., *Scrutiny of the glutamine-fructose-6-phosphate transaminase 1 (GFPT1) locus reveals conserved haplotype block structure not associated with diabetic nephropathy.* Diabetes, 2004. **53**(3): p. 865-9.

121. Kunika, K., et al., *Effect of +36T>C in intron 1 on the glutamine: fructose-6-phosphate amidotransferase 1 gene and its contribution to type 2 diabetes in different populations.* J Hum Genet, 2006. **51**(12): p. 1100-9.

122. Schwarz, J.M., et al., *MutationTaster evaluates disease-causing potential of sequence alterations.* Nat Methods, 2010. **7**(8): p. 575-6.

123. Holt, G.D., et al., *Nuclear pore complex glycoproteins contain cytoplasmically disposed O-linked N-acetylglucosamine.* J Cell Biol, 1987. **104**(5): p. 1157-64.

124. Baskerville, S. and D.P. Bartel, *Microarray profiling of microRNAs reveals frequent coexpression with neighboring miRNAs and host genes.* RNA, 2005. **11**(3): p. 241-7.

125. Beuvink, I., et al., *A novel microarray approach reveals new tissue-specific signatures of known and predicted mammalian microRNAs.* Nucleic Acids Res, 2007. **35**(7): p. e52.

126. Shingara, J., et al., *An optimized isolation and labeling platform for accurate microRNA expression profiling.* RNA, 2005. **11**(9): p. 1461-70.

127. Liang, Y., et al., *Characterization of microRNA expression profiles in normal human tissues.* BMC Genomics, 2007. **8**: p. 166.

128. McCarthy, J.J., *MicroRNA-206: the skeletal muscle-specific myomiR.* Biochim Biophys Acta, 2008. **1779**(11): p. 682-91.

129. Rao, P.K., et al., *Myogenic factors that regulate expression of muscle-specific microRNAs.* Proc Natl Acad Sci U S A, 2006. **103**(23): p. 8721-6.

130. Cummins, J.M., et al., *The colorectal microRNAome.* Proc Natl Acad Sci U S A, 2006. **103**(10): p. 3687-92.

131. Kim, H.K., et al., *Muscle-specific microRNA miR-206 promotes muscle differentiation.* J Cell Biol, 2006. **174**(5): p. 677-87.

132. Wang, Z., *The guideline of the design and validation of MiRNA mimics.* Methods Mol Biol, 2011. **676**: p. 211-23.

133. Xiao, J., et al., *Novel approaches for gene-specific interference via manipulating actions of microRNAs: examination on the pacemaker channel genes HCN2 and HCN4.* J Cell Physiol, 2007. **212**(2): p. 285-92.

134. Clop, A., et al., *A mutation creating a potential illegitimate microRNA target site in the myostatin gene affects muscularity in sheep.* Nat Genet, 2006. **38**(7): p. 813-8.

135. McQuillen, M.P., *Familial limb-girdle myasthenia.* Brain, 1966. **89**(1): p. 121-32.

136. Muller, J.S., et al., *Phenotypical spectrum of DOK7 mutations in congenital myasthenic syndromes.* Brain, 2007. **130**(Pt 6): p. 1497-506.

137. Palace, J., et al., *Clinical features of the DOK7 neuromuscular junction synaptopathy.* Brain, 2007. **130**(Pt 6): p. 1507-15.

138. Ben Ammar, A., et al., *Phenotype genotype analysis in 15 patients presenting a congenital myasthenic syndrome due to mutations in DOK7.* J Neurol, 2010. **257**(5): p. 754-66.

139. Abicht, A., et al., *A common mutation (epsilon1267delG) in congenital myasthenic patients of Gypsy ethnic origin.* Neurology, 1999. **53**(7): p. 1564-9.

140. Muller, J.S., et al., *The congenital myasthenic syndrome mutation RAPSN N88K derives from an ancient Indo-European founder.* J Med Genet, 2004. **41**(8): p. e104.

141. Love, D.C., M.W. Krause, and J.A. Hanover, *O-GlcNAc cycling: emerging roles in development and epigenetics.* Semin Cell Dev Biol, 2010. **21**(6): p. 646-54.

142. Martin, P.T., *Glycobiology of the synapse.* Glycobiology, 2002. **12**(1): p. 1R-7R.

143. Hedou, J., et al., *Mapping of O-linked beta-N-acetylglucosamine modification sites in key contractile proteins of rat skeletal muscle.* Proteomics, 2009. **9**(8): p. 2139-48.

144. Cieniewski-Bernard, C., et al., *Identification of O-linked N-acetylglucosamine proteins in rat skeletal muscle using two-dimensional gel electrophoresis and mass spectrometry.* Mol Cell Proteomics, 2004. **3**(6): p. 577-85.

145. Cieniewski-Bernard, C., et al., *O-GlcNAc level variations are associated with the development of skeletal muscle atrophy.* J Appl Physiol, 2006. **100**(5): p. 1499-505.

146. Ohno, K., et al., *Congenital myasthenic syndrome caused by decreased agonist binding affinity due to a mutation in the acetylcholine receptor epsilon subunit.* Neuron, 1996. **17**(1): p. 157-70.

147. Prives, J. and D. Bar-Sagi, *Effect of tunicamycin, an inhibitor of protein glycosylation, on the biological properties of acetylcholine receptor in cultured muscle cells.* J Biol Chem, 1983. **258**(3): p. 1775-80.

148. Engel, A.G., et al., *End-plate acetylcholine receptor deficiency due to nonsense mutations in the epsilon subunit.* Ann Neurol, 1996. **40**(5): p. 810-7.

149. Rodolico, C., et al., *Limb-girdle myasthenia: clinical, electrophysiological and morphological features in familial and autoimmune cases.* Neuromuscul Disord, 2002. **12**(10): p. 964-9.

150. Bret, C., et al., *Expression of genes encoding for proteins involved in heparan sulphate and chondroitin sulphate chain synthesis and modification in normal and malignant plasma cells.* Br J Haematol, 2009. **145**(3): p. 350-68.

151. Gotting, C., et al., *Molecular cloning and expression of human UDP-d-Xylose:proteoglycan core protein beta-d-xylosyltransferase and its first isoform XT-II.* J Mol Biol, 2000. **304**(4): p. 517-28.

152. Kuhn, J., et al., *First isolation of human UDP-D-xylose: proteoglycan core protein beta-D-xylosyltransferase secreted from cultured JAR choriocarcinoma cells.* J Biol Chem, 2001. **276**(7): p. 4940-7.

153. Boshart, M., et al., *A very strong enhancer is located upstream of an immediate early gene of human cytomegalovirus.* Cell, 1985. **41**(2): p. 521-30.

154. Muscat, G.E. and L. Kedes, *Multiple 5'-flanking regions of the human alpha-skeletal actin gene synergistically modulate muscle-specific expression.* Mol Cell Biol, 1987. **7**(11): p. 4089-99.

155. Brennan, K.J. and E.C. Hardeman, *Quantitative analysis of the human alpha-skeletal actin gene in transgenic mice.* J Biol Chem, 1993. **268**(1): p. 719-25.

156. Sayeski, P.P. and J.E. Kudlow, *Glucose metabolism to glucosamine is necessary for glucose stimulation of transforming growth factor-alpha gene transcription.* J Biol Chem, 1996. **271**(25): p. 15237-43.

157. Walgren, J.L., et al., *High glucose and insulin promote O-GlcNAc modification of proteins, including alpha-tubulin.* Am J Physiol Endocrinol Metab, 2003. **284**(2): p. E424-34.

158. Watty, A. and S.J. Burden, *MuSK glycosylation restrains MuSK activation and acetylcholine receptor clustering.* J Biol Chem, 2002. **277**(52): p. 50457-62.

159. Xia, B. and P.T. Martin, *Modulation of agrin binding and activity by the CT and related carbohydrate antigens.* Mol Cell Neurosci, 2002. **19**(4): p. 539-51.

160. Kim, M.L., et al., *O-fucosylation of muscle agrin determines its ability to cluster acetylcholine receptors.* Mol Cell Neurosci, 2008. **39**(3): p. 452-64.

161. Comer, F.I. and G.W. Hart, *O-Glycosylation of nuclear and cytosolic proteins. Dynamic interplay between O-GlcNAc and O-phosphate.* J Biol Chem, 2000. **275**(38): p. 29179-82.

162. Broschat, K.O., et al., *Kinetic characterization of human glutamine-fructose-6-phosphate amidotransferase I: potent feedback inhibition by glucosamine 6-phosphate.* J Biol Chem, 2002. **277**(17): p. 14764-70.

163. Kenig, M., E. Vandamme, and E.P. Abraham, *The mode of action of bacilysin and anticapsin and biochemical properties of bacilysin-resistant mutants.* J Gen Microbiol, 1976. **94**(1): p. 46-54.

164. Pogell, B.M., *Enzyme purification by selective elution with substrate from substituted cellulose columns.* Biochem Biophys Res Commun, 1962. **7**: p. 225-30.

165. Callahan, M., A. Tourian, and W.Y. Hung, *A sensitive, specific radioisotope assay for L-glutamine-D-fructose-6-phosphate aminotransferase.* Anal Biochem, 1981. **115**(2): p. 347-52.

166. Conne, B., A. Stutz, and J.D. Vassalli, *The 3' untranslated region of messenger RNA: A molecular 'hotspot' for pathology?* Nat Med, 2000. **6**(6): p. 637-41.

167. Mignone, F., et al., *Untranslated regions of mRNAs.* Genome Biol, 2002. **3**(3): p. REVIEWS0004.

168. Chabanon, H., I. Mickleburgh, and J. Hesketh, *Zipcodes and postage stamps: mRNA localisation signals and their trans-acting binding proteins.* Brief Funct Genomic Proteomic, 2004. **3**(3): p. 240-56.

169. Xie, X., et al., *Systematic discovery of regulatory motifs in human promoters and 3' UTRs by comparison of several mammals.* Nature, 2005. **434**(7031): p. 338-45.

170. Bandiera, S., et al., *microRNAs in diseases: from candidate to modifier genes.* Clin Genet, 2010. **77**(4): p. 306-13.

171. Bartel, D.P., *MicroRNAs: genomics, biogenesis, mechanism, and function.* Cell, 2004. **116**(2): p. 281-97.

172. Schwarz, D.S., et al., *Asymmetry in the assembly of the RNAi enzyme complex.* Cell, 2003. **115**(2): p. 199-208.

173. Krichevsky, A.M., et al., *A microRNA array reveals extensive regulation of microRNAs during brain development.* RNA, 2003. **9**(10): p. 1274-81.

174. Metzler, M., et al., *High expression of precursor microRNA-155/BIC RNA in children with Burkitt lymphoma.* Genes Chromosomes Cancer, 2004. **39**(2): p. 167-9.

175. Smalheiser, N.R., *EST analyses predict the existence of a population of chimeric microRNA precursor-mRNA transcripts expressed in normal human and mouse tissues.* Genome Biol, 2003. **4**(7): p. 403.

176. Lau, N.C., et al., *An abundant class of tiny RNAs with probable regulatory roles in Caenorhabditis elegans.* Science, 2001. **294**(5543): p. 858-62.

177. Okamura, K., et al., *The regulatory activity of microRNA* species has substantial influence on microRNA and 3' UTR evolution.* Nat Struct Mol Biol, 2008. **15**(4): p. 354-63.

178. Packer, A.N., et al., *The bifunctional microRNA miR-9/miR-9* regulates REST and CoREST and is downregulated in Huntington's disease.* J Neurosci, 2008. **28**(53): p. 14341-6.

179. Han, J., et al., *Molecular basis for the recognition of primary microRNAs by the Drosha-DGCR8 complex.* Cell, 2006. **125**(5): p. 887-901.

180. Denli, A.M., et al., *Processing of primary microRNAs by the Microprocessor complex.* Nature, 2004. **432**(7014): p. 231-5.

181. Lewis, B.P., C.B. Burge, and D.P. Bartel, *Conserved seed pairing, often flanked by adenosines, indicates that thousands of human genes are microRNA targets.* Cell, 2005. **120**(1): p. 15-20.

182. Grimson, A., et al., *MicroRNA targeting specificity in mammals: determinants beyond seed pairing.* Mol Cell, 2007. **27**(1): p. 91-105.

183. Nielsen, C.B., et al., *Determinants of targeting by endogenous and exogenous microRNAs and siRNAs.* RNA, 2007. **13**(11): p. 1894-910.

184. Lai, E.C., B. Tam, and G.M. Rubin, *Pervasive regulation of Drosophila Notch target genes by GY-box-, Brd-box-, and K-box-class microRNAs.* Genes Dev, 2005. **19**(9): p. 1067-80.

185. Lai, E.C., *Micro RNAs are complementary to 3' UTR sequence motifs that mediate negative post-transcriptional regulation.* Nat Genet, 2002. **30**(4): p. 363-4.

186. Brennecke, J., et al., *Principles of microRNA-target recognition.* PLoS Biol, 2005. **3**(3): p. e85.

187. Doench, J.G. and P.A. Sharp, *Specificity of microRNA target selection in translational repression.* Genes Dev, 2004. **18**(5): p. 504-11.

188. Lewis, B.P., et al., *Prediction of mammalian microRNA targets.* Cell, 2003. **115**(7): p. 787-98.

189. Stark, A., et al., *Animal MicroRNAs confer robustness to gene expression and have a significant impact on 3'UTR evolution.* Cell, 2005. **123**(6): p. 1133-46.

190. Grun, D., et al., *microRNA target predictions across seven Drosophila species and comparison to mammalian targets.* PLoS Comput Biol, 2005. **1**(1): p. e13.

191. Shin, C., et al., *Expanding the microRNA targeting code: functional sites with centered pairing.* Mol Cell, 2010. **38**(6): p. 789-802.

192. Lim, L.P., et al., *The microRNAs of Caenorhabditis elegans.* Genes Dev, 2003. **17**(8): p. 991-1008.

193. Simon, D., et al., *A mutation in the 3'-UTR of the HDAC6 gene abolishing the post-transcriptional regulation mediated by hsa-miR-433 is linked to a new form of dominant X-linked chondrodysplasia.* Hum Mol Genet, 2010. **19**(10): p. 2015-27.

194. Abelson, J.F., et al., *Sequence variants in SLITRK1 are associated with Tourette's syndrome.* Science, 2005. **310**(5746): p. 317-20.

195. Zuchner, S., et al., *Mutations in the novel mitochondrial protein REEP1 cause hereditary spastic paraplegia type 31.* Am J Hum Genet, 2006. **79**(2): p. 365-9.

196. Beetz, C., et al., *REEP1 mutation spectrum and genotype/phenotype correlation in hereditary spastic paraplegia type 31.* Brain, 2008. **131**(Pt 4): p. 1078-86.

197. Chi, S.W., et al., *Argonaute HITS-CLIP decodes microRNA-mRNA interaction maps.* Nature, 2009. **460**(7254): p. 479-86.

198. Guo, H., et al., *Mammalian microRNAs predominantly act to decrease target mRNA levels.* Nature, 2010. **466**(7308): p. 835-40.

199. Sempere, L.F., et al., *Expression profiling of mammalian microRNAs uncovers a subset of brain-expressed microRNAs with possible roles in murine and human neuronal differentiation.* Genome Biol, 2004. **5**(3): p. R13.

200. Gregory, R.I., et al., *Human RISC couples microRNA biogenesis and posttranscriptional gene silencing.* Cell, 2005. **123**(4): p. 631-40.

201. Rand, T.A., et al., *Argonaute2 cleaves the anti-guide strand of siRNA during RISC activation.* Cell, 2005. **123**(4): p. 621-9.

202. Matranga, C., et al., *Passenger-strand cleavage facilitates assembly of siRNA into Ago2-containing RNAi enzyme complexes.* Cell, 2005. **123**(4): p. 607-20.

203. Czech, B., et al., *Hierarchical rules for Argonaute loading in Drosophila.* Mol Cell, 2009. **36**(3): p. 445-56.

204. Hu, H.Y., et al., *Sequence features associated with microRNA strand selection in humans and flies.* BMC Genomics, 2009. **10**: p. 413.

205. Okamura, K., N. Liu, and E.C. Lai, *Distinct mechanisms for microRNA strand selection by Drosophila Argonautes.* Mol Cell, 2009. **36**(3): p. 431-44.

206. Seitz, H., M. Ghildiyal, and P.D. Zamore, *Argonaute loading improves the 5' precision of both MicroRNAs and their miRNA* strands in flies.* Curr Biol, 2008. **18**(2): p. 147-51.

207. Wu, H., et al., *Alternative processing of primary microRNA transcripts by Drosha generates 5' end variation of mature microRNA.* PLoS One, 2009. **4**(10): p. e7566.

208. Liu, N., et al., *microRNA-206 promotes skeletal muscle regeneration and delays progression of Duchenne muscular dystrophy in mice.* J Clin Invest, 2012. **122**(6): p. 2054-65.

209. Lagos-Quintana, M., et al., *Identification of novel genes coding for small expressed RNAs.* Science, 2001. **294**(5543): p. 853-8.

210. Zeng, Y. and B.R. Cullen, *Sequence requirements for micro RNA processing and function in human cells.* RNA, 2003. **9**(1): p. 112-23.

211. Shi, R. and V.L. Chiang, *Facile means for quantifying microRNA expression by real-time PCR.* Biotechniques, 2005. **39**(4): p. 519-25.

212. Benes, V. and M. Castoldi, *Expression profiling of microRNA using real-time quantitative PCR, how to use it and what is available.* Methods, 2010. **50**(4): p. 244-9.

213. Zipper, H., et al., *Investigations on DNA intercalation and surface binding by SYBR Green I, its structure determination and methodological implications.* Nucleic Acids Res, 2004. **32**(12): p. e103.

214. Schara, U. and H. Lochmuller, *Therapeutic strategies in congenital myasthenic syndromes.* Neurotherapeutics, 2008. **5**(4): p. 542-7.

215. Haeuptle, M.A. and T. Hennet, *Congenital disorders of glycosylation: an update on defects affecting the biosynthesis of dolichol-linked oligosaccharides.* Hum Mutat, 2009. **30**(12): p. 1628-41.

216. Chen, J.M., C. Ferec, and D.N. Cooper, *A systematic analysis of disease-associated variants in the 3' regulatory regions of human protein-coding genes I: general principles and overview.* Hum Genet, 2006. **120**(1): p. 1-21.

217. Hresko, R.C., et al., *Glucosamine-induced insulin resistance in 3T3-L1 adipocytes is caused by depletion of intracellular ATP.* J Biol Chem, 1998. **273**(32): p. 20658-68.

218. Weigert, C., et al., *Palmitate-induced activation of the hexosamine pathway in human myotubes: increased expression of glutamine:fructose-6-phosphate aminotransferase.* Diabetes, 2003. **52**(3): p. 650-6.

K Abbreviations

aa	amino acid
ab	antibody
Acetyl-CoA	Acetyl-CoenzymeA
ACh	Acetylcholine
AChE/*ACHE*	Acetylcholinesterase/gene
AChR	Acetylcholine receptor (nicotinic)
αAChR	Acetylcholine receptor, alpha-subunit
βAChR	Acetylcholine receptor, beta-subunit
δAChR	Acetylcholine receptor, delta-subunit
γAChR	Acetylcholine receptor, gamma-subunit
εAChR	Acetylcholine receptor, epsilon-subunit
BCA	bicinchonin acid
BLAST	basic local alignment search tool
bp	base pair/s
BSA	bovine serum albumin
°C	Grad Celsius
cDNA	complementary DNA
ChAT/*CHAT*	Cholin-Acetyltransferase/gene
CHRNA1	gene coding for the alpha-subunit of the AChR
CHRNB1	gene coding for the beta-subunit of the AChR
CHRND	gene coding for the delta-subunit of the AChR
CHRNE	gene coding for the epsilon-subunit of the AChR
ColQ/*COLQ*	collagen tail/gene
CMS	Congenital myasthenic syndrome
CSK	cytoskeletal buffer
d	day/s
ddH_2O	double-distilled water
DMSO	dimethyl sulfoxide
DNA	deoxyribonucleic acid
dNTPs	mixture of all 4 deoxy ribonucleotides dATP, dTTP, dCTP, dGTP
DTT	Dithiothreitol
E.coli	*Escherichia coli*
EDTA	ethylenediaminetetraacetic acid

ELISA	enzyme-linked immunosorbent assay
HEK	Human embryonic kidney
e.g.	exempli gratia, for example
et al.	et alii, and others
etc.	et cetera
FCS	fetal calf serum
g	gram
GAPDH	Glyceraldehyde 3-phosphate dehydrogenase
GFP	green fluorescent protein
GFPT1/*GFPT1*	glutamine-fructose-6- phosphate transaminase 1/gene (human)
Gfpt1/*Gfpt1*	glutamine-fructose-6- phosphate transaminase 1/gene (mouse)
GFPT1-L/GFAT1-L	muscle-specific variant of glutamine-fructose-6- phosphate transaminase 1
h	hour/hours
hpf	hours post fertilization
HRP	horseradish peroxidise
hsa	Homo sapiens
IF	Immunofluorescence
l	liter
kb	kilobase
kDa	kilodaltons
LB	Luria-Bertani
LOD	Logarithm of odds
min	minutes
M	molar
ml	millilitre
mM	millimolar
mRNA	messenger ribonucleic acid
MuSK/*MUSK*	Muscle specific kinase/gene
mut	mutant
Myc	*myelocytomatosis* oncogene
ng	nanogram
nm	nanometer
NTPs	nucleotide triphosphate mixture containing adenosine, guanidine, uridine and cytosine
oan	Ornithorhynchus anatinus
o.n.	over night

ORF	open reading frame
PBS	phosphate buffered saline
PCR	polymerase chain reaction
PMSF	phenylmethylsulfonyl fluoride
pol	RNA-polymerase II
qRT-PCR	quantitative reverse transcription PCR
Rapsyn/*RAPSN*	Receptor-associated protein of the synapse/gene
RNA	ribonucleic acid
rpm	revolutions per minute
rt	room temperature
RT	reverse transcription
RT-PCR	reverse transcription polymerase chain reaction
SCCMS	Slow-Channel CMS
SCN4A	gene coding for the sodium channel
sec	seconds
SNP	Single nucleotide exchange polymorphism
TE	Tris-EDTA
Tris	Tris-(hydoxymethyl)-amminomethan
UTR	untranslated region
wt	wild-type
WB	Western blot
µg	microgram
µl	microliter
µM	micromolar

L List of Figures

PUBLICATIONS

Senderek J[#], Muller JS[#], **Dusl M**, Strom TM, Guergueltcheva V, Diepolder I, Laval SH, Maxwell S, Cossins J, Krause S, Muelas N, Vilchez JJ, Colomer J, Mallebrera CJ, Nascimento A, Nafissi S, Kariminejad A, Nilipour Y, Bozorgmehr B, Najmabadi H, Rodolico C, Sieb JP, Steinlein OK, Schlotter B, Schoser B, Kirschner J, Herrmann R, Voit T, Oldfors A, Lindbergh C, Urtizberea A, von der Hagen M, Hubner A, Palace J, Bushby K, Straub V, Beeson D, Abicht A, Lochmuller H. Hexosamine biosynthetic pathway mutations cause neuromuscular transmission defect. *Am J Hum Genet* 2011;88(2):162-72.

Chaouch A, Muller JS, Guergueltcheva V, **Dusl M**, Schara U, Rakocevic-Stojanovic V, Lindberg C, Scola RH, Werneck LC, Colomer J, Nascimento A, Vilchez JJ, Muelas N, Argov Z, Abicht A, Lochmuller H. A retrospective clinical study of the treatment of slow-channel congenital myasthenic syndrome. *J Neurol* 2012;259(3):474-81.

Guergueltcheva V[#], Muller JS[#], **Dusl M**, Senderek J, Oldfors A, Lindbergh C, Maxwell S, Colomer J, Mallebrera CJ, Nascimento A, Vilchez JJ, Muelas N, Kirschner J, Nafissi S, Kariminejad A, Nilipour Y, Bozorgmehr B, Najmabadi H, Rodolico C, Sieb JP, Schlotter B, Schoser B, Herrmann R, Voit T, Steinlein OK, Najafi A, Urtizberea A, Soler DM, Muntoni F, Hanna MG, Chaouch A, Straub V, Bushby K, Palace J, Beeson D, Abicht A, Lochmuller H. Congenital myasthenic syndrome with tubular aggregates caused by GFPT1 mutations. *J Neurol* 2011;259(5):838-50.

Abicht A, **Dusl M**, Gallenmuller C, Guergueltcheva V, Schara U, Della Marina A, Wibbeler E, Almaras S, Mihaylova V, von der Hagen M, Huebner A, Chaouch A, Muller JS, Lochmuller H. Congenital myasthenic syndromes: achievements and limitations of phenotype-guided gene-after-gene sequencing in diagnostic practice: a study of 680 patients. *Hum Mutat* 2012;33(10):1474-84.

Kriegmair MC, Frenz S, **Dusl M**, Franz WM, David R, Rupp RA. Cardiac differentiation in Xenopus is initiated by mespa. *Cardiovasc Res* 2013;97(3):454-63.

Gallenmuller C, Muller-Felber W, **Dusl M**, Stucka R, Guergueltcheva V, Blaschek A, von der Hagen M, Huebner A, Muller JS, Lochmuller H, Abicht A. Salbutamol-responsive limb-girdle congenital myasthenic syndrome due to a novel missense mutation and heteroallelic deletion in MUSK. *Neuromuscul Disord* 2014;24(1):31-5.

Dusl M, Müller JS, Pertl A, Stucka R, Senderek J ,Lochmüller H, David R[#], Abicht A[#]. A 3'-UTR mutation creates a potential microRNA target site in the *GFPT1* gene of LG-CMS patients. Im Begutachtungsverfahren.

[#] These authors contributed equally to this work

M Eidesstattliche Versicherung

Dusl Marina

Ich erkläre hiermit an Eides statt,

dass ich die vorliegende Dissertation mit dem Thema

Novel pathomechanisms implicated in defects of neuromuscular transmission

selbständig verfasst, mich außer der angegebenen keiner weiteren Hilfsmittel bedient und alle Erkenntnisse, die aus dem Schrifttum ganz oder annähernd übernommen sind, als solche kenntlich gemacht und nach ihrer Herkunft unter Bezeichnung der Fundstelle einzeln nachgewiesen habe.

Ich erkläre des Weiteren, dass die hier vorgelegte Dissertation nicht in gleicher oder in ähnlicher Form bei einer anderen Stelle zur Erlangung eines akademischen Grades eingereicht wurde.

München, den …… ……

Marina Dusl